Feasibility of Using Force Myography (FMG) for Estimating Hand Force and Wrist Torque

by

Maram Sakr

B.Sc. (Hons), Mansoura University, 2012

Thesis Submitted in Partial Fulfillment of the
Requirements for the Degree of
Master of Applied Science

In the
School of Engineering Science
Faculty of Applied Sciences

SIMON FRASER UNIVERSITY

Spring 2018

Approval

Name:	**Maram Sakr**
Degree:	**Master of Applied Science**
Title:	**Feasibility of Using Force Myography (FMG) for Estimating Hand Force and Wrist Torque**
Examining Committee:	**Chair:** **Rodney Vaughan** Professor
	Carlo Menon Senior Supervisor Professor
	Jie Liang Supervisor Professor
	Kamal Gupta Internal Examiner Professor
Date Defended/Approved:	[October 12th, 2017]

Ethics Statement

The author, whose name appears on the title page of this work, has obtained, for the research described in this work, either:

a. human research ethics approval from the Simon Fraser University Office of Research Ethics

or

b. advance approval of the animal care protocol from the University Animal Care Committee of Simon Fraser University

or has conducted the research

c. as a co-investigator, collaborator, or research assistant in a research project approved in advance.

A copy of the approval letter has been filed with the Theses Office of the University Library at the time of submission of this thesis or project.

The original application for approval and letter of approval are filed with the relevant offices. Inquiries may be directed to those authorities.

Simon Fraser University Library
Burnaby, British Columbia, Canada

Update Spring 2016

Abstract

Hand force estimation is critical for applications that involve physical human-machine interactions for force monitoring and machine control. Force Myography (FMG) is a potential technique to be used for estimating hand force/torque. The FMG signals represent the volumetric changes in the arm muscles due to muscle contraction or expansion during force/torque exertion. The aim of this thesis is to explore the suitability of FMG for hand force/torque estimation.

Studying the feasibility of using FMG for torque estimation was preliminary investigated by using 1-DOF torque sensor for labeling the FMG during torque exertion. A custom designed force-sensing resistors (FSRs) band was donned on the forearm muscle belly for measuring FMG signals, while the participants exerted torque around three axes. A regression model was created for each torque axis and trained using the corresponding data. The average R^2 was 0.89 for pronation-supination, flexion-extension, and radial-ulnar deviations.

Using 1-DOF torque sensor for labeling the data needs a new custom-rig for capturing each torque axis. To overcome this limitation, a 6-DOF force/torque load cell was used for labeling the FMG data during force/torque exertion in any direction. In addition, a total number of 60 FSRs were embedded into four bands to be worn on the arm for measuring FMG signals during force/torque exertion. Healthy participants were recruited in this study and were asked to exert isometric force along three perpendicular axes, torque about the same three axes, and force and torque freely in any direction. Three cases were considered to explore the performance of the FMG bands in estimating force/torque in single- and multi- axis. These cases are: (1) 6 axes force/torque individually; (2) 3-DOF force and 3-DOF torque; and (3) 6-DOF force and torque simultaneously. In addition, a comparison between all possible combinations of the four bands was held to provide guidelines about the best placement of the FMG measurements in each case.

The results show a promising potential of FMG to estimate isometric force/torque. Specifically, the following average R^2 accuracies were obtained using the four bands on the arm in cross-validation evaluation: 0.97 when the 6 force/torque axes were considered individually; 0.98 and 0.96 for the 3-DOF force and torque, respectively; and 0.95 for 6-DOF force/torque estimation.

Keywords: Hand Force/Torque Estimation; Human-machine Interface; Force Myography; Wearable Sensors.

To my father's soul

Acknowledgements

First, I would like to express my sincere gratitude to my senior supervisor, Dr. Carlo Menon for his support and guidance during my Masters. I am very grateful for all I have learned from him and for his continuous help in all stages of this thesis. I would also like to thank Drs. Kamal Gupta, Jie Liang, and Rodney Vaughan for their valuable time to review my work and participate in my oral defense.

I would also like to thank all my colleagues in the Menrva laboratory. It was truly pleasure and honor learning and working with all of you. I would like to specially acknowledge: Xianta Jiang, Mona Lisa Delva, Zhen Xiao, Gautam Sadarangani and Carlolyn Levy, for their valuable time and thoughts throughout my research.

Finally, I would like to express my loving thanks to my family for their endless love, support, and prayers. My gratitude to my father who was always in my thoughts on this journey. I would like also to express my deepest love and gratefulness for my mother, brother, and sister. Thank you for all the encouragement, love, Skype calls and support when I was so far from home. I also owe thanks to a very special person; my husband, Alaa for his extraordinary love, support, and inspiration. You were always around at times I thought that it is impossible to continue, you helped me keep things in perspective. I greatly value his contribution, thoughts and volunteering in my research work, and deeply appreciate his faith in me. Lastly, I am grateful to the support of my friend Zainab, who was always beside me during the happy and hard moments to push and motivate me.

Table of Contents

List of Figures

List of Tables

List of Acronyms

Term	Initial components of the term
FMG	Force Myography
FSR	Force Sensitive Resistor
EMG	Electromyography
ZIF	Zero Insertion Force
PCB	Printed Circuit Board
KRR	Kernel Ridge Regression
GRNN	General Regression Neural Network
ANN	Artificial Neural Network
SVM	Support Vector Machine
SVR	Support Vector Regression
sEMG	Surface Electromyography.
PTF	Polymer Thin Film
SFU	Simon Fraser University
GPR	Gaussian Processes Regression
MLP	Multilayer Perceptron
SE	Squared Exponential
GP	Gaussian Process
RBF	Radial Basis Function
NRMSE	Normalized Root Mean Square Error
ANOVA	Analysis of Variance
RF	Random Forest
DOF	Degree of freedom
ADL	Activities of Daily Living
MAL	Muscle Activation Level
RR	Ridge Regression
RFF	Random Fourier Features
HRI	Human-robot interaction

List of Symbols

Term	Initial components of the term
$\mathbf{F_X}$	Force in X-axis
$\mathbf{F_Y}$	Force in Y-axis
$\mathbf{F_Z}$	Force in Z-axis
$\mathbf{T_X}$	Torque around X-axis
$\mathbf{T_Y}$	Torque around Y-axis
$\mathbf{T_Z}$	Torque around Z-axis
$\mathbf{R^2}$	Coefficient of determination
P/S	Pronation/Supination
F/E	Flexion/Extension
R/U	Radial/Ulnar

Chapter 1.

Introduction

1.1. Chapter Overview

This chapter begins by outlining the background and motivation of this thesis in **1.2.** Subsequently, three research objectives for advancing the field of research are defined in **Section 1.3.** Finally, the layout of the remaining chapters of this thesis is presented in **Section 1.5.**

1.2. Background and Motivation

In the context of physical human-machine interaction, it is crucial to track and monitor human actions e.g. forces and movements, to guarantee human safety during the interaction. A 2013 report from Safe Work Australia [1] highlights an alarming high number of workers known to have sustained an injury of severity requiring admission to hospital. In fact, workers operating and maintaining automated machinery are at risk of serious injuries. US statistics suggest that 18,000 amputations and over 800 fatalities in the United States each year are attributable to such causes [2]. The most common cause of work related injury is exposure to inanimate mechanical forces, which accounts for 46% of work related hospitalizations with the most common bodily location being the wrist or hand (38%) [1]. Furthermore, 4.9% of wrist and hand injuries involve amputations with more than one in ten involving a manufacturing employee [1]. A study performed in the US confirms that injuries to the hand and wrist are particularly high in automotive plants, especially in foundries and assembly plants [3]. In the light of these statistics, it is crucial to monitor hand movements and forces to avoid morbidity and disability associated with close interaction between human and machines.

Over the past several decades, many studies have been carried out to characterize dynamic [4] and kinematic aspects of human movements [5]. In particular, force measurements of human body have become an important aspect in various fields, including human-robot interaction (HRI) [6][7], rehabilitation [8][9], and neuromuscular

diagnostics [10]. Force/torque can be measured either using direct measurements, the involve using the commercial force/torque sensors which have to be attached directly to the human body to measure the force/torque, or indirect force measurements, which require some muscles information to predict the force/torque values. In direct force measurements by commercial force/torque transducers, these transducers require to be attached directly to human body which limit human movements. In addition, they are bulky and expensive. Thus, indirect force measurement is appropriate to keep human hands empty and helps to not limit human movements. Wearable sensing systems incorporating Myography sensors were considered as a good alternative of the direct force measurement methods. Examples of these wearable systems include surface electromyography (sEMG) and force Myography (FMG). sEMG is a good source of information about muscle activity by registering electrical activity due to muscle contraction as the result of motor neuron firing [11]. But, the electrical signals that the sEMG electrodes are measuring is very faint. Thus, the electrodes require an accurate placement and excellent contact to the skin. In addition, complex signal processing is required to make use of the signals. On the other hand, FMG measures the volumetric changes on the arm muscles due to contraction/expansion of the muscles during hand activates. FMG presents many advantages including electrical robustness [12], not requiring special skin preparation [13], minimal signal processing [14], and being cost effective [15]. However, FMG is not a well-establish technique like the sEMG, but it shows a promising potential in various applications of rehabilitation [16][17], prosthetic control [18][19], and gesture identification [20][21].

As discussed before, it is clearly shown that FMG technique has merits over the traditional methods of measuring hand force either direct measurements using force/torque transducer or using sEMG for estimating the force. A wearable FMG-based system can be used on the arm to track the muscles pattern changes, and these signals can be fed to a regression model to estimate hand force/torque. The aim of this thesis is to contribute to the realization of the FMG wearable system in estimating hand force/torque in isometric conditions which has a potential in different applications.

1.3. Objectives

Considering the background presented previously in **Section 1.2**, which is discussed in detail in **Chapter 2**, this thesis seeks to explore the suitability of using FMG signals for estimating hand force/torque. The literature shows that the FMG has been used for predicting grip force [22] and finger forces [23][24]. Up to the best of our knowledge, no one used the FMG for predicting hand force/torque. To this end, this thesis has three main objectives.

- **Objective 1**: Studying the feasibility of using FMG to predict hand force/torque in single-axis.
- **Objective 2**: Studying the feasibility of using FMG to predict hand force/torque in multi-axis simultaneously.
- **Objective 3**: Finding the best placement(s) among four landmarks on the arm for the FMG measurements for estimating single- and multi-axis force/torque.

The experimental protocol which is explained in **Chapter 4**, was designed to explore the viability of using the FMG for predicting single- and multi-axis isometric force/torque. In addition, four custom bands were used for measuring FMG signals in four positions: the wrist, the forearm midway, the forearm muscle belly, and the upper arm. The motivation behind this to find the best placement among these landmarks which is **Objective 3.**

1.4. Contribution to Body of Knowledge

This work provides several contributions to the body of knowledge in the areas of human-machine interface and FMG. For human-machine interface, this body of research presents an alternative sensing modality for hand force/torque estimation that could be used to complement other technologies being explored to guarantee human safety during the interaction with machines. With respect to Force Myography (FMG), this work proposes using FMG for estimating hand force/torque in single- and multi-axis simultaneously. In addition, guidelines for FMG sensors placement are provided for best

force/torque sensation and in turn higher estimation accuracy. To date, FMG has been used for different applications like: rehabilitation, prosthesis control and gesture identification, as discussed in **Chapter 2**. However, up to our knowledge, there is no work that introduces FMG for hand force/torque estimation or provides guidelines for the FMG measurements placement on the arm for better estimation accuracy.

1.5. Document Outline

The remainder of this thesis is organized as follows:

Chapter 2 provides a detailed overview about the FMG technology and the state-of-art of FMG development research in different applications.

Chapter 4 the design of the FMG wearable system as well as the force/torque acquisition systems is discussed. This followed by an explanation of the experimental protocol that the participants followed to acquire the data. Then, an overview of the data analysis and the performance measurement is provided.

Chapter 3 a detailed description for the 5 regression algorithms that will be used to create FMG-based model to predict the isometric hand force/torque in single- and multi-axis, is provided.

Chapter 5 investigates the suitability of using FMG to predict hand force/torque in single-axis using different data acquisition systems to address **Objective 1** of this thesis. In addition, the recruitment criteria for the participants in all experiments is discussed. Finally, a comparison between different band(s) placement combinations is provided to find the best one for single-axis force/torque prediction which addresses part of **Objective 3**.

Chapter 6 explores the feasibility of using FMG to predict isometric hand force/torque in 3-axis simultaneously using different data acquisition systems, which addresses part of **Objective 2** of this thesis. Moreover, a regression model was created using all possible band(s) combinations of the 4 bands to find the best placement for the FMG measurements for 3-axis force/torque estimation which handles part of **Objective 3**.

Chapter 7 provides a study on the possibility of using FMG to predict 6-DOF hand force/torque simultaneously which addresses part of **Objective 2** of this thesis. Furthermore, a comparison between all possible band(s) combinations is held to find the best placement among the 4 proposed landmarks.

Chapter 8 a discussion of the results is presented to give more insight about the findings of the previous chapters.

Chapter 9 concludes the thesis, and summarizes its engineering and scientific contribution.

Chapter 2.

Literature Review

2.1. Chapter Overview

This chapter begins by introducing an overview about hand force/torque estimation techniques in **Section 2.2**. Then, an overview about the FMG technology is provided in **Section 2.3**. Subsequently, the state-of-art FMG literature is discussed in **Section 2.4** based on three categories: areas of research, placement of FMG measurements, and machine learning algorithms. Finally, the summary of this chapter is provided in **Section 2.5**.

2.2. Hand Force/Torque Estimation

Humans constantly use their hands to interact with the environment and perform a wide variety of activities of daily living (ADLs) [25]. To move and manipulate objects, people exert forces and torques on the object [26]. All such force/torque exertion are generated by the activation of the corresponding muscles on the arm Measurement of the intensity of a muscle contraction can be translated into hand force/torque value [27]. Hand force/torque measurement is of interest in many applications such as control of prostheses [28][29][30], rehabilitation [8][9][31][32], human-machine interaction [6][7][33], teleoperation [34], gait analysis [35][36][37], and ergonomic design [38][39].

Many methodologies can be used for measuring hand force/torque. They could be mainly classified into two categories: direct and indirect measurement. In the direct measurement, the traditional force/torque sensors, such as ATI Mini45 6-DOF force/torque sensor [40] could be used for measuring force directly. However, these commercial sensors are not appropriate in some applications because they are bulky, expensive, and should be attached to the object. The indirect measurement has two approaches: physics-based approach and data-driven approach. In physics-based approach, muscle model is developed to predict the exerted force such as Hill-type muscle model [41]. The problem of using such models is that they need data about the length of

muscle fiber, muscle activation level and other information which is very difficult to obtain [42].

In data-driven approach, different types of sensors were used to measure the changes on the arm muscles due to force/torque exertion, changing on hand gesture, and wrist movements. Using machine learning techniques, these measurements can be mapped into the force/torque values or different hand/wrist postures. Hand force/torque is generated by the activation or contraction of the corresponding muscles on the arm, and is a function of the Muscle Activation Level (MAL) [43]. Thus, muscular signals generated from the activated motor units can be picked up at the surface of the skin in the vicinity of the sensing electrode. Therefore, muscular sensing techniques such as the electromyography (EMG) can be used to estimate hand force/torque [44][45]. EMG electrodes detect the electric potential generated by the muscle cells when the cells are electrically or neurologically activated [46][47]. The signal can be acquired by an intramuscular sensor, that need the insertion of needle electrodes, or by surface electrodes placed in direct contact with the skin. The latter represents a non-invasive technique suitable to implement a non-invasive control strategy and the electrodes are called surface Electromyography (sEMG). The EMG signals are correlated with the applied contraction level; therefore, they suit well to decode the intentions of the human body. The literature shows that the sEMG was used for estimating hand/wrist force/torque [48][45][49][50] and also was used for detecting hand grasp force [51][44][52][53][54] which is crucial for hand prosthetics control. In addition, sEMG was used widely for regression finger forces [55][56][57]. Moreover, sEMG was employed for estimating hand/wrist/forearm stiffness [58] which is important for rehabilitation [9], skills transfer from human to robots [59] and teleoperation [34][60]. Unfortunately, there are several challenges associated to using surface electromyography (sEMG) due to various sources of noise. These sources include inherent noise in the electrode, movement artifacts, electromagnetic noise, skin formation, blood flow velocity, measured skin temperatures, and the measuring site [61].

Given the challenges associated with sEMG, there has been recent interest in the development of alternative technologies that are easier-to-use and inexpensive for detecting hand movements and forces such as Force Myography (FMG).

2.3. FMG Overview

Muscle activity is associated with changes of muscle shape. In particular in the limbs, these changes are noticeable on the surface of skin as certain parts of the muscle inflate or deflate. FMG measures the patterns in surface pressure caused by the volumetric changes that occur with muscle contraction [62]. This pressure signature could be used to detecting different hand movements or forces. Force Myography is also referred to as Pressure Myography (PMG) [63], Topographic Force Mapping (TFM) [13], Residual Kinetic Imaging (RKI) [64], and Surface Muscle Pressure (SMP) [36].

The FMG has gained momentum in innovative and novel device design, typically dominated by EMG [65], for several reasons. These include that it: (1) is robust to external electrical interference and sweating [12] (2) does not require for sensors to be placed at specific anatomical points on the body or extensive skin preparation [13][66], (3) does not require the same level of signal processing required in EMG datasets [14][67], (4) can be a cost effective method of tactile sensing, with off-the-shelf discrete force-sensing resistors (FSRs) sensors costing less than $10 [68], and (5) FMG signals are less variability in time and provide more repeatable patterns [69].

2.4. State-of-art FMG Literature

FMG has been shown to be an effective method for various applications that ranges from rehabilitation [70]–[73], prosthetic control [18], [19], [28], [74], exoskeleton control [75], and gesture identification [14], [20], [21], [76], [77]. A review was performed on FMG related research and the findings are tabulated and summarized based on three factors

1. Areas of research.
2. Placement of the FMG measurements.
3. Machine learning algorithms used in FMG research either for classification or regression.

Based on the results from this review and up to our knowledge, no work has been done to either explore the suitability of using force myography (FMG) signals for predicting hand force/torque nor finding experimentally the best placement of the FMG measurements among different positions for predicting hand force/torque accurately. Thus, the main contribution to body of knowledge is to introduce and explore the viability of using FMG for estimating hand force/torque in single- and multi-axis. In addition, provide a comparison between 4 landmarks for the FMG measurement placements, to find the best one or combination of them.

Areas of Research

The areas of research that the FMG signals has been used in is summarized in **Table 2.1**. From the table, it is clearly shown that FMG has been widely used in gesture classification which is crucial for different application like rehabilitation [76][78][77] and prosthetic control [19][17]. In addition, FMG was used for measuring active and passive behavior of muscles during gait [79]. For regression forces, FMG was used for regressing grip force generated in repetitive grasping tasks for proportional control [62]. Also, tracking finger forces [80][28] and movements [74] was done using FMG to establish a reliable prosthetic hand control for amputees. However, based on our review, no work was published on using the FMG for estimating hand force/torque except [81][82], which are the thesis work as is presented in **Chapter 5** and **Chapter 6**.

Table 2.1. Areas of research that FMG has been applied

Area	References
Regression of grip force	[62]
Regression of finger forces	[28][23][65][83][80]
Regression of finger movement	[74]
Regression of 1-DOF wrist torque	[82]
Regression of 3-DOF wrist torque	[81]
Hand prosthetic control	[13][83][63][18][84][19][64]
Exoskeleton control	[75]
Gesture classification	[78][14][85][86][77][69][20][17][67][76][19][87]

Gait analysis	[37]

Placement of FMG Measurements

A review about the placement of the FMG measurements on human body was done for all research areas that FMG has been utilized. The different placement landmarks are summarized in **Table 2.2**. From the table, it is clearly shown that FMG was commonly used on the forearm muscle belly for different application either regression or classification. The volumetric changes of the forearm are associated with the hand and wrist movement because the movement is controlled by both intrinsic and extrinsic muscles of the forearm. However, FMG captures the overall volumetric change of the muscles, therefore, the effect of the intrinsic muscle movement is less apparent than the one of the extrinsic muscles. FMG extracted from the bulk region of the forearm is able to capture information associated with hand and wrist movement [27]. However, there are much research used the FMG measurements on the wrist, forearm midway and forearm cuff and have a good accuracy [14].

Given the results from the review on the placement positions of the FMG measurement son the arm, there are a few research [14][77] was held to provide guidelines about the best placement for each application. In [77] and [14], they provide an experimental comparison between the placement on the wrist, midway, and forearm muscle belly for gesture classification. Moreover, in [77] they compare between different band combinations to find the best among 3 locations for gesture classification. They found that increasing the spatial coverage of the FMG measurements from a single landmark to combinations of multiple landmarks either 2 or 3 resulted in similar classification accuracy. These studies guided us in designing an experimental protocol that include different placement positions for the FMG measurements and compare between them based on the regression accuracy. This will provide a guidance for future studies about the positioning of the FMG sensors.

Table 2.2. Placement positions of the FMG measurements on the arm

Placement position	**References**

Wrist	[14][77][76][67][88][89]
Forearm midway	[77][65][18][69]
Forearm muscle belly	[14][77][81][82][28][71][74][21][75][63][89]
Forearm cuff	[62][23][90][91][17][19][87][64]

Machine Learning Algorithms

Table 2.3 provides a summary of the machine learning algorithms for regression and classification problems utilized in FMG research. The majority of FMG related works employed supervised learning approach to predict activities of the limb, e.g. forces, gestures or movements of the hand and wrist. In this approach, the FMG data is first obtained during a data collection session namely, the training session. The purpose of this session is to extract relevant information from the collected data to associate these data with targeted activities. For each collected FMG sample, a unique label corresponding to a gesture or movement is assigned. The collected FMG samples and the labels are used to generate a prediction model using machine learning techniques. This model describes the relationship between the input data and the corresponding labels explicitly or implicitly depending on the selected techniques. Once the model is generated, it can be used to predict the labels of the untrained data.

In this thesis, 3 machine learning algorithms from the literature are used. These algorithms are Support Vector Regression (SVR), Ridge Regression (RR), and General Regression Neural Network (GRNN) which is a special type of ANN that was developed for regression problems and has more merits than ANN. In addition, we used 2 machine learning algorithms: Gaussian Processes Regression (GPR) and Random Forest (RF), that were not used before in the literature within the FMG research, to explore their capabilities. A description of the machine learning algorithms used in this thesis is provided in **Chapter 3**.

Table 2.3. Machine Learning algorithms used in FMG research

Machine Learning Algorithm	Problem Type	References
Support Vector Machine (SVM)	Classification	[86][88][67][17][23]
	Regression	[82][81][76][74][28]
Artificial Neural Network (ANN)	Classification	[92][87][93][91][71]
	Regression	[82][81]
Linear Discriminant Analysis (LDA)	Classification	[93][14][63][77][19]
K-nearest neighbor (KNN)	Classification	[93][89]
Ridge Regression with Random Fourier Features (RR-RFF)	Regression	[28][69][94]
Extreme Learning Machine (ELM)	Classification	[18][75][21]

2.5. Chapter Summary

In this chapter, an overview about the hand force/torque estimation importance for different applications was proposed. In addition, the techniques that can be used for monitoring hand force/torque were described. They can mainly be classified into two categories: direct and indirect measurement. Direct measurement means that a force sensor should be attached directly to the hand to measure the force which is not appropriate in some applications. While the indirect measurements overcome the problems of the direct method. In this method, sensors are used to track the muscles changes and using machine learning techniques, these changes can be mapped into hand forces or movements, this called data-driven approach.

After that, an overview about the Force Myography (FMG) was provided and followed by the state of the art in the FMG research-related. The literature was summarized based on three factors: 1) areas of research that the FMG has successfully been utilized, 2) the placemat positions of the FMG measurement, and 3) the Machine learning algorithms used in the FMG research.

Chapter 3.

Hand Force/Torque Regression Models

3.1. Chapter Overview

In this chapter, a description for the regression algorithms that will be used to create FMG-based model to predict the isometric hand force/torque in single- and multi-axis, is provided. These algorithms are kernel ridge regression (KRR), general regression neural network (GRNN), Gaussian processes regression (GPR), support vector machine (SVR), and random forest (RF).

3.2. Kernel Ridge Regression

Kernel Ridge Regression (KRR) is a simple but powerful regression method [95] that maps the input data through a nonlinear mapping φ into a kernel feature space. KRR method aims to obtain a linear regression model in the reproducing kernel Hilbert space (RKHS) [96] as in **Equation 3.1**:

$$y = f(x) = \varphi(x)^T w \tag{3.1}$$

by optimizing the following objective in **Equation 3.2**:

$$\min_w \frac{1}{2} \left\| X_\varphi w - y \right\|^2 + \frac{\lambda}{2} \|w\|^2 \tag{3.2}$$

Where λ is a hyper-parameter that balances the trade-off between minimizing the errors and regularizing the solution. Using kernel trick [97][98] allows the algorithm to be performed implicitly in a potentially infinite dimensional feature space. Here, we used the Gaussian kernel function as in **Equation 3.3**:

$$k(x, x') = \exp\left(-\frac{\|x - x'\|^2}{2\sigma^2}\right) \tag{3.3}$$

Where $\|x - x'\|^2$ is the squared Euclidean distance between the two feature vectors and σ is the bandwidth of the Gaussian function. To avoid computational problem,

the kernel trick allows calculating the scalar product between two points in the infinite-dimensional space by simply calculating the kernel function in **Equation 3.3** of the data in input space [98].

3.3. General Regression Neural Network

Among the machine learning techniques, artificial neural network (ANN) is one of the most widely employed model due to its powerful capabilities in numerical prediction and pattern recognition [99]. In addition, ANNs are able to handle multiple classification/regression outputs by setting a number of neurons in the output layer corresponding to the target outputs; the training process (back-propagation algorithm) adjusts the weights of the network according to the training data and the true labels [100][101]. The regression algorithm called General Regression Neural Network (GRNN) used in this study was initially proposed by Donald F. Specht [102] in 1991. It falls into the category of probabilistic neural networks. The GRNN works as a one-pass learning algorithm with a highly parallel structure. Even with sparse data in a multidimensional space, the network provides smooth transitions from one observed value to another. In addition, the structure of a GRNN is relatively simple and static with 2 layers, namely pattern and summation layers. Compared with the standard feedforward neural network, GRNN has several advantages as follows:

1) GRNN is a fast learning network.

2) It converges to the optimal regression surface as the number of samples becomes very large.

3) The estimated values are bounded by the minimum and maximum of the observations.

4) It converges to the global minima [102].

Figure 3.1 demonstrates the structure of the GRNN used in this study where the number of inputs is equal to the number of FMG sensors used, and the number of output nodes is equal to the number of degrees of freedom that the GRNN model will estimate. The GRNN network consists of four layers [102][103]. First, the input layer has as many

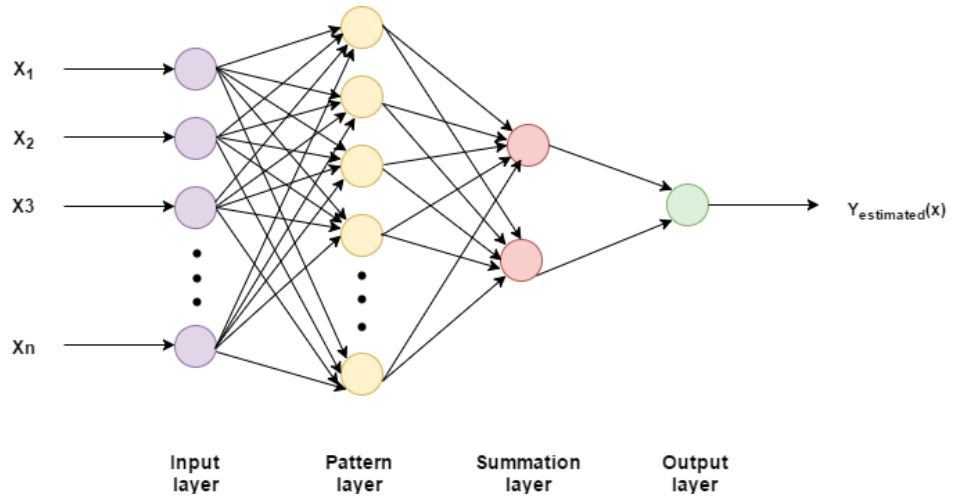

Figure 3.1. An example of GRNN architecture for single-output network. The inputs x_1, …, x_n are the FMG sensors readings, and the output is the estimated force/torque in one degree of freedom.

neurons as the number of input variables. Once the input goes through each unit in the pattern layer, the relationship between the input and the response would be recorded and stored in the unit. Thus, the number of units in the pattern layer is equal to the number of observations in the training sample. Then, the summation units perform a dot product between a weight vector and a vector composed of the signals from the pattern units. There are only two neurons in the summation layer for each output. One neuron is the denominator summation unit and the other is the numerator summation unit. The denominator summation unit adds up the weight values coming from each of the hidden neurons. The numerator summation unit adds up the weight values multiplied by the actual target value for each hidden neuron, as in **Equation 3.4**. The addition of one element in the output vector requires only one summation neuron and one output neuron.

$$\hat{Y}(X) = \frac{\sum_{i=1}^{n} Y_i \exp\left[\frac{-D_i^2}{2\sigma^2}\right]}{\sum_{i=1}^{n} \exp\left[\frac{-D_i^2}{2\sigma^2}\right]} \tag{3.4}$$

Where $D_i^2 = (X - X_i)^T . (X - X_i)$

Where X is the input sample and X_i is the training sample memorized in the unit in the pattern layer. The output of the input sample X_i is Y_i. D_i^2 is the Euclidean distance from the X and X_i. It signifies how much the training samples can contribute to the estimated

output of that particular test sample. If the distance D_i^2 is small, then the exponential in **Equation 3.4** will be a large value which means that the training sample will contribute more to the output prediction and vice versa. While if D_i^2 is zero, then the exponential returns one which means that the predicted output is the same as the training sample output. Finally, σ is the only unknown parameter which called spread constant. It was tuned in the training process to get the optimum value where the error is very small.

3.4. Gaussian Processes Regression

Gaussian Processes Regression (GPR) is a kernel-based machine learning method for non-linear regression problems. It employs Gaussian process (GP) models to formulate a Bayesian framework for regression. Gaussian process (GP) is a random process that has a Gaussian probability distribution for any finite number of points in the continuous input space. The advantage of the Gaussian process formulation is that the combination of the prior and noise models can be carried out exactly using matrix operations [104]. A GP is specified by its mean and covariance functions, known as the hyper parameters, which provide the prior for Bayesian inference [105]. After providing the GP prior with training data to yield the posterior GP, the hyper parameters are updated in the light of training data. This is typically done by selecting hyper parameters that maximize the probability of observing the training data. The most common used covariance function is the Squared Exponential (SE) function, as in **Equation 3.5**:

$$k_{SE}(x_i, x_j) = \sigma_0^2 \exp\left(-\frac{1}{2}\left(x_i - x_j\right)^T \Lambda^{-1}\left(x_i - x_j\right)\right) \tag{3.5}$$

Where Λ is a diagonal matrix determining how quickly the covariance decreases for each input dimension. The parameters of the SE covariance function are the variance σ_0^2 and the length scales Λ. The hyper parameters are trained by maximizing the log marginal likelihood in **Equation 3.6** using gradient descent.

$$\log p(y|X) = -\frac{1}{2}\, y^T (K + \sigma_n^2 I)^{-1} y - \frac{1}{2} log|K + \sigma_n^2 I| - \frac{n}{2}\log 2\pi \tag{3.6}$$

Where K is n by n covariance matrix, which is calculated by evaluating the covariance function between each pair of the training inputs. This causes a computational complexity of the GPR which scales cubically with the number of training inputs $O(n^3)$.

However, this complexity in the computation did not affect the data processing in this study as all the computation were done offline.

3.5. Support Vector Regression

Support Vector Regression (SVR) is one of the Support Vector Machine (SVM) techniques which used for handling regression problems. SVR maps the input data to a higher-dimensional feature space where the data can be separated using the linear regression [106][107]. SVR does not suffer from the local minim problem since model parameter estimation involves solving a convex optimization problem [108].

The LIBSVM library [109] in the MATLAB® environment was used for offline processing of the collected data. Nu Support Vector Regression (ν-SVR) was used, as the ν parameter used to control the number of support vectors in the resulting model. We used the Radial Basis Function (RBF) kernel as in **Equation 3.7** it enables nonlinear mapping for the input data. Besides it has a small number of hyper parameters, which reduces model selection complexity [110].

$$k(x,y) = e^{-\frac{\|x-y\|^2}{2\sigma^2}} \tag{3.7}$$

10-fold cross validation and grid search are used to find the optimal values for the model parameters (cost and gamma), where the average accuracy of the 10 iterations is considered as the metric to compare between the different values for both the cost and gamma, as it is usually done in common practice [111][54].

3.6. Random Forest Regression

Random Forest is a technique that can be used in regression and classification problems. It was introduced by Leo Breiman [112] in 2001. The main idea is to train several decision trees, constituting a “Forest”, using a random sample of the dataset. After that, each tree is used independently to predict the output of a new data point. The final output of the whole forest is the combination of all these predictions, for example by averaging all of them. By using decision trees, a complex problem is splitted into smaller ones, which can be tackled efficiently using simple predictors.

The Random Forest algorithm [113] starts by randomly drawing a sample of the training data before building the tree. To grow a random-forest tree, a subset of the input features is selected randomly. Then, for each terminal node of the tree, a split point among the training data is chosen such that the information gain is maximized. This node is then splitted into two children nodes. These steps are done recursively until a minimum node size is reached. The output is a Forest of ensemble trees $\{T_b\}_1^B$, where T_b is the tree number b and B is the total number of trees in the forest. In regression problems (like the case in this thesis), when a new point x is fed to the random forest, the predicted output F(x) is calculated according to **Equation 3.8:**

$$F(x) = \frac{1}{B} \sum_{b=1}^{B} T_b(x) \tag{3.8}$$

Criminisi et al [114] studied the effects of several parameters on the performance of the random forests. For example, they found that under fitting is likely to happen when the tree depth is small. In addition, increasing the depth may lead to the problem of overfitting. They also showed that as the forest size becomes larger, the decision boundaries reached by the random forest becomes better and smoother. When to comes to classification problems, the number of classes has almost no effect on the performance of the random forest.

Chapter 4.

Methodology

4.1. Chapter Overview

The purpose of this chapter is to provide a description for the instrumentations that have been used to collect the Force Myography (FMG) signals and the force/torque data. Then, we present an explanation for the experimental protocol that the participants followed to acquire the data. Finally, the data analysis and the performance measures is proposed.

4.2. Participants

Participants were recruited from the students, faculty, and staff of Simon Fraser University. Inclusion criteria for participation required that participants can follow instructions of the experimental protocol and perform the required tasks to completion. Exclusion criteria were limited to self-identified neurological or musculoskeletal barriers to functional movements of the upper extremities. The subjects were given a detailed oral description of the procedure. All participants affirmed their voluntary participation in an informed and written consent which was approved by the office of Research Ethics at Simon Fraser University. Except for muscle fatigue, there was little to no risk to participants.

4.3. Instrumentations

There were two data acquisition systems that were used to acquire the Force Myography (FMG) data and the isometric hand force/torque. The detailed description of the acquisition systems is provided below.

4.3.1. The First Data Acquisition System

The data acquisition system composed of two parts: the first one is for capturing FMG signals using a wearable band and the other one is for measuring the exerted torque in different axes. A detailed description for each part is provided below.

Force Myography Band

A custom band was designed to measure the Force Myography (FMG) signals. Force Myography relies on tracking patterns of skin deformation caused by volumetric changes in underlying musculature used to generate the functional movement [62]. The FMG band used in this study consists of an array of 16 force sensitive resisters (FSR) and a control unit, as shown in **Figure 4.1**. The FSR is a polymer thick film (PTF) device, which exhibits decreasing resistance as increasing force is applied to the active area. The FSR sensors are custom-printed on the band, each 1.3 cm in diameter and 0.3 cm apart each other. The characteristic of the printed FSR sensor is the same as the one of FSR402 from Interlink [115]. The total length of the FSR band is of 38 cm and the width is 2.1 cm. The band is longer than the average forearm muscle belly size of the participants in this study (24.6 cm ± 1.3 cm), so the number of active sensors, which were in contact with the forearm skin was recorded during the data collection. Then in the data analysis, we used the active sensors data only and ignore the others. A Velcro strap was placed on the back of the band to fix it on the participant's arm. A Zero insertion force (ZIF) connector was inserted in one end of the band to connect the FSRs to the control unit.

The control unit was built on a double sided printed circuit board (PCB) with a 5V battery to power its components. An ATMega328 microprocessor [116] was used to facilitate data collection and transmission. A Bluetooth module was used to transmit the data to an on-site computer. Each FSR was sampled at approximately 10 Hz, with raw analog values converted to a digital signal ranging from 0 to 1023 (0.00361 V/bit). As the frequency of human hand motion is typically < 4.5 Hz, the 10 Hz sampling rate is sufficient for the purposes of the study [117][63].The FSRs were incorporated into a voltage divider

circuit as in **Figure 4.1**. The base resistor in the voltage divider circuit which controls the sensitivity of the FSRs has a value of 4.7 kΩ.

1-DOF Torque Acquisition

Three custom-build rigs were designed for measurement the isolated upper extremity movements: wrist pronation-supination, wrist flexion-extension and wrist radial-ulnar deviation. A Transducer Techniques (TRT-100) torque sensor, was placed where its axis of rotation is aligned with the axis of rotation of the movement. The torque sensor was connected to an amplifier from Transducer Techniques (LCA-RTC) to adjust the sensor's output and increase the sensitivity of the sensor. The output of the amplifier is connected to data acquisition device (DAQ) from National Instruments (NI USB 6210). The torque sensor's amplifier was calibrated using pre-defined weights, to get the calibration equation that maps the amplifier readings to the torque values in Newton meters (Nm). Participant's forearm was secured to the rig using the Velcro tapes which restrict the arm movement.

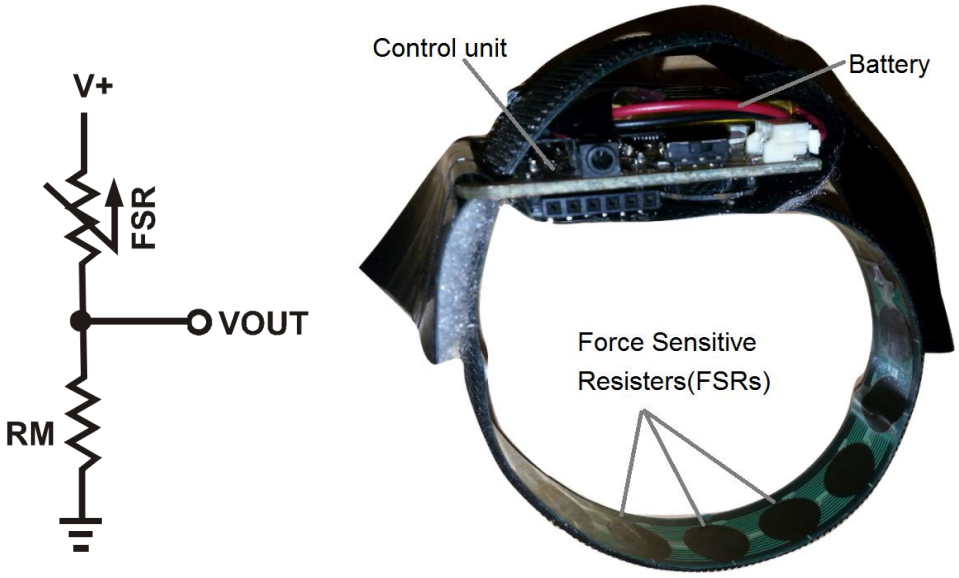

Figure 4.1. (Left) the voltage divider circuit. (Right) View of the Force Sensitive Resistor (FSR) band used to collect the Force Myography (FMG) data.

Pronation-Supination Acquisition Setup

The setup consists of two aluminum plates with the torque sensor connecting them to each other as in **Figure 4.2**. One of these plates is fixed to a table, while the other plate holds a handler that the participant holds on and pronate-supinate the wrist isometrically.

Figure 4.2. The setup that was used to collect the isometric pronation-supination data with the FSRs band wrapped around the participant's forearm.

Flexion-Extension Acquisition Setup

As shown in **Figure 4.3**, the setup composed of two parts: a wooden base that holds the participant's forearm with Velcro straps to fix the forearm, and two aluminum plates that connected to each other through the same torque sensor, one of these plates is settled to the wooden base. While the other plate holds the participant's hand and a

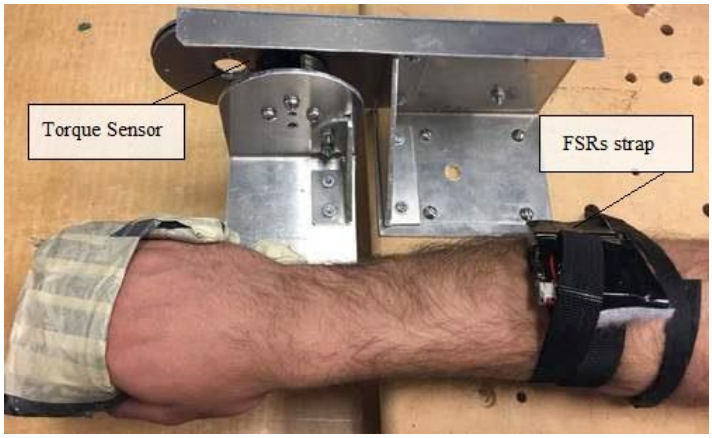

Figure 4.3. The setup that was used to collect the flexion-extension data with the FSRs band donned around the participant forearm.

band was used to maintain the fingers on the same position during the isometric wrist flexion and extension exertion.

Radial-Ulnar Acquisition Setup

Figure 4.4 shows the setup that was used to collect the radial-ulnar data. It is mainly the same as the flexion-extension setup except the torque sensor placement, which is under the participant's wrist to capture the radial-ulnar deviations.

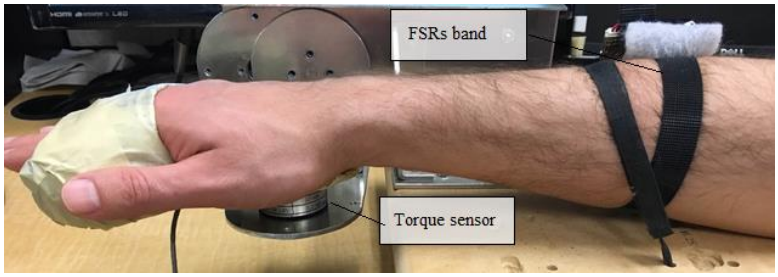

Figure 4.4. The setup that was used to collect the radial-ulnar data with the FSRs band donned around the participant forearm.

4.3.2. The Second Data Acquisition System

The second data acquisition system was designed to overcome the limitations of the first system, either on the FMG band or the custom-rig. These limitations are explained deeply in **Section 5.4.1** and **Section 6.4.1**. The second acquisition system is composed of two parts: the first one is a custom wearable force-sensing band for measuring FMG signals and the other one is a custom-rig that housed a 6-DOF load cell which can measure the force/torque in all directions. A detailed description for each part is provided below.

Force Myography Band

Four customized force-sensing bands were designed to record FMG signals from the participant's working arm on different placements, to find the best placement on the arm among 4 positions. Each band contains 16 force sensing resistors (FSRs, Model 402 from Interlink Electronics) [115], except the wrist band which has 12 FSRs. The FSRs were arranged in series in the band and spaced around 0.5 cm apart from each other.

Snaps were placed on either side of the force-sensing band to allow the band to be securely donned. The FSRs used are similar to that described in **Section 4.3.1**, because they are cheap, flexible, low-profile dimensions and can be easily embedded into portable devices. The control unit in this band is the same as in **Section 4.3.1** except we connect the components directly to each other without using a PCB. **Figure 4.5** shows a view of the FMG band with the control unit connected to it.

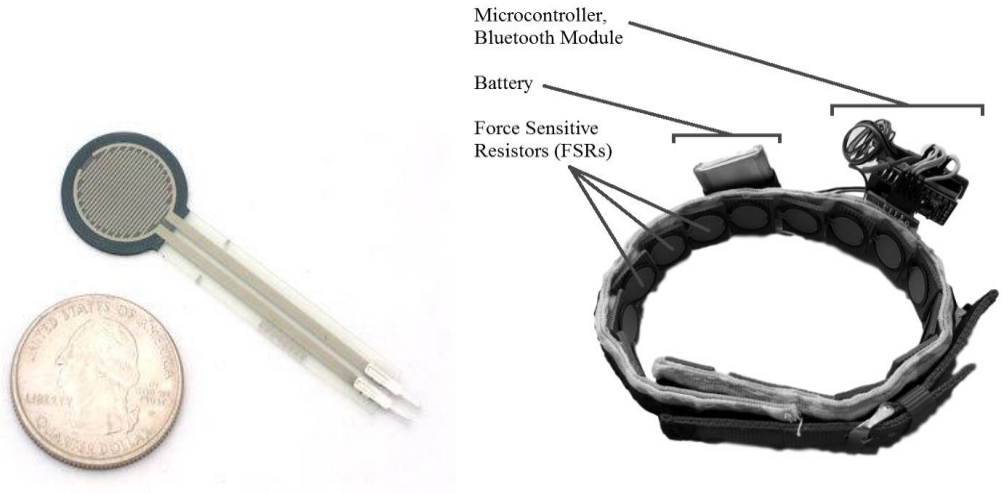

Figure 4.5. (Left) the FSR that was used in the band. (Right) view of the Force Sensitive Resistor (FSR) band used to gather Force Myography (FMG) data.

6-DOF Force/Torque Acquisition

A custom-built rig was designed to measure the isometric hand forces and torques exerted onto the load cell in X, Y and Z axes, denoted as F_X, F_Y, F_Z, T_X, T_Y, and T_Z, respectively, in the rest of the thesis. **Figure 4.6** shows the custom-rig used for collecting the exerted force/torque. It is composed of a base that holds a hollow plastic sphere accommodating an ATI Mini45 6 DOF force/torque transducer [40].The resolution of F_X, F_Y and F_Z is 1/8 N and the resolution of T_X and T_Y is 1/376 Nm and T_Z is 1/752 Nm, respectively. The surface of the sphere was made rough to prevent hand slippage during the experiments. The transducer was connected to an interface power supply box to power it, as well as conditioning its signals to be used with a data acquisition system. The output

of the interface power supply was connected to a data acquisition device (DAQ) from National Instruments (NI USB 6210).

4.4. Protocol

In this section, a description for the experimental protocol to collect the FMG signals as well as the isometric force/torque will be provided. The devices discussed in **Section 4.3** were utilized in 2 experimental protocols.

4.4.1. The First Experimental Protocol

This experimental protocol was done using the first data acquisition system that was described in **Section 4.3.1**. The previously defined setups were used to collect three degree of freedom data individually created with isolated upper extremity movements: wrist pronation-supination, wrist flexion-extension and wrist radial-ulnar. Three data collection sessions for each wrist deviation were carried out. Each session lasted for one minute to minimize the muscle fatigue. The data were collected with a sampling frequency of 10 HZ, which means that we collect 600 samples per session and a total of 1800 samples were collected for each setup.

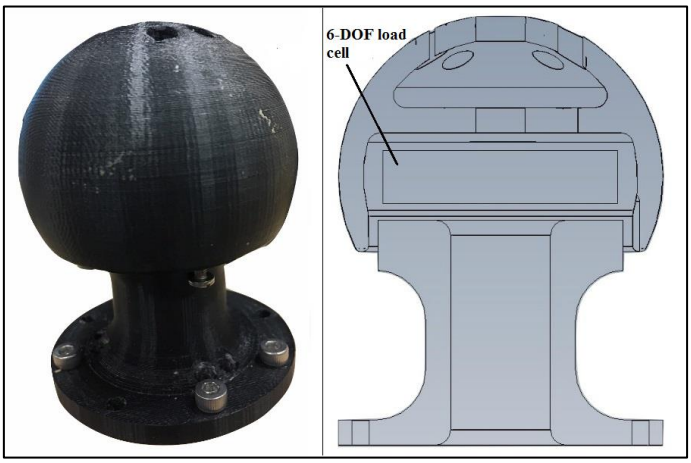

Figure 4.6. The 6 DOF force and torque data acquisition system. In the left is the plastic sphere that houses the 6 DOF load cell and in the right a cross section sketch of the rig shows the inside load cell.

A custom program was designed in LabVIEW (© 2014) to facilitate data collection and recording for offline analysis. First, the FMG band was tied on the forearm muscle belly of the dominant arm of each participant. Then, the participant rested his hand on the defined place of the custom rig. To collect the pronation-supination deviation, the participant was asked to alternately pronate and supinate his wrist to form an approximate sinusoidal wave, for one minute. Then, the participant rests his hand if needed and redo the same procedure for three sessions.

For collecting flexion-extension data, the participant placed his/her forearm on the platform of the rig, the wrist on the top of the axis of rotation of the load cell, and the palm on the aluminum plate. The participant's forearm and palm were secured to the custom rig using the Velcro tapes. With this arm position, the data were collected for both of the FMG signals and the flexion-extension isometric torque for three sessions.

Finally, the data are collected for the wrist radial and ulnar deviations using the same arm position used in the flexion-extension data collection session but with the third setup, for three sessions. In every data collection session, there was a visual chart on LabVIEW that displays the exerted torque value with the result wave to visually help the participant to maintain the sinusoidal wave form. All the data acquired from the nine sessions were stored in a csv file for off-line processing and analysis.

4.4.2. The Second Experimental Protocol

This experimental protocol was done using the second data acquisition system that was described in **Section 4.3.2.** An experimental protocol was designed to collect the FMG signals and the exerted force/torque data in single-axis at a time and freely in multi-axis combinations for evaluating the feasibility of using FMG to predict isometric hand forces and torques in single- and multi- axis. Moreover, four bands were used in this protocol to find the best band(s) combination on the arm within four placement locations.

A custom program was designed in LabVIEW (© 2014) to facilitate data collection and recording for offline analysis. Initially, each participant sat comfortably on a height-adjustable office chair, maintaining an upright position where the elbow angle is about 90° and the shoulder angle is approximately 45°. The four bands were firmly and comfortably worn on specified spots on the participant's arm: the wrist, the forearm midway, the forearm muscle belly and the upper arm, as in **Figure 4.7**. Band (1) was placed approximately 2.25 cm proximal to the wrist, identified by the surface landmarks of the radial and ulnar styloid processes. Band (2) was placed midway between the band at position 1 and the point on the forearm with the widest circumference. Band (3) was placed at the point on the forearm with the widest circumference, and finally band (4) was placed on the upper arm, about 2 inches above the elbow. These landmarks were chosen from the literature which was discussed in **Section 2.4**. Then, the participant held the sphere on the custom-rig as in **Figure 4.6** with his/her palm and start exerting isometric force/torque in one of the 6-DOF with a predetermined order and duration. Each participant performed the experiment for five trials. In each trial, the participant tried to exert isometric forces in X, Y and Z axes sequentially for 40 seconds for each axis while intended to keep the elbow and shoulder fixed in the initial position, the resultant force values are forming an approximate sinusoidal wave in each axis. Then, the participant exerted torques around the wrist joint: pronation-supination (T_X), flexion-extension (T_Y)

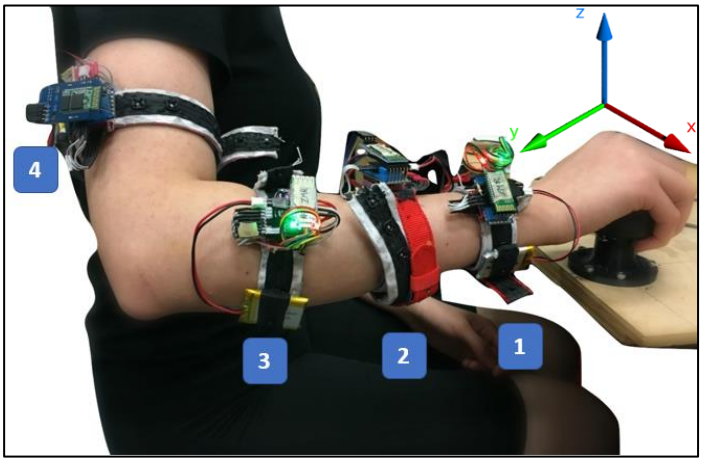

Figure 4.7. The participant holds the plastic sphere that accommodate the 6 DOF load cell during the data collection. The shoulder angle is about 45° and the elbow angle is approximately 90°. The four bands positions are labeled as (1) is the wrist band, (2) is the midway band, (3) is the muscle belly band, and (4) is the upper arm band.

and radial-ulnar (T_Z) sequentially for 40 seconds for each axis. After that, the participant exerted both force and torque freely in any axis and a combination of different axes, we called this session 'free-degree session'. Afterwards, the participant rests his/her hand for a while if needed then repeated the previously described procedure for 5 trials. During each trial, the FMG signals from the four bands and the 6 force/torque readings from the load cell were recorded and saved. In each trial, there was a visual chart on LabVIEW that displayed the exerted force/torque values with the resultant waves, to visually help the participant to maintain the sinusoidal wave form (except in the free-degree sessions) but without any limitations on the values or the speed of exerting forces and torques.

4.5. Data Analysis

The data that were collected using the two acquisition systems, were the FMG data as the input and the labels were the force/torque in single- or multi-axis. These data were preprocessed before feeding it to the regression model for training. A detailed description of the regression algorithms that are used in this thesis is provided in **Chapter 3**. In order to compare between different regression models, two main performance measures were considered:

1) **Coefficient of Determination (R^2):** it is a number that indicates how well the model fits the data, with R^2 of 1 indicating the model perfectly fits the data and R^2 of 0 represents that the model does not fit the data [118]. It is calculated as in **Equation 4.1**.

$$R_i^2 = 1 - \frac{\sum_{n=1}^{n=N}(\hat{y}_i(n) - y_i(n))^2}{\sum_{n=1}^{n=N}(y_i(n) - \overline{y_i(n)})^2} \quad (4.1),$$

Where N is the number of data points, $y_i(n)$ is the true value of the i^{th} force/torque, $\hat{y}_i(n)$ is the corresponding estimate value and $\overline{y_i(n)}$ is the mean of the i^{th} force/torque sequence over N data points.

2) **Normalized Root Mean Square Error (NRMSE):** it is a dimensionless metric which is a measure of the error percentage between the estimated and the true values over the range of the true values. It is calculated as in **Equation 4.2**.

$$NRMSE = \frac{\sqrt{\frac{\sum_{n=1}^{n=N}(\widehat{y_i}(n)-y_i(n))^2}{N}}}{y_{max}- y_{min}} \quad (4.2),$$

Where N is the number of data points, $y_i(n)$ is the true value of the i[th] force/torque. y_{max} and y_{min} are the maximum and minimum values of the i[th] force/torque.

In the coming two subsections, a detailed demonstration of the preprocessing stages for the data and the experiments will be provided.

4.5.1. Data Analysis for the First Study

Data processing and analysis were done offline in MATLAB®. Initially, the number of sensors that were in touch with skin during data collection was recorded for each participant. Then in the data processing, we only consider the active sensors and ignore the others. The number of active sensors varied from one participant to another based on the size of the participant's arm at the band's position. The average number of the active sensors used was 12 for the band on the forearm muscle belly. Two cases using these data were considered to explore the feasibility of using the FMG to predict the wrist torque in single- and multi- axis at a time. We used 10-fold cross validation scheme in the two cases. The data were divided randomly into 10 subsets, in each validation cycle, one of the subsets was saved for testing purpose while the other nine subsets were used for training the model.

The first case is about predicting the wrist torque around a single axis at a time. The collected data using the 3 custom rigs were the isometric wrist torque in 3-axis: pronation supination, flexion-extension and radial ulnar individually. A regression model was created for each wrist deviation values prediction. The FMG data of each axis were normalized using the global minimum and maximum of each participant's data. Then, the normalized FMG data were used to train the regression model, while a subset of the data was saved in the beginning for testing the trained model.

The second case proposed a procedure for a preliminary investigation of using the FMG to predict the isometric wrist torque in 3-axis simultaneously. First, the data from pronation-supination, flexion-extension, and radial-ulnar sessions were merged to be

processed as a single dataset to predict multi-axis torque. The input in the combined data set is the FMG channels and the target is the torque values around 3-axis. For each sample in the data set, one out of the three outputs has a value while the others are zeros e.g. if the first output has a value of 4 Nm, that means the input is the FMG signals corresponding to the pronation torque with a value of 4 Nm and the other two outputs are zeros that indicates the flexion-extension and radial-ulnar torques are zero. Then, the FMG data was normalized using the global maximum and minimum of each participant's data. Through that data set, the torque magnitude and direction across the three deviations data can be estimated using the FMG signals. **Figure 4.8** shows the procedure for combining the three data sets as well as the preprocessing for the data before feeding it to the regression model to predict the isometric wrist torque in 3-axis.

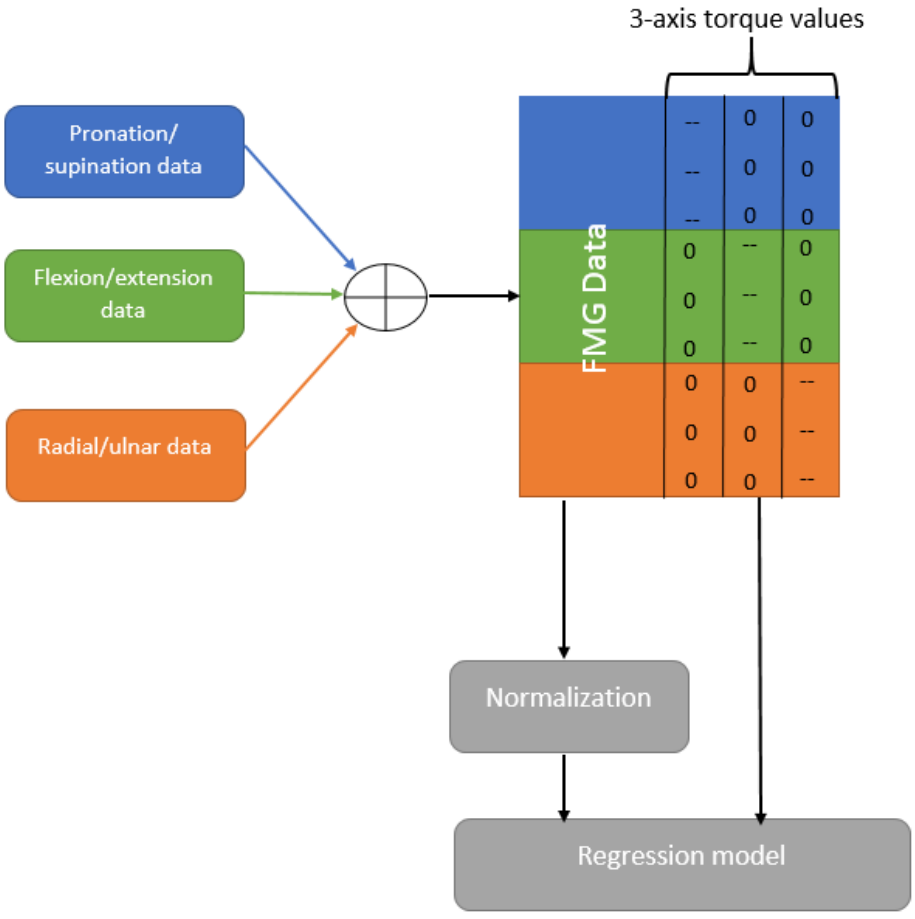

Figure 4.8. Merging the three data sets to predict 3-axis wrist torque all together. Followed by the normalization for the FMG signals, before feeding it to the regression model to train it.

4.5.2. Data Analysis for the Second Study

This section provides a description for the data processing and analysis of the data that were collected using the second acquisition system. A MATLAB® script was designed to preprocess the data before feeding it to the regression models. First, the number of sensors that were in touch with the participant skin during the data collection were manually recorded and then the other inactive sensors were removed during the data processing. The number of active sensors varied from one participant to another based on the size of the participant's arm at the bands' positions. The average number of the active sensors used was 9, 10, 12 and 14 for band 1, band 2, band 3 and band 4, respectively. After that, the raw FMG signals were normalized using the global minimum and maximum of the FMG data of each participant. Then, the linear trend of each channel in the FMG signals was removed to eliminate the muscles fatigue effect on the signals. The linear trend line was calculated using the least-squares fit of the FMG data and then the resulting straight line is removed from this data. For the true label, a low pass Butterworth filter with a cut-off frequency of 1.5 Hz with an order selected empirically for each participant, was applied to the forces and torques signals to remove the noise. **Figure 4.9** presents a diagram for the preprocessing steps on both the FMG data and the labels before feeding then to the regression models.

Two experiments using different regression models were carried out to study the feasibility of using the FMG signals for predicting the force/torque in single- and multi- axis which is addressing **Objectives 1 and 2**. The first one was the 10-fold cross-validation

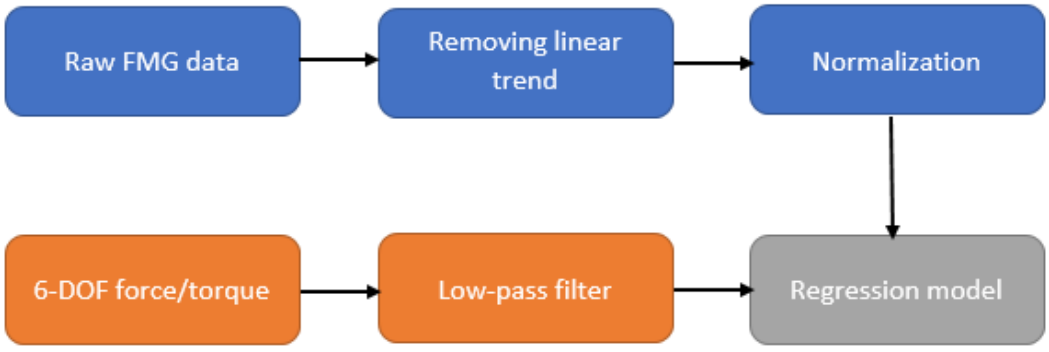

Figure 4.9. Data preprocessing sequence.

where ten different random permutations of the data set were generated, and then the models were trained each time on nine subsets of the data and were tested on the remaining set. The second one was the cross-trial, where one trial within each subject's data was left for testing while the remaining four trials were used to train the regression model, this was done 5 times where in each time the testing data was different. Then the average accuracy was calculated across the 5 trials. The resulting accuracy and error values were averaged across the ten subjects in both experiments to be presented. In the two experiments, the regression models were trained using all possible bands combinations: single, double, triple and all the 4 bands that were used in the data collection to find the best band combination to address **Objective 3**.

Three cases were considered to explore the viability of using FMG to predict hand force/torque and to find the best band(s) combination for each axis and for the combined axes using various regression algorithms. We used 10-fold cross validation and cross-trial evaluation schemes in the three cases. All possible band combinations were used with the three cases to find the best placement within 4 landmarks in each case.

- **The first case** is to evaluate the performance of FMG in predicting force/torque in one axis at a time. In this case, the data from each of the 6 force and torque axes were used to train and test a regression model individually. In addition, towards finding the best placement of the FMG measurements on the arm to estimate the force/torque in 6 axes individually, the regression model was trained using all possible band combinations.

- **The second case** explored the feasibility of using FMG for predicting force and torque in 3-axes where a one regression model was trained to predict the force in 3-axes: X, Y, and Z axes and another model was trained to predict the torque around the same axes. The input to the force model was the FMG signals collected during the trials of force exertion in X, Y, and Z, and the input to the torque model was the FMG signals of the torque exertion trials.

- **The third case** was more extensive where only one model was used to predict the force/torque in 6-DOF. This model was trained using all trials that focused on one axis at a time as well as the free-degree trials. This case aimed to study the feasibility of using FMG signals to predict the hand force/torque in 6-DOF simultaneously.

A three-way ANOVA was conducted to examine the effect of the three independent variables, the regression algorithms, FMG band combinations, and the hand force/torque components to the dependent variable of the force/torque estimation accuracy R^2, based on the first and second case. While, a two-way ANOVA was conducted to examine the effect of the independent variables, the regression algorithms and FMG band combinations to the dependent variable of the force/torque estimation accuracy R^2, in the third cases. Post Hoc pair comparison (Tukey HSD) was further conducted if there was any significant effect of the variables on the accuracy. The significance level was set to p-value = .05.

4.6. Chapter Summary

In this chapter, a description of the data acquisition systems was provided as well as the experimental protocol and the analysis for the data that were collected using the acquisition systems. Two acquisition systems were mainly used. The first one included the FMG band that has an array of 19 Force Sensitive Resistors (FSRs) and a control unit to sampling the FMG signals and facilitate sending the signals to an on-site computer for offline processing and analysis. 1-DOF torque sensor was used with it to label the FMG signals. The limitations of this setup are: 1) some bumps on the FMG band are coming up when it was wrapped around the forearm, this distort the signals from some sensors, and 2) different setups were needed to capture different wrist/hand force and torque, this is because the setup has only 1-DOF load cell that can capture single-axis at a time.

The previously mentioned limitations motivated us to design another system to overcome these drawbacks. First, 16 Force Sensitive Resistors (FSRs) were embedded into a fabric band and keep around 0.5 cm between them to capture all the muscles contraction/expansion when donned around the arm. In addition, fabric band keep the flexibility of the FSRs and make it easy to use without any pumps coming up. Towards

finding the best placement for the FMG band on the arm, 4 bands were designed and placed on 4 different locations. The regression model was trained using all possible band combinations data to compare between them based on the performance measures and find the best band(s) combination within the 4 landmarks.

Furthermore, the experimental protocol was designed to capture the isometric force/torque in single- and multi- axis to address **Objectives 1 and 2** using the two acquisition systems. Then, the data analysis procedure was provided with a description for the experiments to address all the portions of the thesis objectives.

Chapter 5.

Feasibility of Using Force Myography (FMG) for Estimating Single-axis Force/Torque

5.1. Chapter Overview

The work described in this chapter was intended to address **Objective 1** and portion of **Objective 3** of this work, which was studying the feasibility of using an FMG based sensing system to predict the hand force/torque in single-axis at a time and finding the best placement for the FMG measurements for each axis of the hand force/torque. **Section 5.2** demonstrates an overview of the study. **Section 5.3** outlines the participants' demographics. Results and conclusion remarks are provided in **Section 5.4 and 5.5.** Finally, **Section 5.6** provides a summary of the chapter.

5.2. Study Overview

The purpose of this study was to explore the feasibility of using FMG to predict hand force/torque in single-axis at a time. The instrumentation that have been used in this study were previously described in **Section 4.3.** In addition, a full demonstration of the experimental protocol and data analysis was provided in **Sections 4.4** and **4.5.** The results of the two studies will be presented in this chapter.

5.3. Participant Demographics

5.3.1. The First Study Participants

Seven healthy participants with no known neuromuscular disorders (4 females and 3 males) aged (24.9 ± 2.9 years old) participated in this study. The forearm muscle belly circumference was measured for each participant, **Table 5.1** shows the participant demographics. The average circumference of their forearm muscle belly, where the FMG band was placed, is 25.6 ± 1.3 cm. All participants provided informed and written consent, and the test procedure was approved by the Simon Fraser University of Research Ethics.

Table 5.1. First Study Participant Demographics

Participant	Gender	Age	Forearm belly Circumference
1	Male	25	26
2	Female	25	22
3	Female	27	24
4	Male	30	25
5	Male	22	25
6	Female	23	25
7	Female	22	25
Average	---------	24.9 ± 2.9	24.6 ± 1.3

5.3.2. The Second Study Participants

Ten healthy participants with no known neuromuscular disorders (5 females and 5 males) aged (24.1 ± 2.1 years old) participated in this study. Two anthropometric measurements of the forearm were also taken. The first measurement taken was of the forearm length, which was taken from the ulnar styloid process (bony prominence of the wrist on the side of the pinky) to the olecranon (the bony prominence of the elbow). The second measurement taken was of the circumference of the arm at each band landmarks shown in **Figure 5.1**. The average forearm length was 27.7 ± 2.5 cm for all ten participants with circumferences of 16.9 ± 1.5 cm, 20.9 ± 2.5 cm, 26.4 ± 2.7 cm, and 27.4 ± 2.7 cm at landmarks 1, 2, 3, and 4 respectively. Participant demographics data are shown in **Table 5.2**. All participants provided informed and written consent, and the test procedure was approved by the Simon Fraser University of Research Ethics.

Table 5.2. Second Study Participant Demographics

Participant	Gender	age	Forearm length (cm)	Circumference (cm)			
				Position 1	Position 2	Position 3	Position 4
1	Female	28	26	15.5	19	25.5	27
2	Female	25	25	14	16.5	22	24
3	Female	20	28	15.5	18.5	23	24
4	Male	24	29	18	21.5	25.5	26.5
5	Male	25	31	18	22.5	28.5	28.5
6	Male	26	29	18.5	25	30	30
7	Male	23	28.5	17	21	26.5	28
8	Female	23	24	16.5	20	25	25
9	Male	24	31	18.5	23.5	30	32.5
10	Female	23	25	17	21	28	28.5
Average	-----	24.1 ± 2.1	27.7 ± 2.5	16.9 ± 1.5	20.9 ± 2.5	26.4 ± 2.7	27.4 ± 2.7

5.4. The First Study Results

The data were successfully collected from 7 participants for 3 trials for each wrist deviation of: pronation-supination, flexion-extension and radial-ulnar. Thus, there were a total number of 5400 samples for each subject (3 trials times 3 wrist deviations, and 600 samples per trial). **Figure 5.2** shows an example of the FMG signals which are centralized to the mean value and normalized using the global maximum and minimum on one trial versus the pronation-supination deviation values. The number of peaks in the torque graph represents the transition speed between the pronation and supination deviations during the data collection. It is clearly shown that there is a correlation pattern between the FMG signals and the exerted torque.

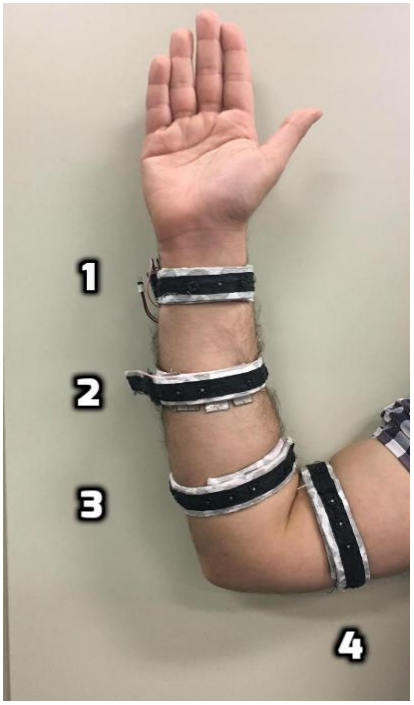

Figure 5.1. Placement of 4 customized FMG bands on participant's arm. (1) approximately 2.25 cm proximal to the wrist, identified by the surface landmarks of the radial and ulnar styloid processes (2) midway between the band at position 1 and the point on the forearm with the widest circumference, (3) the point on the forearm with the widest circumference, and (4) on the upper arm about 2 inches above the elbow.

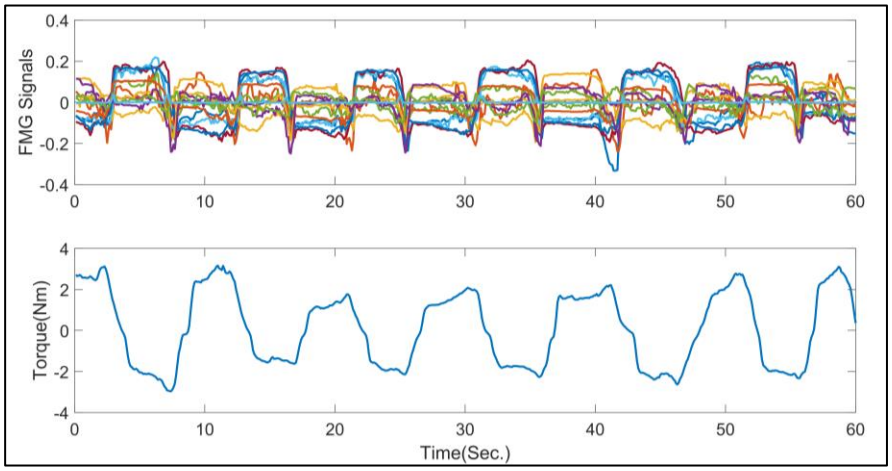

Figure 5.2. An example of the FMG signals in one trial versus the pronation-supination deviation values.

A regression model was created to predict each deviation individually. The input for the model was the FMG signals corresponding to the wrist torque that the model will predict. A total number of 1800 data points (3 trials times 600 samples per trial) were used to train and test the regression model. Five regression algorithms that were described in **Chapter 4**, were used to create the FMG-based model and the performance metrics in **Section 3.5** were used to compare between the resultant models. 10-fold cross validation evaluation was used for analysing the data. **Figure 5.3-a** shows the average R^2 across all participants for the 10-fold cross validation evaluation for three torque axes using 5 regression algorithms. While **Figure 5.3-b** shows the average NRMSE across all participants for the 10-fold cross validation evaluation for three torque axes using 5 regression algorithms. It is clearly shown that all regression algorithms perform similarly in terms of R^2 and NRMSE except the random forest which has a lower accuracy than the others with about 0.10. The Kernel Ridge Regression (KRR) achieves average accuracy of 0.91 ± 0.04, 0.88 ± 0.04, and 0.89 ± 0.05 for pronation-supination, flexion-extension, and radial-ulnar respectively and the error has a relatively low value with 8.39 ± 2.8%, 9.63 ± 2.56%, and 8.62 ± 2.37% for the three wrist deviations. While General Regression Neural Network (GRNN) has a slight decrease in the accuracy and increase in the error, that reaches 0.90 ± 0.04, 0.87 ± 0.05 and 0.88 ± 0.05 for the three wrist deviations respectively. Gaussian Processes Regression (GPR) achieves a similar R^2 and error as the KRR. Whereas the accuracy from Support Vector Regression (SVR) slightly decline

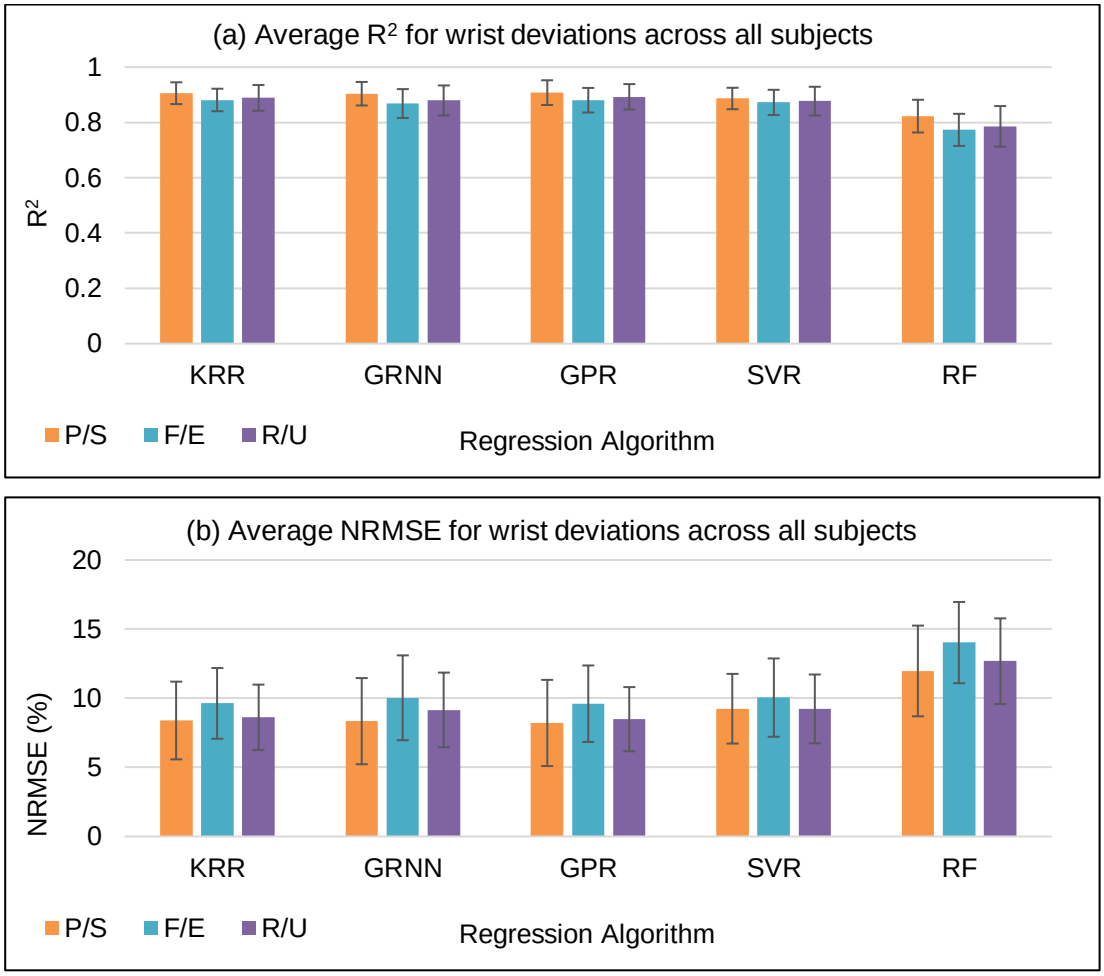

Figure 5.3. (a) The average R^2 for wrist deviations: pronation-supination(P/S), flexion-extension(F/E), and radial-ulnar(R/U) for 10-fold cross validation averaged across 7 participants using KRR, GRNN, GPR, SVR, and RF. (b) The average NRMSE for wrist deviations: pronation-supination, flexion-extension, and radial-ulnar for 10-fold cross validation averaged across 7 participants using KRR, GRNN, GPR, SVR, and RF.

to 0.89 ± 0.04, 0.87 ± 0.05, and 0.88 ± 0.05 for pronation-supination, flexion-extension, and radial-ulnar respectively. Finally, Random Forest (RF) has a degradation in the accuracy that reaches 0.82 ± 0.06, 0.77 ± 0.06 and 0.79 ± 0.07 for pronation-supination, flexion-extension, and radial-ulnar respectively. While the error was higher compared to the other algorithms with 11.97 ± 3.28, 14.03 ± 2.94, and 12.68 ± 3.1 for the three wrist torque axes respectively.

5.4.1. Limitations of the First Study

Despite the good accuracy using the first experimental setup, there are some limitations in the acquisition system used in this study. The acquisition system composed two parts: the FMG band for capturing the FMG data, and the rig that has a torque sensor for detecting the torque value. First for the FMG band, it wasn't stretchable when placing a Velcro tape on its back. This makes some sensors bumps up when the band was wrapped around the participant's forearm, which in turn deform the signals. During the data analysis, we exclude the deformed sensors signals and use the others in the regression process. However, this may affect the consistency and the reproducibility of the results. This problem guides us to design another band that overcome these problems that was described in **Section 4.3.2**. The new band will be used in the second study.

Using 1-DOF torque sensor in the rig for labeling the data may not be efficient in terms of the need for a new rig to capture the torque in different axis. Instead, using 6-DOF load cell that able to capture the torque around three axes and the force in three axes all together is more efficient. Thus, having one setup that can be used for capturing the force and torque in all axes at a time and this is the second setup that overwhelmed this constrain. The second rig was described in **Section 4.3.2**.

5.5. The Second Study Results

The data were successfully collected from all 10 participants for 5 trials, except the last trial of subject 6. This trial was excluded due to the band slipping during the data collection. Thus, there were a total of 12,000 data points for each subject (5 trials times 6 axes sessions, and 400 samples on each session). For subject 6, the data included only 10,000 samples and the cross-trial was conducted in 4-fold and the average accuracy was from only four trials. During the data collection sessions, some subjects reported feeling slightly fatigue in their arm muscles and rested their hands between the sessions for a few minutes. **Figure 5.4** shows a sample trial of the normalized FMG signals with the linear trend removed from the band 3 with the exerted force in X axis (F_X). It is shown that the FMG signals have a correlated pattern like that of F_X.

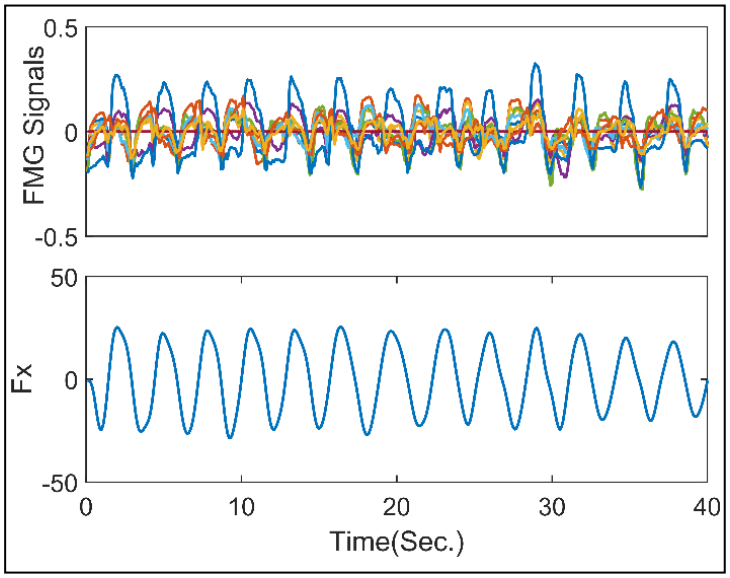

Figure 5.4. Sample of the normalized FMG signals from band 3 vs the force exerted in X axis in one trial for 40 seconds.

This study is about predicting single-axis force/torque using the Force Myography (FMG) signals. A regression model was created for each axis individually to examine how well the FMG can predict isometric force/torque in single-axis at a time. In addition, towards finding the best band(s) combination placement within four locations, the regression model of each axis was trained using data from all the possible band combinations.

The input for each model was the FMG signals recorded during the trials where the participant was focusing on a specific axis which the model will predict. A number of 2000 data points (5 trials times 400 samples per trial) was used for training and testing the model of each axis. Two experiments using different regression models were carried out to study the feasibility of using the FMG signals for predicting the force/torque in single-axis. The first one is 10-fold cross validation which was previously described in **Section 4.5.2**. **Figure 5.5-a** shows the average accuracy (R^2) of the isometric force prediction in X-axis, averaged across all subjects in the 10-fold cross validation for all possible band combinations. While **Figure 5.5-b** shows the average NRMSE from the 10-fold cross-validation across all subjects for F_X prediction. It is shown that Gaussian Processes Regression (GPR) outperform all other algorithms in terms of high accuracy and low error, using any band combination while the Kernel Ridge Regression (KRR), General

Regression Neural Network (GRNN), Support Vector Regression (SVR) and Random Forest (RF) have a less accuracy (R^2) with an average of 0.07, 0.08, 0.10, and 0.04 than GPR. Using single band, the band on forearm muscle belly (band 3) achieved the best performance among all 4 locations throughout all algorithms, with an average accuracy (using GPR) of 0.92 ± 0.03, compared to 0.83 ± 0.11, 0.85 ± 0.07, and 0.86 ± 0.11 for band 1, 2, and 4, respectively. In addition, the NRMSE has a lowest value using band 3 with 6.75 ± 1.69%.

Increasing the spatial coverage of FMG measurements from a single band to using two bands contributes to enhancing the accuracy. It is noticeable that the double

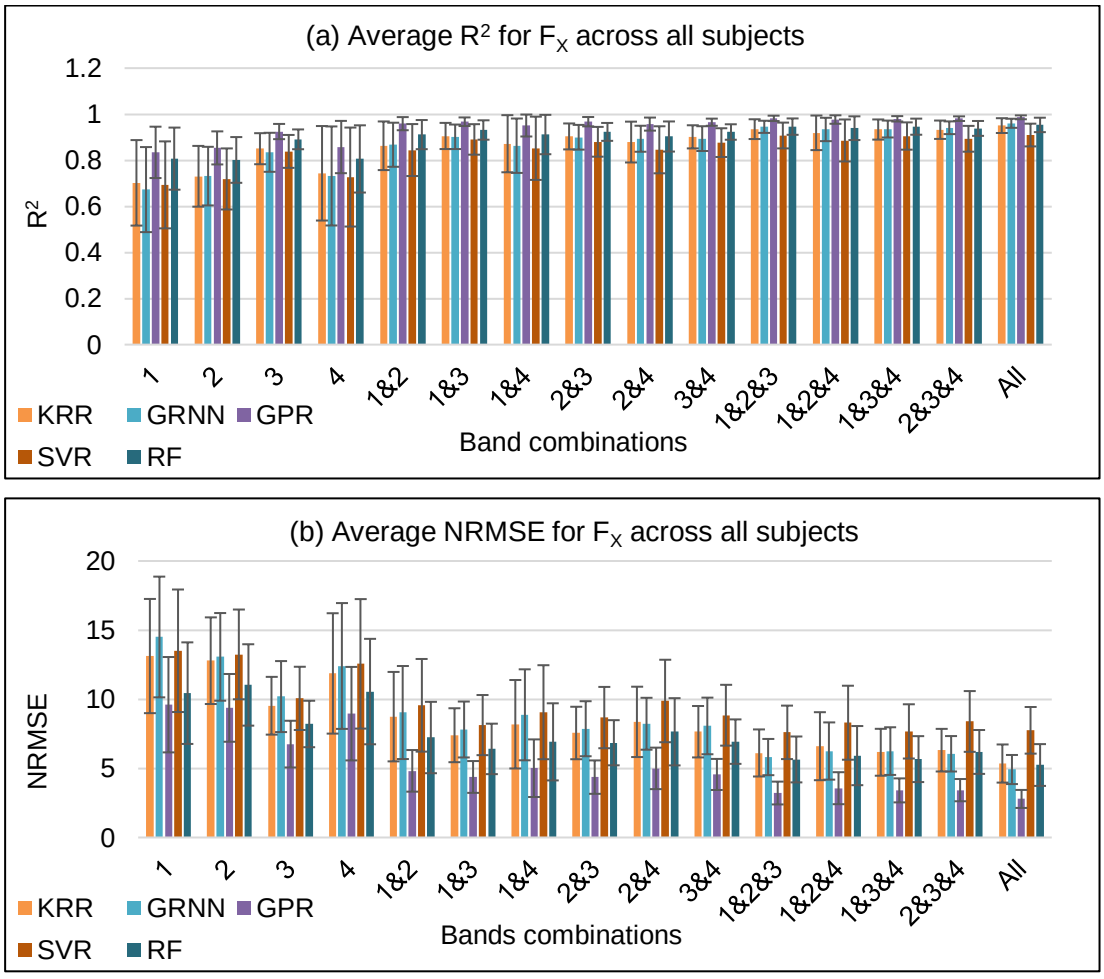

Figure 5.5. (a) The average R^2 for F_X prediction across 10 participants for 10-fold cross validation. (b) The average NRMSE for F_X prediction across ten participants for 10-fold cross validation.

combinations that have band 3 as one of its items achieves higher accuracy than the other combinations. Combination of bands 1 and 3, combination of bands 2 and 3, and combination of bands 3 and 4 achieves accuracies of 0.97 ± 0.03, 0.97 ± 0.02, and 0.97 ± 0.02, respectively, while the other combinations has less accuracy with about 0.02 using GPR. Using 3 bands increased the accuracy slightly to 0.98 ± 0.01 using combination of bands 1, 2, and 3. In addition, using all bands increased the accuracy slightly with 0.01 and the NRMSE reaches 2.79 ± 0.65.

Figure 5.6-a shows the average accuracy (R^2) of the isometric force prediction in Y-axis, averaged across all subjects in the 10-fold cross validation for all possible band

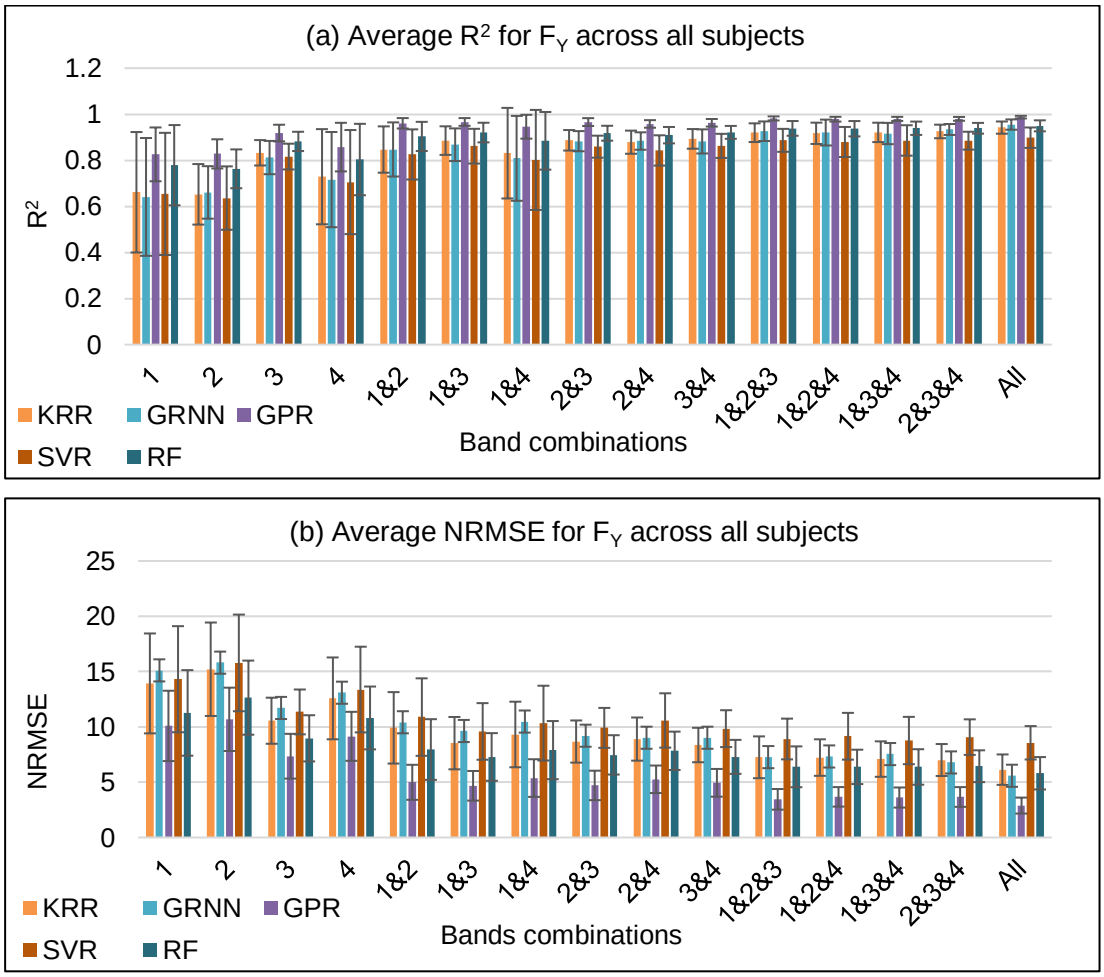

Figure 5.6. (a) The average R^2 for F_Y prediction across 10 participants for 10-fold cross validation. (b) The average NRMSE for F_Y prediction across ten participants for 10-fold cross validation.

combinations. While **Figure 5.6-b** shows the average NRMSE from the 10-fold cross-validation across all subjects for F_Y prediction. Similar to F_X prediction accuracy, GPR achieves the highest accuracy and lowest variance among the five algorithms using and band combination. While KRR, GRNN, SVR and RF have a less accuracy (R^2) with an average of 0.09, 0.10, 0.12 and 0.05 than GPR. Using a single FMG band, band 3 (on the forearm muscle belly) achieved the best performance compared to the other landmarks, with an average accuracy (using GPR) of 0.92 ± 0.04, compared to 0.83 ± 0.12, 0.83 ± 0.06, and 0.86 ± 0.11 for band 1, 2, and 4, respectively. Increasing the FMG measurements from single band to multiple enhance the accuracy gradually. The accuracy increased to 0.97 ± 0.02, 0.98 ± 0.01, and 0.99 ± 0.01 using bands 1 and 3, bands 1, 2, and 3, and all bands, respectively. In addition, the NRMSE decreased gradually from 7.35 ± 2.02% using single band to 4.67 ± 1.34%, 3.45 ± 0.93% and 2.88 ± 0.72% using double, triple and all bands, respectively.

Figure 5.7-a shows the accuracies R^2 of the isometric force prediction in Z-axis, averaged across all subjects in the 10-fold cross validation for all possible band combinations. While **Figure 5.7-b** shows the average NRMSE from the 10-fold cross-validation across all subjects for F_Z prediction. Similar to F_X and F_Y prediction results, GPR hits the highest accuracy among all regression algorithms for all band combinations. While the other algorithms: KRR, GRNN, SVR and RF have a less accuracy (R^2) with an average of 0.04, 0.06, 0.05 and 0.03, respectively than GPR, which shows a relatively consistent estimation accuracy among different algorithms. Using a single FMG band, the band on the forearm muscle belly (band 3) achieves the best performance compared to other positions. The R^2 of band 3 is 0.93 ± 0.02 and the NRMSE is 6.9 ± 1.4% compared to R^2 of 0.88 ± 0.04, 0.85 ± 0.06, 0.88 ± 0.04, and 0.90 ± 0.03 and NRMSE of 8.9 ± 0.93%, 9.8 ± 1.57%, 8.99 ± 1.07%, and 7.99 ± 1.19% for KRR, GRNN, SVR and RF, respectively. Increasing the bands used to two, the accuracy improved using any double-band combinations, but the relatively highest one is the combination of bands 2 and 3 with accuracy of 0.97 ± 0.02. Using 3 bands, the accuracy increased slightly reaching 0.98 ± 0.01 using bands 1, 2, and 3. Finally, using all bands together the accuracy increased to 0.99 ± 0.004 while the NRMSE reaches its lowest value of 2.98 ± 0.55%.

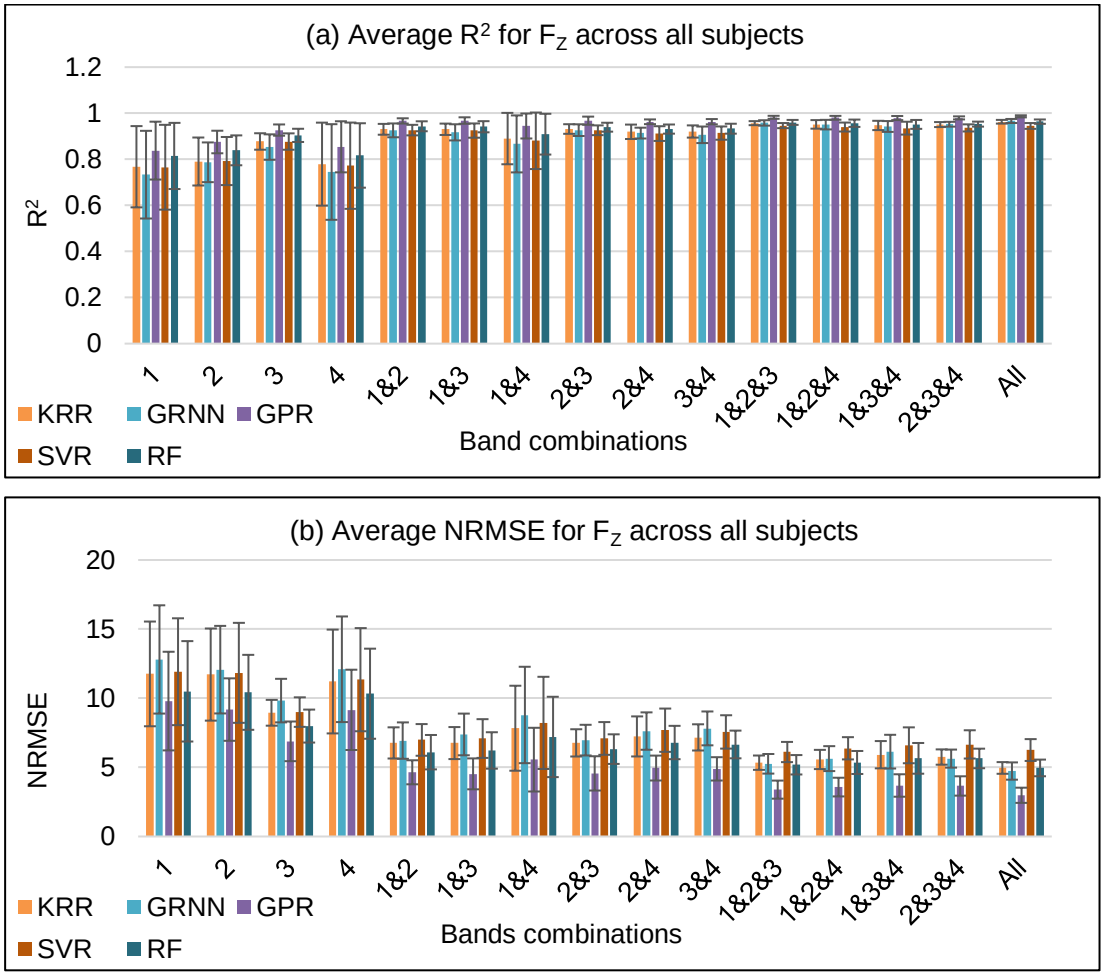

Figure 5. 7. (a) The average R^2 for F_Z prediction across 10 participants for 10-fold cross validation. (b) The average NRMSE for F_Z prediction across ten participants for 10-fold cross validation.

Figure 5.8-a shows the accuracies R^2 of the isometric torque prediction in X-axis, averaged across all subjects in the 10-fold cross validation for all possible band combinations. While **Figure 5.8-b** shows the average NRMSE from the 10-fold cross-validation across all subjects for T_X prediction. Similar to force prediction results, GPR still achieves the highest accuracy among all algorithms using any bands combination. The average degradation in the accuracy using the other algorithms compared to GPR is 0.32, 0.24, 0.10 and 0.13 using KRR, GRNN, SVR, and RF, respectively. Using single-band, band 2, band 3, and band 4 achieves similar accuracy while band 1 is the lowest one. The accuracy using band 3 is 0.59 ± 0.10 and the NRMSE is 9.75 ± 2.11%. Considering double-band to predict the torque, combination of band 2 and 3 has the highest accuracy

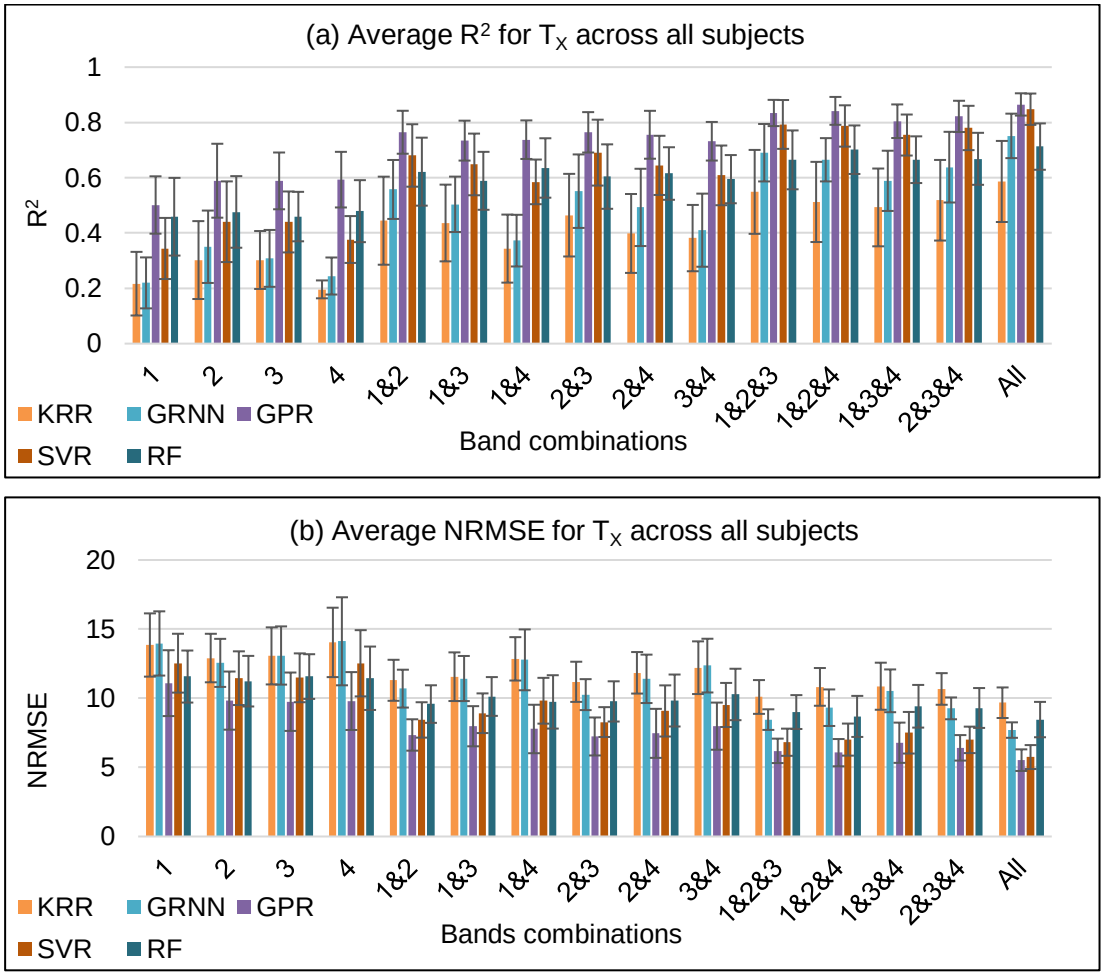

Figure 5.8. (a) The average R^2 for T_X prediction across 10 participants for 10-fold cross validation. (b) The average NRMSE for T_X prediction across ten participants for 10-fold cross validation.

of 0.76 ± 0.07. Then, the accuracy improved to 0.84 ± 0.05 using the combination of bands 1, 2, and 4, which has the highest accuracy among triple combinations. Finally, using all bands increased the accuracy and it reached 0.87 ± 0.04 and the NRMSE is 5.52 ± 0.78%.

Figure 5.9-a shows the accuracies R^2 of the isometric torque prediction in Y-axis, averaged across all subjects in the 10-fold cross validation for all possible band combinations. While **Figure 5.9-b** shows the average NRMSE from the 10-fold cross-validation across all subjects for T_Y prediction. Like the previous results, GPR achieves the best accuracy among all algorithms. The accuracy decreased with an average of 0.07,

0.08, 0.02, and 0.04 using KRR, GRNN, SVR, and RF compared to GPR. Using single-band, band 3 still the best among the 4 landmarks. The R^2 using band 3 was 0.89 ± 0.04 and the NRMSE was 8.09 ± 1.61%. Increasing the FMG measurement spatial coverage to 2 landmarks, the accuracy significantly surged to 0.96 ± 0.02 using combination of bands 2 and 3, which is the best combination among double-band combinations. Using 3 bands, the accuracy slightly increased to 0.98 ± 0.01 using the combination of bands 1, 2, and 3. Finally, using the 4 bands together keeps the accuracy steady at 0.98 and the NRMSE was 3.31 ± 0.55%.

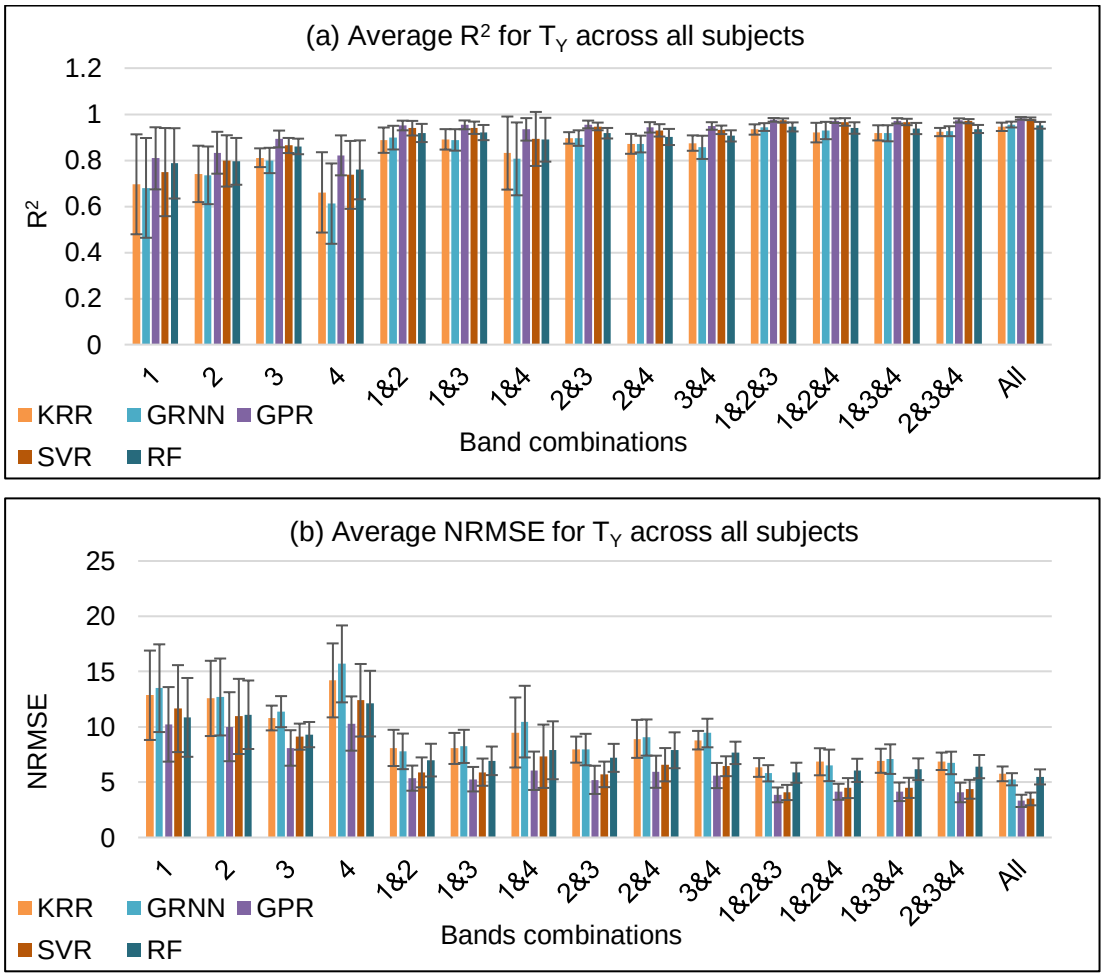

Figure 5.9. (a) The average R^2 for T_Y prediction across 10 participants for 10-fold cross validation. (b) The average NRMSE for T_Y prediction across ten participants for 10-fold cross validation.

Figure 5.10-a shows the accuracies R^2 of the isometric torque prediction in Z-axis, averaged across all subjects in the 10-fold cross validation for all possible band combinations. While **Figure 5.10-b** shows the average NRMSE from the 10-fold cross-validation across all subjects for T_Z prediction. Similar to the previous results, GPR achieves the highest accuracy among the other algorithms. The accuracy decreased by 0.11, 0.11, 0.06, and 0.05 using KRR, GRNN, SVR, RF, respectively compared to GPR. Using single-band, band 3 (on the forearm muscle belly) is the best among the 4 positions. The accuracy using band 3 was 0.89 ± 0.04 compared to 0.80 ± 0.12, 0.83 ± 0.09, and 0.74 ± 0.08 using band 1, band 2, and band 4, respectively. Using the combination of bands 2 and 3, which is the best among all double-band combinations, the accuracy

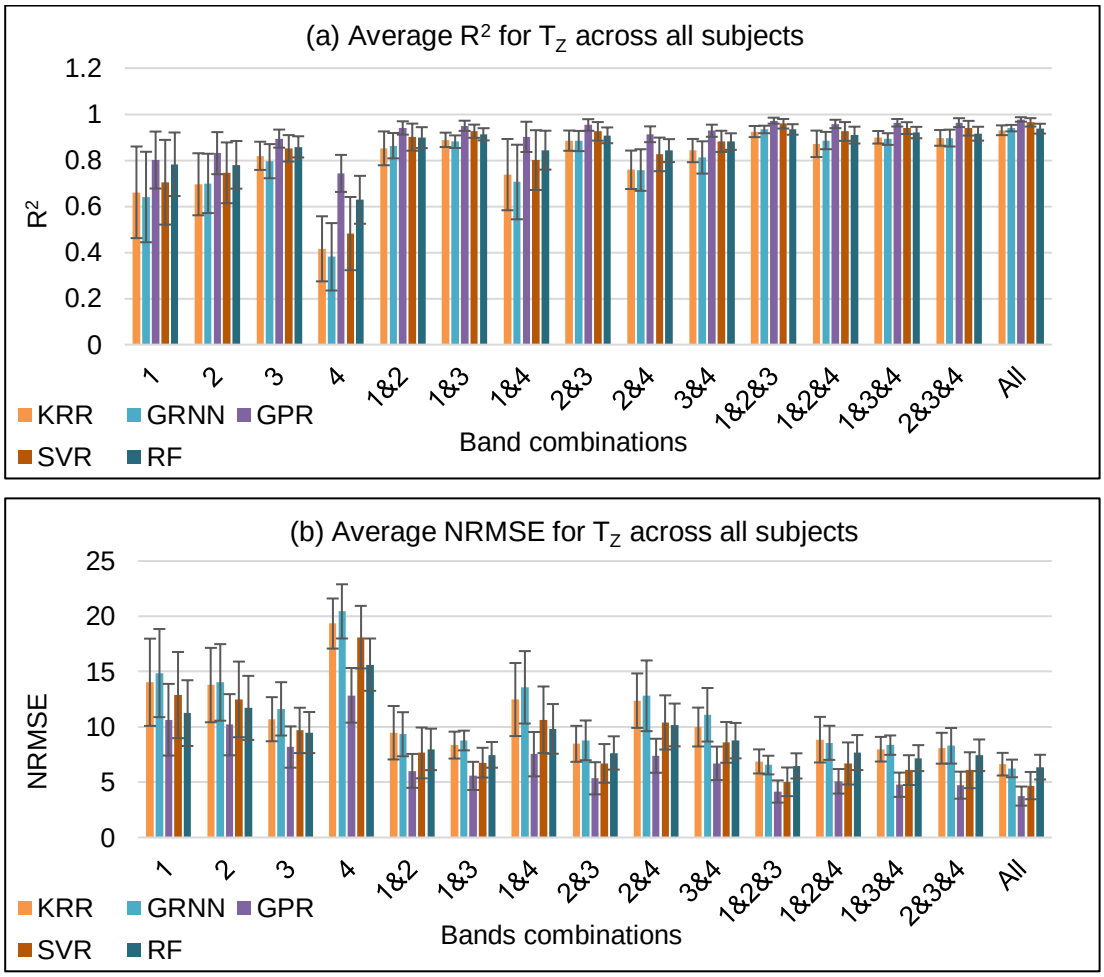

Figure 5.10. (a) The average R^2 for T_Z prediction across 10 participants for 10-fold cross validation. (b) The average NRMSE for T_Z prediction across ten participants for 10-fold cross validation.

improved significantly to 0.95 ± 0.03 and the NRMSE was 5.35 ± 1.45%. Using 3 bands, the accuracy increased slightly to 0.97 ± 0.01 using the combination of bands 1, 2, and 3. Finally using all bands together, the accuracy increased to 0.98 ± 0.01 and the NRMSE was 3.74 ± 0.86%.

Three-way analysis of variance (ANOVA) was performed to examine the effect of the three independent variables: regression algorithm, band combinations and force/torque axis to the dependent variable of the force/torque estimation accuracy R^2. The significant factors at $p < 0.05$ for regression algorithm, band combinations, force/torque axis and their intersections are shown in **Table 5.3**. The table also shows the sum of squares (i.e., squared residuals from the average), the degrees of freedom, the mean square (sum of squares divided by the degrees of freedom) and the test statistics for each factor. For the test statistics, the value of the test statistic F and the probability that the variable variance is due to chance are reported. The three-way ANOVA showed the significant effects of regression algorithm ($F_{4, 4330} = 244.26$, $p < .00001$), bands combination ($F_{14, 4330} = 256.28$, p

Table 5.3. Three-way ANOVA for cross-validation evaluation for single-axis force/torque prediction.

Significant Factor	Sum of Squared	Degrees of Freedom	Mean Squares	F	Probability
Regression Algorithm	8.175	4	2.0437	244.26	0
Band Combinations	30.021	14	2.14444	256.28	0
Force/torque Axis	61.029	5	12.2058	1458.76	0
Algorithm * Band Combinations	1.611	56	0.0288	3.44	0
Algorithm * Force/torque axis	5.583	20	0.2791	33.36	0
Band Combinations* Force/torque Axis	4.629	70	0.0661	7.9	0
Error	36.23	4330	0.0084		
Total	147.278	4499			

< .00001) and force/torque axis ($F_{5, 4330}$ = 1458.76, p < .00001) to the estimation accuracy R^2 for the cross-validation evaluation. In addition, the interaction between the regression algorithm and band combinations is statistically significant ($F_{56, 4330}$ = 3.44, p < .00001), the interaction between the regression algorithm and the force/torque axis is statistically significant ($F_{20, 4330}$ = 33.36, p < .00001), and the interaction between the band combinations and the force/torque axis is statistically significant ($F_{70, 4330}$ = 7.9, p < .00001) to the prediction accuracy R^2.

The Post Hoc test (Turkey HSD) on the effect of regression algorithm to the estimation accuracy R^2 showed that using the GPR was significantly higher (p < .0001) than all other regression algorithm. Also, DF was significantly higher (p < .0001) than KRR, GRNN and SVR. Furthermore, there was no significant difference between the KRR and the GRNN.

The Post Hoc test (Tukey HSD) on the effect of band combination showed that the accuracy of using the 4 bands together was significantly higher (p < .00001) than those of using single-, double-, and triple-band combinations except the combination of bands 1, 2, and 3, and the combination of bands 2, 3, and 4. The accuracies of all triple combinations were significantly higher (p < .05) compared to using single or double-band except the combination of bands 2 and 3 which was not significantly lower than combination of bands 1, 2, and 4. However, there was no significant difference between any of the 4 combinations using triple-band. The accuracies of the 6 combinations of double-band were significantly higher (p < .00001) than the accuracies using single-band except combination of bands 1 and 4 which was not significantly higher than band 3. Among the 4 single bands, band 3 was significantly higher than all other band positions, which confirms that the band on the forearm muscle belly (band 3) is the best for isometric force/torque sensing.

The Post Hoc test (Tukey HSD) on the effect of force/torque axis showed that the accuracies of F_Z was significantly higher (p < .00001) than those of F_X, F_Y, T_X, T_Y, and T_Z, whereas the accuracy of T_X was significantly lower (p < .00001) than all other force/torque axes. In addition, the accuracy of F_X was significantly higher (p < 0.05) than F_Y, T_X and T_Z and there was no significant difference between F_X and T_Y.

The second experiment which is cross-trial evaluation was motivated by studying the data consistency across different trials and it is closer to the real situation. In each trial, the regression model was trained using four data sets and was tested on the remaining set. The resulting accuracy concludes the same trend as cross-validation in increasing the spatial coverage of the FMG results in improving the prediction accuracy. The degradation in the cross-trial accuracies compared to the cross validation is because the data was not consistent between different trials.

From cross-validation results, the GPR algorithm shows the highest accuracy among all algorithms which in turn was used for cross-trial evaluation. **Figure 5.11-a** shows the average R^2 for cross-trial evaluation averaged across all participants using GPR for all isometric force/torque axes. Agreed with the cross-validation analysis, using all bands achieves the peak accuracy with 0.87 ± 0.08, 0.86 ± 0.06, 0.92 ± 0.01, 0.77 ± 0.12, 0.88 ± 0.04, and 0.86 ± 0.06 for F_X, F_Y, F_Z, T_X, T_Y and T_Z respectively. While using 3 bands decreased the accuracy slightly for some axes and remained steady in other axes. The R^2 using combinations of bands 1, 2, and 3 was 0.86 ± 0.08, 0.82 ± 0.09, 0.91 ± 0.01, 0.76 ± 0.12, 0.87 ± 0.05, and 0.85 ± 0.07 for F_X, F_Y, F_Z, T_X, T_Y and T_Z respectively. Then the accuracy decreased significantly when using double-band combination, the R^2 was 0.81 ± 0.09, 0.75 ± 0.11, 0.87 ± 0.04, 0.69 ± 0.13, 0.82 ± 0.07, and 0.80 ± 0.06 for F_X, F_Y, F_Z, T_X, T_Y and T_Z respectively using combination of bands 1 and 3. Finally, using single-band declined the accuracy dramatically to 0.71 ± 0.13, 0.66 ± 0.12, 0.79 ± 0.07, 0.60 ± 0.15, 0.70 ± 0.09, and 0.71 ± 0.12 for F_X, F_Y, F_Z, T_X, T_Y and T_Z respectively using band 3.

In addition, the error NRMSE represented in the **Figure 5.11-b** shows the same pattern as the cross-validation in terms of increasing the number of bands used, the error and variance decrease significantly. The NRMSE using band3 was 16.21 ± 2.69%, 17.48 ± 2.00%, 13.95 ± 1.89%, 16.33 ± 1.98%, 15.04 ± 2.42%, and 14.40 ± 2.92%, for F_X, F_Y, F_Z, T_X, T_Y and T_Z respectively. Then the error declined significantly to 11.22 ± 2.29, 11.84 ± 1.75, 8.90 ± 1.28, 12.59 ± 1.59, 9.79 ± 1.23, and 10.28 ± 1.84, for F_X, F_Y, F_Z, T_X, T_Y and T_Z respectively using all bands together.

Two-way analysis of variance (ANOVA) was performed to examine the effect of the two independent variables: the band combinations and the force/torque axis to the dependent variable of the force/torque estimation accuracy R^2. The significant factors at p

< 0.05 for band combinations and force/torque axis are shown in **Table 5.4**. The table shows the sum of squares (i.e., squared residuals from the average), the degrees of freedom, the mean square (sum of squares divided by the degrees of freedom) and the test statistics for each factor. For the test statistics, the value of the test statistic F and the probability that the variable variance is due to chance are reported. The two-way ANOVA showed both significant effects of the bands combination ($F_{14, 810} = 45.15$, $p < .00001$) and force/torque axis ($F_{5, 810} = 39.62$, $p < .00001$) to the estimation accuracy R^2 for the cross-trial evaluation

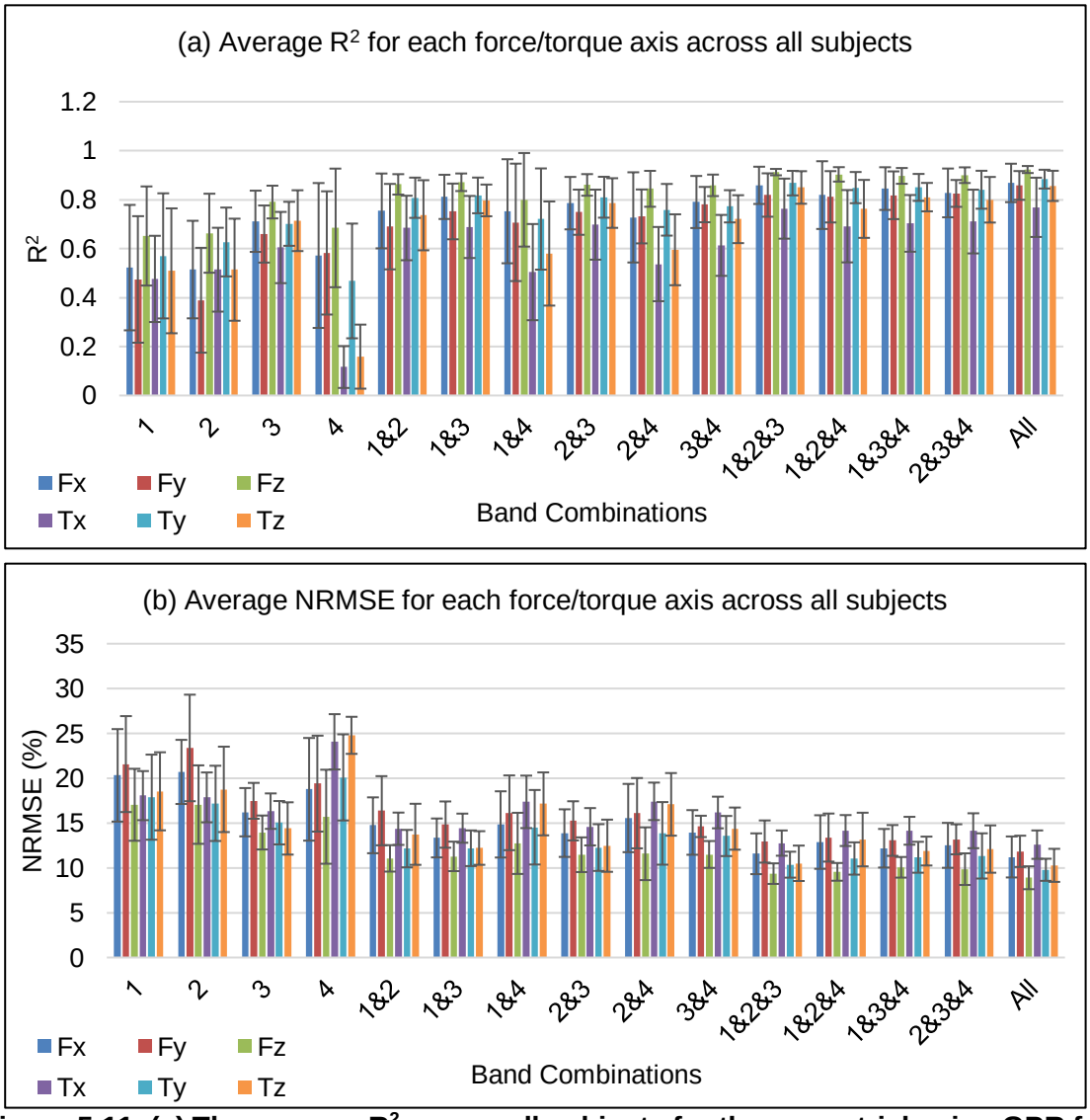

Figure 5.11. (a) The average R^2 across all subjects for the cross-trial using GPR for the force/torque estimated values in X, Y and Z axes. (b) The average NRMSE across all subjects for the cross-trial evaluation.

using GPR. In addition, the interaction between the band combinations and the force/torque axis is statistically significant ($F_{70, 810} = 1.67$, $p < .001$) to the prediction accuracy R^2.

Figure 5.12 shows an example of GPR prediction for forces in X, Y, and Z axes and the torque around the same axes vs the actual values. The example showed is from subject 9 data when the last trial used as the testing data while the first four trials was used for training the GPR regression model. The average accuracy across the 6 axes was 0.93.

The Post Hoc test (Tukey HSD) on the effect of band combinations showed that the accuracy of using all 4 bands was significantly higher ($p < .05$) than the all other band combinations except combination of bands 1 and 3, combination of bands 2 and 3, and all triple-band combinations. The accuracies of all triple-band combinations were significantly higher ($p < .00001$) than using single-band and double-band combinations except the combinations that has band 3 as one of its items and the combination of bands 1 and 2. However, there was no significant difference between any of the 4 triple-band combinations. Among all the 6 double-band combinations, combination of band 1 and 3 is the only one that is significantly higher ($p < .00001$) all single-band accuracies. Furthermore, all other double-band combinations are significantly higher ($p < .00001$) than all single-band except

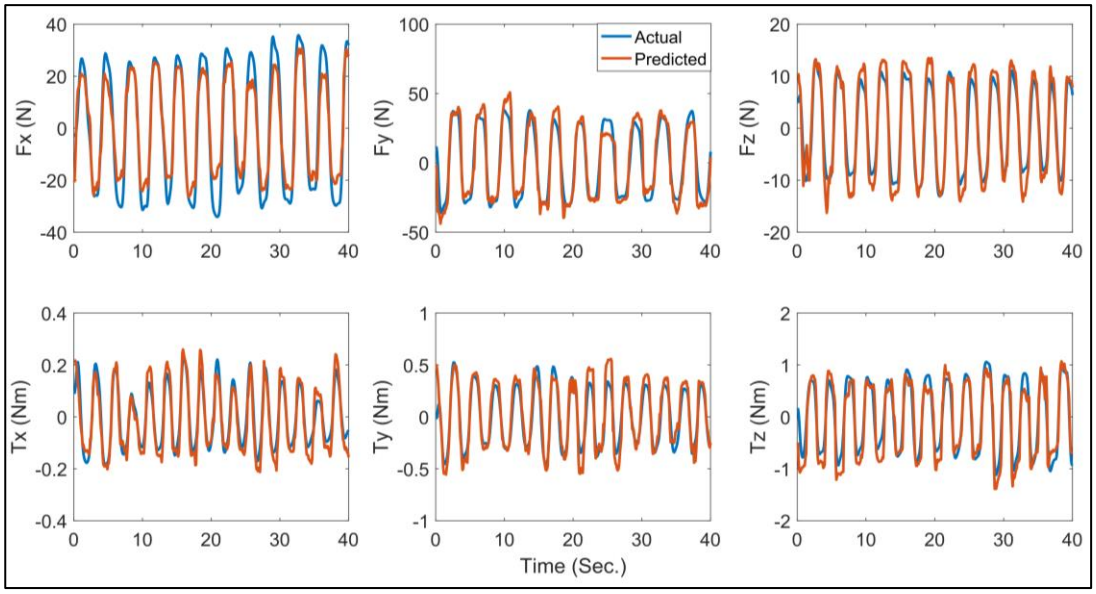

Figure 5. 12. An example of the force and torque actual values in X, Y, and Z axes vs the predicted values using GPR in cross-trial evaluation.

Table 5.4. Two-way ANOVA for the cross-trial evaluation for single-axis force/torque prediction.

Significant Factor	Sum of Squared	Degrees of Freedom	Mean Squares	F	Probability
Band Combinations	13.6898	14	0.97784	45.15	0
Force/torque Axis	4.2899	5	0.85798	39.62	0
Band Combinations * Force/torque Axis	2.5387	70	0.03627	1.67	0.0007
Error	17.5414	810	0.02166		
Total	38.0598	899			

band 3. Among the 4 single bands, band 3 is significantly higher ($p < .00001$) than other single bands, which means that the band on the forearm muscle belly is the best for force/torque sensing in any axis.

The Post Hoc test (Tukey HSD) on the effect of force/torque axis showed that the prediction accuracy of F_Z is significantly higher ($p < 0.0005$) than all other force/torque axes. Whereas the accuracy of T_X is significantly lower ($p < 0.0005$) than all other force/torque axes. In addition, there is no significant difference between the prediction accuracies of F_X, F_Y, and T_Y. The accuracies of F_X, F_Y, and T_Y are significantly higher ($p < .05$) than F_Z, T_X, and T_Z, but there is neither significant difference between F_X, F_Z, and T_Y nor between F_Y, T_X, and T_Z.

5.6. Chapter Summary

In this chapter, the viability of using the FMG to predict hand force/torque in single-axis was explored. Two studies were proposed, the first one using a single-axis torque sensor which measure the torque in single-axis at a time. In addition, using a band with custom-printed FSRs on the forearm muscle belly, the FMG signals was captured during the torque exertion. After that, a regression model was created to predict the torque in single-axis based on the FMG signals. This first study has a constrain of the need for developing different rigs to measure the wrist torque in different axis. To overcome this

limitation, a 6-DOF force/torque load cell was used to measure hand force/torque in 6-axis simultaneously which was used in the second study. In addition, a custom-fabricated FMG band was designed in-house instead of the first one that has some sensors bumps up when the band wrapped around the participant's forearm which may distort the signals. In the second study, the data of the hand force/torque in 6-axis was collected individually using the same rig. To capture the FMG signals, 4 FMG bands were used in 4 landmarks. Then, a regression model was trained using all band(s) combinations to find the best placement within these 4 positions: the wrist, the forearm midway, the forearm muscle belly and the upper arm.

The accuracy from both cross-validation and cross-trial evaluation was 0.96 and 0.86 averaged across all axes and participants. This accuracy proposed the potential of using the FMG signals to predict hand force/torque in 6-axis. In addition, the results showed that the band on the forearm muscle belly is the best placement within the 4 proposed locations. If double-band combination was used, all the combinations that has band 3 as one of its items have a higher accuracy than the other combinations. In addition, increasing the FMG measurements spatial coverage to 3 or 4 bands, the accuracy has a slight increase. This result may conclude that single- or double-band combination is enough for prediction hand force/torque in single-axis.

Chapter 6.

Feasibility of Using Force Myography (FMG) for 3-axis Force/Torque Estimation

6.1. Chapter Overview

The work described in this chapter addresses part of **Objectives 2** and **3** of this work. The first study is about exploring the feasibility of using FMG based system to predict hand force in X, Y and Z axes and the torque around the same axes simultaneously. This is more complex study compared to predicting single-axis at a time which is contributing to address part of **Objective 2.** While the second study is about finding the best band combinations placement within four landmarks for accurate 3-DOF force and torque prediction, this addresses part of **Objective 3** of this work. This chapter starts with a study overview in **Section 6.2**. **Section 6.3** outlines the participants' demographics. The results of the studies are explained in **Section 6.4** and **6.5.** Finally, a summary of this chapter is provided in **Section 6.6.**

6.2. Study Overview

In this study, the feasibility of using FMG to predict force/torque in 3-DOF was explored. The data used in this study was collected using two different setups, the first one has 1-DOF torque sensor and the other has 6-DOF load cell. The first setup was used to capture wrist torque in one-axis at a time, then the collected data were merged in one dataset that has the FMG data and its corresponding torque values in 3-DOF. While the second setup was used to capture hand force/torque in 3-DOF simultaneously. After that, different regression algorithms were used to map from the FMG data to 3-DOF force/torque at the same time. One model was trained using the data from the trials of exerting force in X, Y, and Z axes to predict the force in 3-axis. While another model was trained using the data from the trials of exerting torque around the same axes to predict the torque in 3-DOF all together. In addition, towards finding the best placement of the FMG measurements within 4 landmarks, the force and torque models was trained using all possible band(s) combinations. Then, a comparison among all resultant models was

performed based on the accuracy R^2 to find the best placement within these 4 positions: the wrist, the forearm midway, the forearm muscle belly and the upper arm.

6.3. Participants Demographics

The data used in the coming two studies were collected from the participants with their demographics previously described in **Section 5.3**.

6.4. The First Study Results

The data were successfully collected from 7 participants for 3 trials for each wrist deviation of: pronation-supination, flexion-extension and radial-ulnar. Thus, there were a total number of 5400 samples for each subject (3 trials times 3 wrist deviations, and 600 samples per trial). Then, the data from three deviations were merged into one dataset that has the FMG data as the input and the output was the torque deviation in 3-axis. The detailed description of the merging process and the result dataset was previously described in **Section 4.5.1**. **Figure 6.1** shows an example of the FMG signals which are

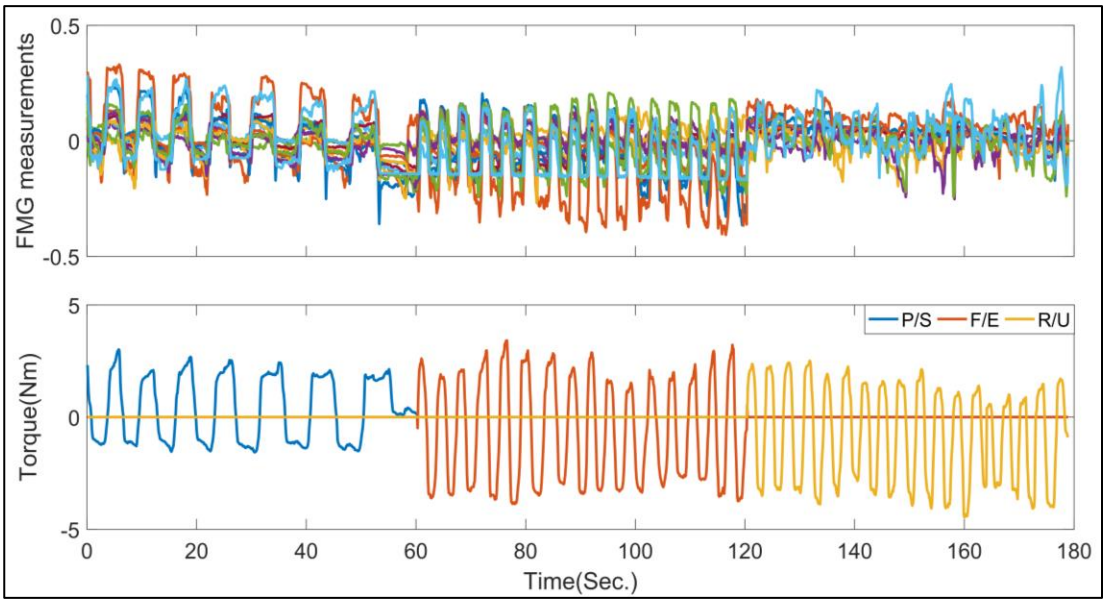

Figure 6.1. An example of the FMG measurements versus the torque deviations in: pronation-supination (P/S), flexion-extension (F/E), and radial-ulnar (R/U).

centralized to the mean value and normalized using the global maximum and minimum on 3 trials versus the values of torque deviations in: pronation-supination, flexion-extension and radial-ulnar. The number of peaks in the torque graph represents the transition speed between the negative and positive direction of each deviation (e.g., the pronation and supination) during the data collection. It is clearly shown that there is a correlation pattern between the FMG signals and the exerted torque. In addition, the FMG signals have different pattern for each deviation.

A regression model was created to predict the wrist torque around 3-axis simultaneously. The input for the model was the FMG signals form the combined dataset that has all FMG signals from 3 wrist deviations, and the output of the model was the torque around 3-axis where one of them has a value while the others two were zeros. A total number of 5400 data points (3 trials times 600 samples per trial times 3 wrist deviations) were used to train and test the regression model. Five regression algorithms that were previously proposed in **Chapter 3**, were used to create the FMG-based model. The performance of the resultant models was compared based on the metrics that was discussed in **Section 4.5**. 10-fold cross validation evaluation was used for analysing the data. The dataset was divided randomly into 10 subsets, in each fold 1 subset was saved for testing while the remaining 9 sets were used for training the model. **Figure 6.2-a** shows the average R^2 across all participants for the 10-fold cross validation evaluation for 3-axis torque prediction using 5 regression algorithms. While **Figure 6.2-b** shows the average NRMSE across all participants for the 10-fold cross validation evaluation for 3-axis torque prediction using 5 regression algorithms. It is clearly shown that all regression algorithms perform similarly in terms of R^2 and NRMSE except the random forest (RF) which has a lower accuracy than the others with about 0.12. Kernel Ridge Regression (KRR) achieved a median R^2 of 0.91 ± 0.04 and an average NRMSE of 4.44 ± 1.51%. While General Regression Neural Network (GRNN) achieved slightly lower accuracy of 0.90 ± 0.04 and lower NRMSE of 4.60 ± 1.64 %. In addition, Gaussian Processes Regression (GPR) has similar R^2 as KRR. The usage of Support Vector Regression (SVR) decreased the R^2 to 0.89 ± 0.04 and the NRMSE was 4.79 ± 1.47%. Finally, Random Forest (RF) has the lower accuracy of 0.79 ± 0.06 and an average NRMSE of 7.02 ± 1.86%.

(a)

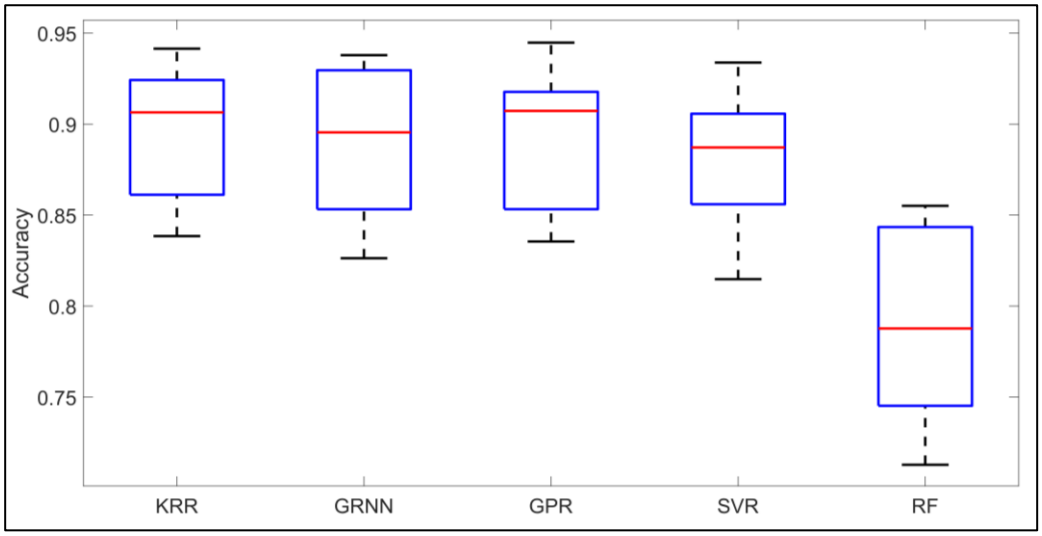

(b)

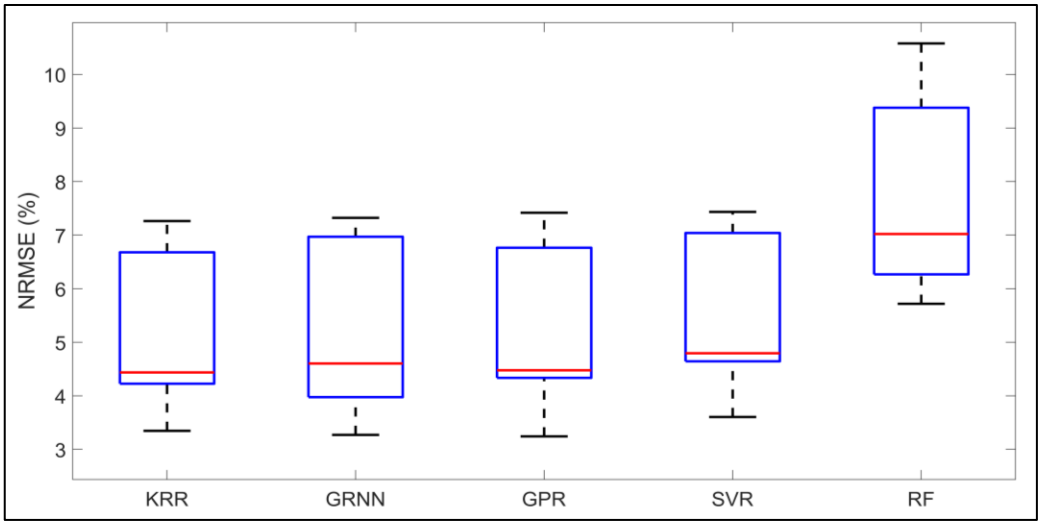

Figure 6.2. (a) The average R^2 for 3-axis wrist deviations for 10-fold cross validation averaged across 7 participants using KRR, GRNN, GPR, SVR, and RF. (b) The average NRMSE for 3-axis wrist deviations for 10-fold cross validation averaged across 7 participants using KRR, GRNN, GPR, SVR, and RF.

6.4.1. Limitations of the First Study

The proposed results preliminary investigated the feasibility of using FMG signals to predict wrist torque in multi-axis simultaneously. The data was collected using a custom rig that has single-DOF torque sensor which capture the torque values in single-axis at a time. The data was collected for three wrist deviations of: pronation-supination, flexion-extension, and radial-ulnar. Then, the data from three deviations was merged into one dataset that has FMG signals were the input and the output was the torque in 3-axis. This current setup has a main drawback that different wrist deviations can not be purely separated. In other words, the participants can not exert pure deviation in single-axis (e.g., pronation-supination) while the other deviations have zero value [119], but there was always more than 1 axis was active during torque exertion even the intention was focusing in 1-axis. This suggests that the suitable and efficient setup for capturing the torque in multi-axis at a time, is using a multi-axis load cell instead of 1-DOF torque sensor.

6.5. The Second Study Results

The data were successfully collected from all 10 participants for five trials, except the last trial of subject 6. This trial was excluded due to the band slipping during the data

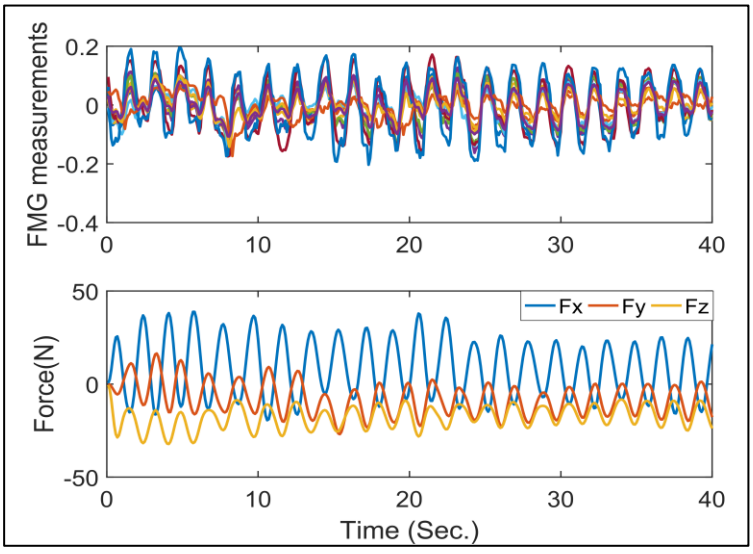

Figure 6.3. A sample of the FMG signals in one trial versus the exerted force values in X, Y, and Z axes.

collection. Thus, there were a total of 12,000 data points for each subject (five trials times six axes sessions, and 400 samples on each session). For subject 6, the data included only 10,000 samples and the cross-trial was conducted in 4-fold and the average accuracy was from only four trials. During the data collection sessions, some subjects reported feeling slightly fatigue in their arm muscles and rested their hands between the sessions for a few minutes. **Figure 6.3** shows a sample trial of the normalized FMG signals from the band 3 with the linear trend removed from it versus the exerted force in X, Y and Z axes. It is shown that the FMG signals have a correlated pattern like that of forces in the three axes. In addition, this trial was intentionally focusing on exerting force in X-axis, however there are values in the other axes: Y and Z.

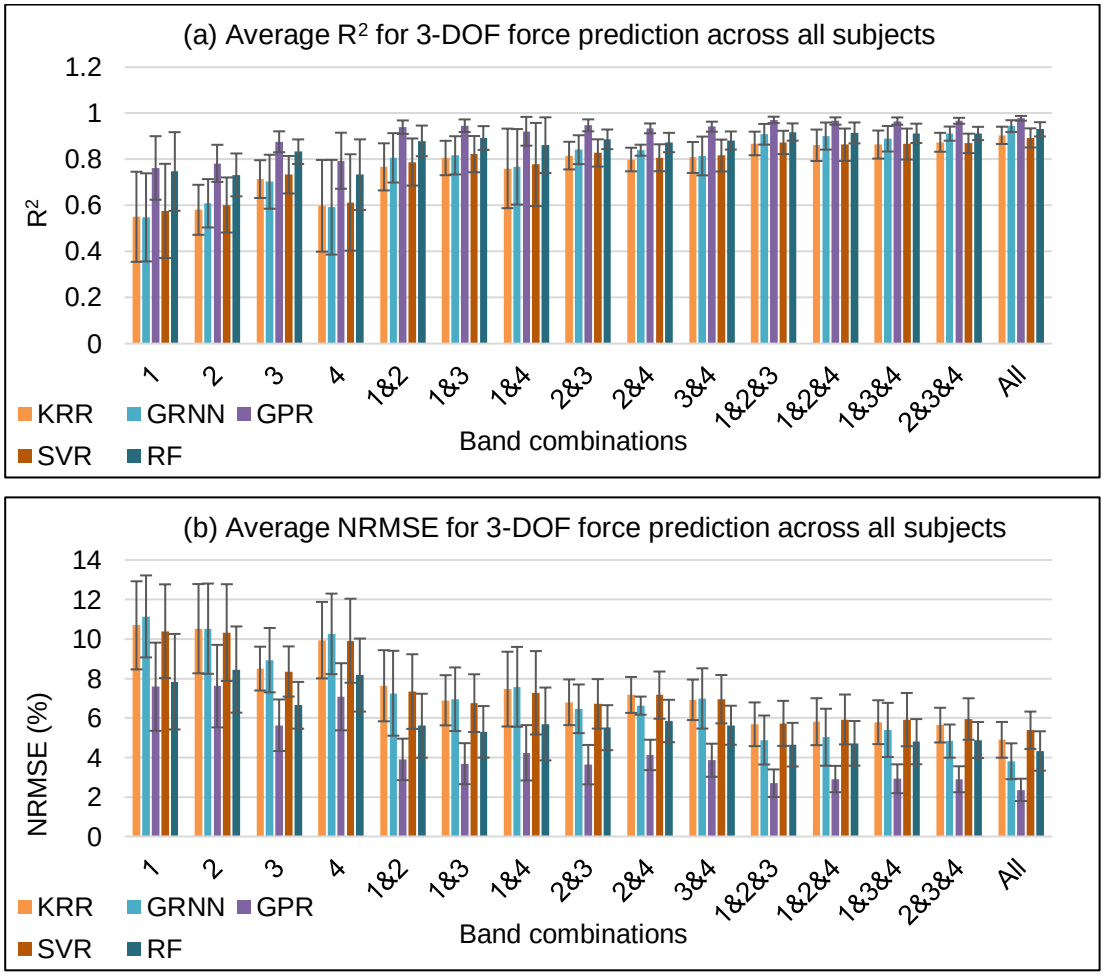

Figure 6.4. (a) The average R^2 across all subjects for force prediction in X, Y, and Z in 10-fold cross validation. (b) The average NRMSE across all subjects for 3-DOF force prediction in 10-fold cross validation.

This study is about predicting the 3-DOF force simultaneously using one model and another model for predicting 3-DOF torque. The input to the force model was the FMG signals collected during the trials of force exertion in X, Y, and Z axes, and the input to the torque model was the FMG signals of the torque exertion trials. Five regression algorithms were used to create the force and torque models, then a comparison between them was performed based of the prediction accuracy R^2 and the NRMSE. Two experiments was performed as discussed before in **Section 04.5.2**. For the cross-validation study, the data from 5 trials was divided into 10 subsets and each time the model was trained using 9 subsets while the remaining set was used for testing purposes. The accuracy and error from testing the model in each fold was calculated and the average across the folds was calculated and reported as mean ± slandered deviation. **Figure 6.4-a** shows the average R^2 of the force in X, Y, and Z axes across all subjects using all band(s) combinations in 10-fold cross validation using 5 regression algorithms. Whereas **Figure 6.4-b** shows the average NRMSE of the force prediction in 3-DOF averaged across all participants.

Agreed with **Chapter 5** results, GPR achieves the highest accuracy R^2 for 3-DOF force prediction among the 5 regression algorithms. While other algorithms have lower accuracy with an average of 0.14, 0.12, 0.13 and 0.05 for KRR, GRNN, SVR and RF, respectively. It is clearly shown that increasing the spatial coverage of FMG measurements contributes in the improvement of the prediction accuracy. Using single-band, the band on the forearm muscle belly (band 3) is the best for prediction with an average accuracy of 0.88 ± 0.05 and a NRMSE of 5.63 ± 1.31%. Increasing the number of bands to two, the usage of bands 2 and 3 combination improved the accuracy significantly to 0.95 ± 0.03 while the NRMSE decreased to 3.64 ± 1.00%. Using triple-band combination, the accuracy slightly increased to 0.97 ± 0.01 using the combination of bands 1, 2 and 3. Finally, using four bands together the accuracy has a 0.01 increase while the NRMSE reached 2.36 ± 0.57%.

Figure 6.5-a shows the average R^2 of the wrist torque prediction in 3-DOF using all band combinations in 10-fold cross validation using 5 regression algorithms. While **Figure 6.5-b** shows the average NRMSE of the torque prediction in 3-DOF averaged across all participants. Similar to the previous results, GPR achieves the highest accuracy among 5 regression algorithms. Whereas using KRR, GRNN, SVR, and RF decreased the accuracy with an average of 0.16, 0.14, 0.06 and 0.06, respectively. Using single-

band, the band on the forearm muscle belly (band 3) is the best position for torque sensing among 4 landmarks, the accuracy using band 3 was 0.80 ± 0.07 and the NRMSE was 7.31 ± 1.36%. Using double-band combination, the accuracy significantly improved to 0.91 ± 0.04 using the combination of bands on the wrist and on the forearm muscle belly (band 1 and 3) and the NRMSE decreased to 4.98 ± 1.18%. Increasing the number of the FMG measurements to 3 positions, the accuracy increased to 0.95 ± 0.02 and the NRMSE decreased to 3.76 ± 0.74% using the combination of bands 1, 2, and 3. Using the combination of the four bands together, the accuracy slightly increased to 0.96 ± 0.01 and the NRMSE marginally decreased to 3.29 ± 0.63%.

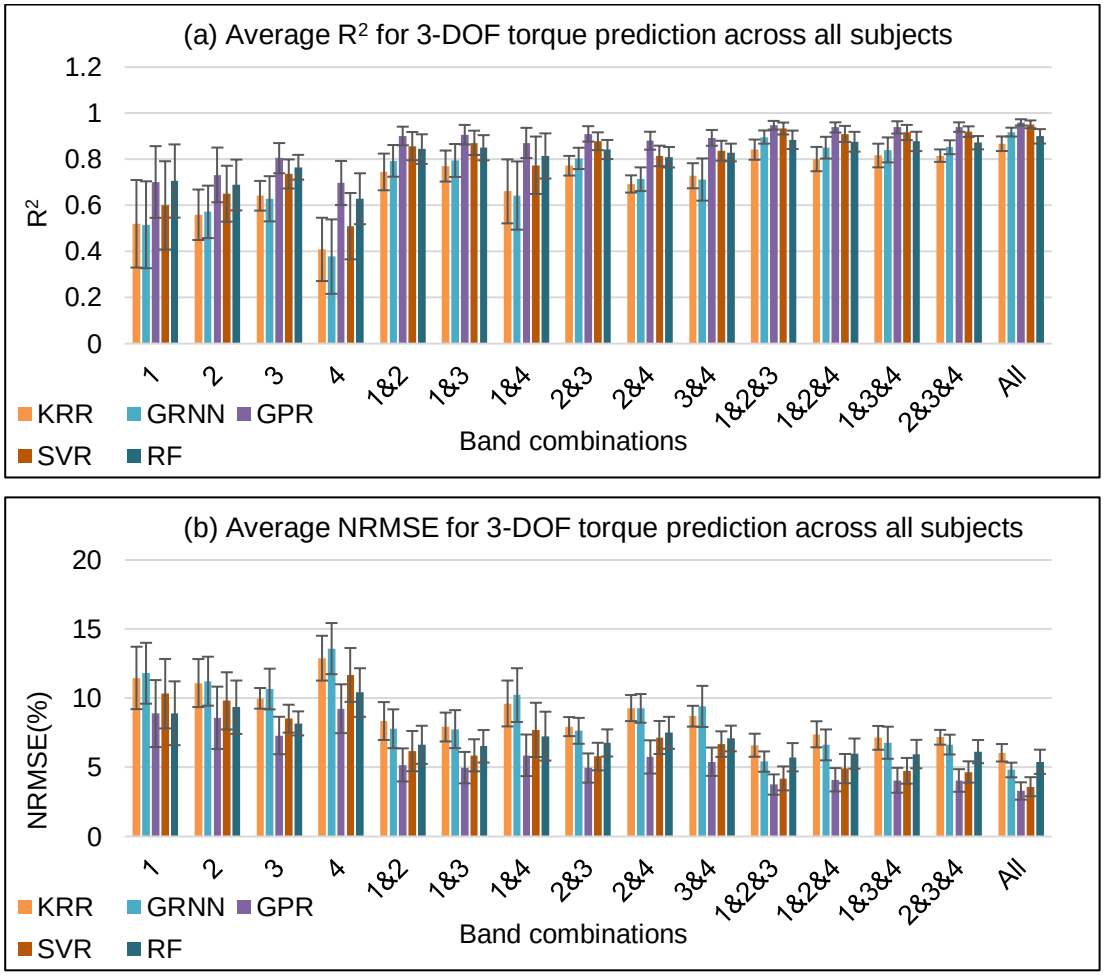

Figure 6.5. (a) The average R^2 across all subjects for torque prediction in X, Y, and Z in 10-fold cross validation. (b) The average NRMSE across all subjects for 3-DOF torque prediction in 10-fold cross validation.

Table 6.1. Three-way ANOVA for the cross-validation evaluation of 3-DOF force and torque estimation.

Significant Factor	Sum of Squared	Degrees of Freedom	Mean Squares	F	Probability
Band Combinations	15.6795	14	1.11996	147.34	1.48705e-263
Regression Algorithm	4.3524	4	1.08811	143.15	1.00659e-102
Component	0.5452	1	0.54517	71.72	6.14963e-17
Band Combinations * Regression Algorithm	0.9654	56	0.01724	2.27	4.82221e-07
Band Combinations * Component	0.4276	14	0.03054	4.02	7.39973e-07
Component * Regression algorithm	0.4463	4	0.11158	14.68	9.41512e-12
Error	10.6871	1406	0.0076		
Total	33.1035	1499			

Three-way analysis of variance (ANOVA) was performed to examine the effect of the three independent variables: regression algorithm, band combinations, and the component (force or torque) to the dependent variable of the estimation accuracy R^2. The significant factors at $p < 0.05$ for regression algorithm, band combinations, component and their intersections are shown in **Table 6.1** The table also shows the sum of squares (i.e., squared residuals from the average), the degrees of freedom, the mean square (sum of squares divided by the degrees of freedom) and the test statistics for each factor. For the test statistics, the value of the test statistic F and the probability that the variable variance is due to chance are reported. The three-way ANOVA showed the significant effects of bands combination ($F_{14, 1406} = 147.34$, $p < .00001$), regression algorithm ($F_{4, 1406} = 143.15$, $p < .00001$) and the component ($F_{1, 1406} = 71.72$, $p < .00001$) to the estimation accuracy R^2 for the cross-validation evaluation. In addition, the interaction between the band combinations and regression algorithm is statistically significant ($F_{56, 1406} = 2.27$, $p < .00001$), the interaction between the band combinations and the component is statistically significant ($F_{14, 1406} = 4.02$,

$p < .00001$), and the interaction between the component and the regression algorithm is statistically significant ($F_{4, 1406} = 14.68$, $p < .00001$) to the prediction accuracy R^2.

The Post Hoc test (Tukey HSD) on the effect of band combinations showed that the accuracy of using the 4 bands together was significantly higher ($p < .00001$) than those of using single-, and double -band combinations. While there was no significant difference between the accuracy using all 4 bands and all triple-band combinations. The accuracies of all triple-band combinations were significantly higher ($p < .001$) compared to using single- or double-band except the combination of bands 1 and 3, and the combination of bands 2 and 3. However, there was no significant difference between any of the 4 triple-band combinations. The accuracies of the 6 combinations of double-band were significantly higher ($p < .00001$) than the accuracies using single-band except the combination of bands 1 and 4 which was not significantly different of band 3. Among the 4 single positions, band 3 was significantly higher ($p < .00001$) than all other band positions, which confirms that the band on the forearm muscle belly (band 3) is the best for isometric force/torque sensing.

The Post Hoc test (Turkey HSD) on the effect of regression algorithm to the estimation accuracy R^2 showed that using the GPR was significantly higher ($p < .00001$) than all other regression algorithm. Also, DF was significantly higher ($p < .00001$) than KRR, GRNN and SVR. Furthermore, KRR was significantly lower than ($p < .05$) all other algorithms. These algorithms can be ordered from the highest accuracy to the lowest as follows: GPR, RF, SVR, GRNN and KRR.

The Post Hoc test (Turkey HSD) on the effect of the component (force or torque) to the estimation accuracy R^2 showed that 3-DOF force prediction was significantly higher ($p < .00001$) than 3-DOF torque prediction.

The second evaluation was the cross-trial where one trial was saved each time for testing purpose and the remaining 4 trials was used for training the regression algorithm. GPR algorithm showed the highest accuracy among all regression algorithms for both force and torque prediction in 3-DOF in cross-validation evaluation, that is why we used the GPR only in the cross-trial evaluation. The degradation in the cross-trial accuracies compared to the cross validation is because the data was not consistent between different trials. **Figure 6.6** shows the average R^2 and NRMSE across all participants for the cross-

trial evaluation using GPR. It is clearly shown that cross-trial shows the same trend as cross-validation in terms of increasing the spatial coverage of the FMG measurements enhance the prediction accuracy for both force and torque. Similar to cross-validation results, band 3 achieved an average accuracy of 0.60 ± 0.10 and 0.58 ± 0.06 for force and torque in 3-DOF respectively and the NRMSE of 11.55 ± 1.11 % and 11.66 ± 1.26% for force and torque in 3-DOF respectively. Using the combination of bands 1 and 3, the accuracy significantly improved to 0.70 ± 0.10 and 0.69 ± 0.08 for 3-DOF force and torque, respectively. Using triple-band combination enhanced the accuracy to 0.77 ± 0.08 and 0.76 ± 0.06 for 3-DOF force and torque, respectively using the combination of bands 1, 2

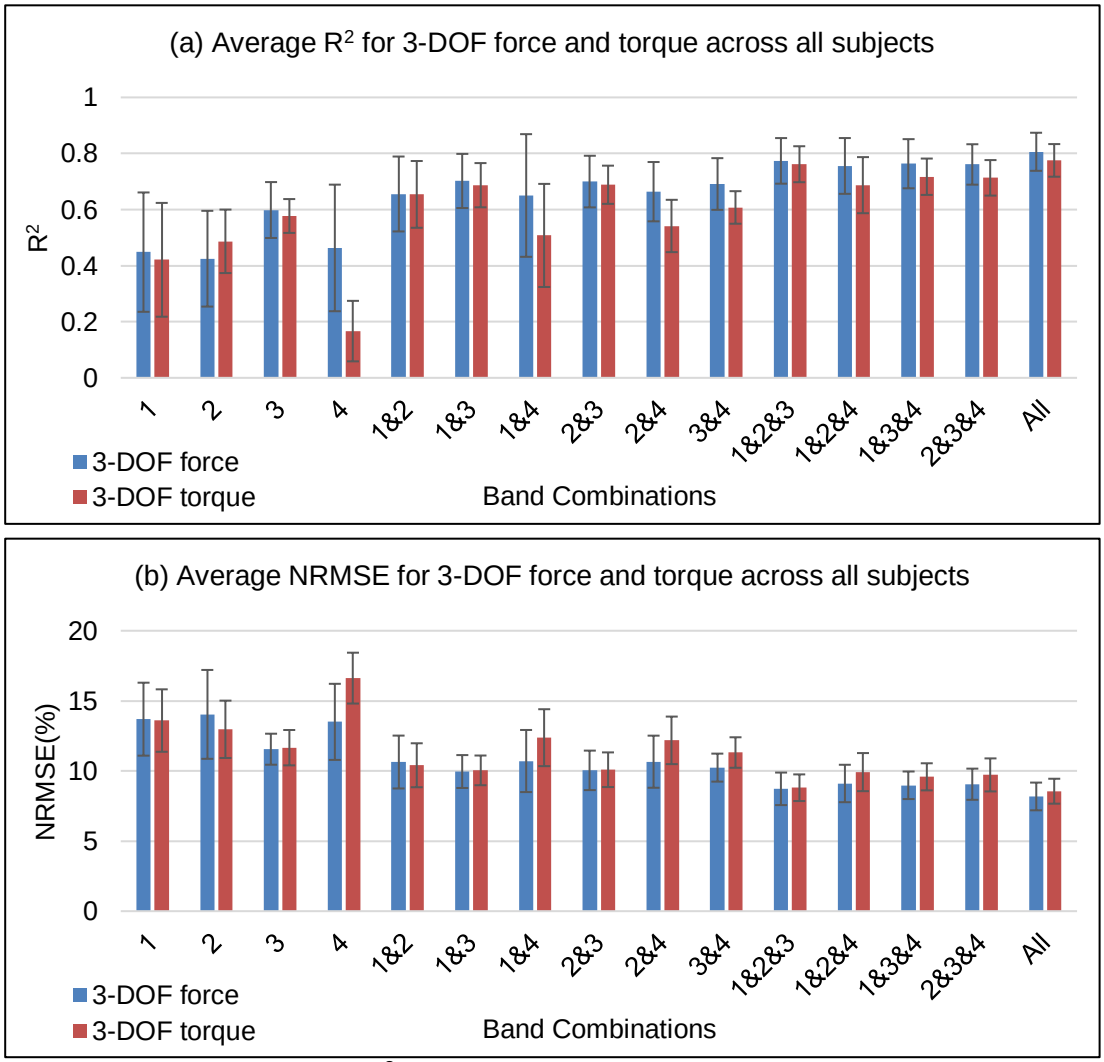

Figure 6.6. (a) The average R^2 across all subjects for the cross-trial using GPR for the 3-DOF force and torque prediction. (b) The average NRMSE across all subjects for the cross-trial of 3-DOF force and torque prediction.

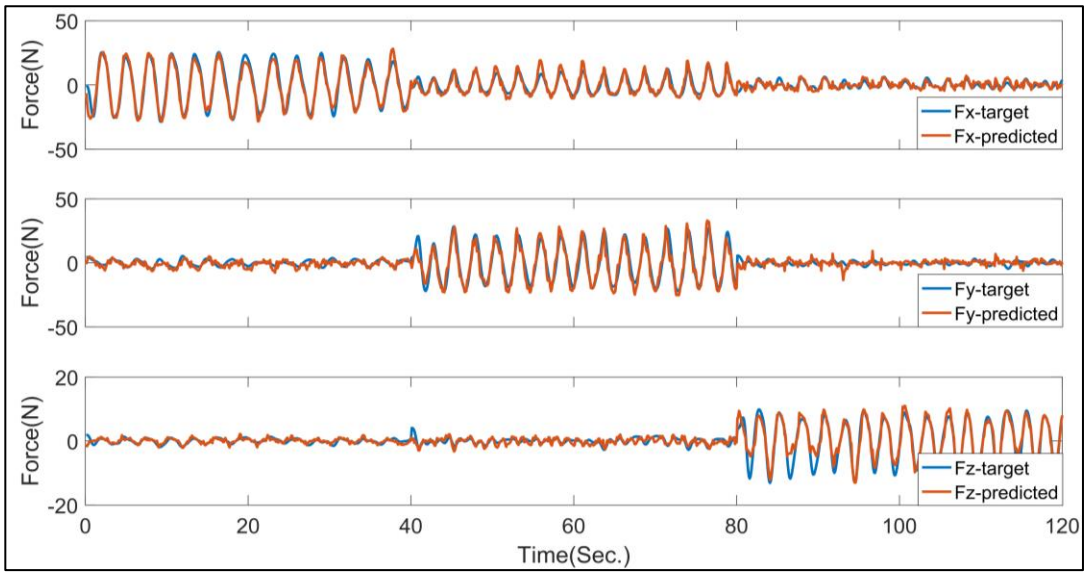

Figure 6.7. An example of 3-DOF force prediction using GPR in cross-trial evaluation.

and 3. Upgrading to 4 bands, the accuracy boosted to 0.81 ± 0.07 and 0.78 ± 0.06 for 3-DOF force and torque, respectively, while the NRMSE decreased to 8.73 ± 1.16 % and 8.80 ± 0.95 %.

Figure 6.7 shows an example of 3-DOF force prediction in X, Y and Z axes using GPR in cross-trial evaluation. This figure was generated using the data from participant 3 when the last trial was used for testing while the first 4 trials were used for training. The accuracy R^2 of this trial was 0.89. It is clearly shown that the GPR model successfully captured the relation between the FMG signals and the force in multi-axis all at once.

Two-way analysis of variance (ANOVA) was performed to examine the effect of the two independent variables: the band combinations and the component (force or torque) to the dependent variable of the accuracy R^2. The significant factors at $p < 0.05$ for band combinations and force/torque axis are shown in **Table 6.2**. The table shows the sum of squares (i.e., squared residuals from the average), the degrees of freedom, the mean square (sum of squares divided by the degrees of freedom) and the test statistics for each factor. For the test statistics, the value of the test statistic F and the probability that the variable variance is due to chance are reported. The two-way ANOVA showed both

Table 6.2. Two-way ANOVA for the cross-trial evaluation of 3-DOF force and torque estimation.

Significant Factor	Sum of Squared	Degrees of Freedom	Mean Squares	F	Probability
Band Combinations	5.17928	14	0.36995	25.32	0
Component	0.24931	1	0.24931	17.06	0
Band Combinations * Component	0.47983	14	0.03427	2.35	0.0045
Error	3.9449	270	0.01461		
Total	9.85331	299			

significant effects of the band combinations ($F_{14, 270} = 25.32$, $p < .00001$) and the component ($F_{1, 270} = 17.06$, $p < .00001$) to the estimation accuracy R^2 for the cross-trial evaluation using GPR. In addition, the interaction between the band combinations and the component (force or torque) was statistically significant ($F_{14, 270} = 2.35$, $p < .005$) to the prediction accuracy R^2.

The Post Hoc test (Tukey HSD) on the effect of band combinations showed that the accuracy of using all 4 bands was significantly higher ($p < .05$) than the all other single-, and double-band combinations except the combination of bands 1 and 3, and the combination of bands 2 and 3. While there was no significant difference between the usage of 4 bands and all triple-band combinations. In addition, all double-band combinations were significantly higher ($p < .05$) than all single-band except the combination of bands 1 and 4 which was not significantly different from band 2 and band 3. Finally, band 3 was significantly higher ($p < .05$) than all other single-band positions.

The Post Hoc test (Turkey HSD) on the effect of the component (force or torque) to the estimation accuracy R^2 showed that 3-DOF force prediction was significantly higher ($p < .00001$) than 3-DOF torque prediction.

6.6. Chapter Summary

In this chapter, the feasibility of using FMG signals to predict 3-DOF hand force/torque was explored. Two studies were carried out: the first one was a preliminary

investigation where a 1-DOF torque sensor was used for data collection and the second one was more realistic where a 6-DOF load cell was used for data collection of multi-axis force/torque. Furthermore, five regression algorithms were used to find the best model based on the prediction accuracy R^2 and the NRMSE. In the first study, the FMG data was collected from a single-band on the forearm muscle belly and 1-DOF torque sensor was used for labeling the data for 3 wrist deviations: pronation-supination, flexion-extension and radial-ulnar. Then a regression model was created to predict the torque around 3-axis all at once using the FMG signals. The main limitation of the first study was the usage of 1-DOF torque sensor to capture multi-axis torque which is not efficient. Instead, 6-DOF load cell was used in the second study to collect hand force/torque in multi-axis simultaneously. In addition, towards finding the best placement and band(s) combination within four landmarks, 4 FMG bands were placed on the arm: the wrist, the forearm midway, the forearm muscle belly, and the upper arm. After that, a regression model was created for force prediction in 3-DOF together and another model was created for 3-DOF torque prediction. Also, both the force and torque models were trained using the FMG data from all possible combinations of the four bands to find the best band(s) combination. The results showed that the prediction accuracy using triple-band increased with an average of 0.09 and 0.15 for 3-DOF force and torque, respectively compared to single-band in cross-validation evaluation and 0.17 and 0.18 in cross-trial evaluation for 3-DOF force and torque, respectively. While the usage of the 4 bands increased the accuracy slightly by 0.01 for both force and torque in cross-validation evaluation, however in cross-trial evaluation the accuracy increased by 0.04 and 0.02 for force and torque, respectively compared to triple-band combination. These results suggested that triple-band may be sufficient for force and torque prediction in 3-DOF. In addition, the combination of bands 1, 2, and 3 (on the wrist, on the forearm midway and on the forearm muscle belly) achieved the highest accuracy among all triple-band combinations. While the combinations that has band 4 (on the upper arm) as one of its items, has lower accuracy.

Chapter 7.

Feasibility of Using Force Myography (FMG) for 6-DOF Force/Torque Estimation

7.1. Chapter Overview

The work described in this chapter addresses part of **Objectives 2 and 3** of this work. The first study is about exploring the feasibility of using FMG based system to predict hand force/torque in 6-DOF. This is an extensive study related to **Objective 2.** While the second study is about finding the best band combinations placement within 4 landmarks for accurate hand force/torque prediction, this addresses part of **Objective 3** of this work. This chapter starts with a study overview in **Section 7.2**, followed by a briefly description of the methodology in **Section 7.3. Section 7.4** follows with a presentation of the results. Finally, a summary of this chapter is provided in **Section 7.5.**

7.2. Study Overview

The purpose of this study was to explore the viability of using one FMG-based model to predict the force/torque in 6-DOF simultaneously. The data for the hand force/torque in 6-DOF and the FMG signals were collected from 10 participants for 5 trials. In each trial, there were 6 sessions for intentionally exerting force/torque in single-axis at a time and 1 session for exerting force/torque freely in any axis or combinations of axes. 4 FMG bands were used to capture the FMG signals from 4 positions: the wrist, the forearm midway, the forearm muscle belly, and the upper arm. Towards finding the best placement of the FMG measurements within 4 landmarks, the regression model was trained using all possible band(s) combinations. Then, a comparison among all resultant models was performed based on the accuracy R^2 and the NRMSE to find the best placement within these 4 positions. In addition, two experiments were carried out: 10-fold cross-validation and cross-trial.

7.3. Methods

7.3.1. Participants

The data used in this chapter were collected from the participants with their demographics previously described in **Section 5.3.2**.

7.3.2. Experimental Protocol

An experimental protocol was designed to collect the FMG signals and the exerted 6-DOF force/torque data for evaluating the feasibility of using FMG to predict isometric hand forces and torques. Moreover, finding the best band(s) combination on the arm within 4 placement locations. The experimental protocol was previously described in **Section 4.4.2.**

The motivation behind focusing on one direction on a time in some sessions in each trial is for the purpose to be easy-to-follow and to cover a relatively full range of each force/torque direction. After that, a free-degree session was done where the participant exerted forces and torques freely in any direction. However, the forces and torques recorded by the 6-DOF load cell show that there are usually more than one degree of force/torque active at the same time even the participant intentionally focused on one direction. **Figure 7.1-a** shows an example of data from subject 7 during sessions where the participant focused on exerting force in one axis X, Y or Z at a time. The force values in X, Y and Z axes were considered as the coordinates of the points in the figure. It is shown that the points from the trial of focusing on one axis (e.g. X axis) has the largest value in X-axis and small values in the remaining axes (Y and Z axes) not zeros. While **Figure 7.1-b** represents an example of the free-degree sessions, where the participant exerted force/torque freely in all axes. It is noticeable that the points are distributed among all three axes as the participant did not focus on a specific axis. Moreover, it is hard to purely separate between different directions while exerting force/torque e.g. wrist flexion-extension and wrist radial-ulnar as in [119]. This phenomenon repeated during all data collection sessions, and was also reported in Kamavuako et al. [120]'s work. In addition, we choose the sinusoidal wave to be the pattern of the exerted forces/toques to cover a relatively full range of each force/torque direction.

(a)

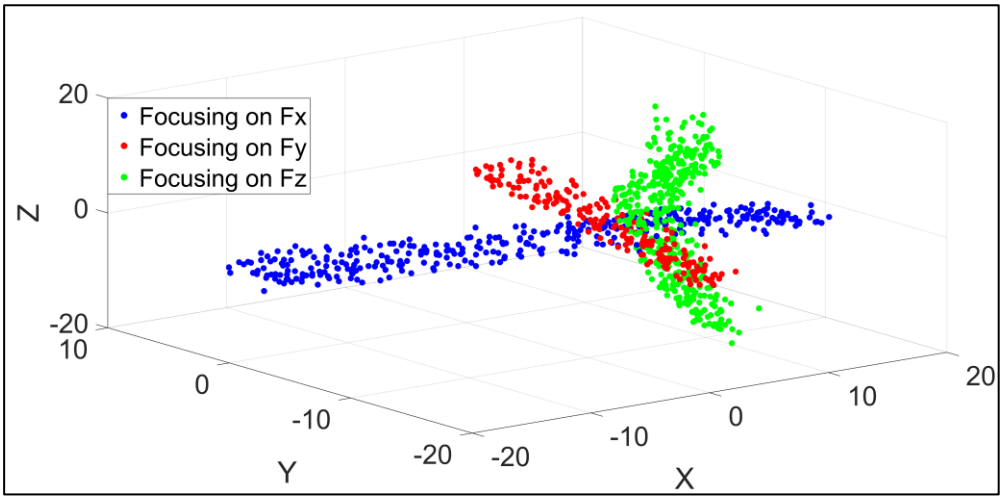

(b)

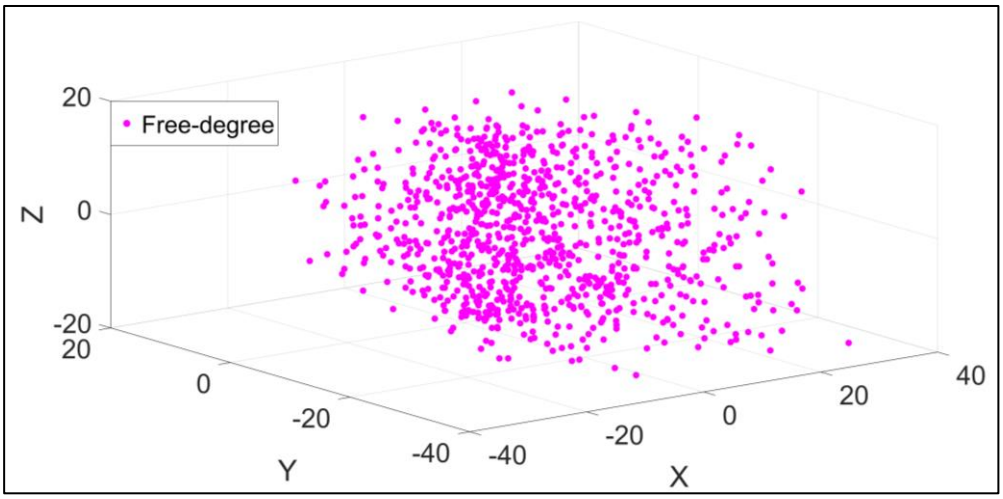

Figure 7.1. An example of the force values in X, Y and Z that participant 7 exerted in few sessions. The coordinates of each point are the force values in 3-DOF. (a) Represents the sessions at which the participant focused on exerting force in one axis at a time. (b) Represents the sessions at which the participant exerted force freely in all axes.

7.4. Results

The data were successfully collected from all 10 participants for five trials, except the last trial of subject 6. This trial was excluded due to the band slipping during the data collection. Thus, there were a total of 14,000 data points for each participant (5 trials times 6 specific axes and 1 free 6-DOF sessions, 400 samples on each session). For subject 6, the data included only 12,000 samples and the cross-trial was conducted in 4-fold and the average accuracy was from only four trials. During the data collection sessions, some participants reported feeling slightly fatigue in their arm muscles and rested their hands between the sessions for a few minutes.

Figure 7.2 shows a sample data of the normalized FMG signals from the band 3 from participant 2 data and the exerted force and torque in X, Y and Z simultaneously. It is shown that the FMG signals have a correlated pattern like that of forces and torques. After preprocessing the data, the data was fed to the regression models to find the best regression model among five machine learning algorithms. In addition, all possible band combinations were considered to find the best band(s) combination for 6-DOF force/torque prediction. In the first experiment which is 10-fold cross validation, the data from all sessions of focusing on a specific axis at a time and the free-degree were combined and randomly divided into ten permutations. Each time the model was trained using 9 subsets while the remaining subset was saved for testing the model. **Figure 7.3** shows the average performance measures (R^2 and NRMSE) for the 10-fold cross validation of the 6-DOF force/torque prediction, averaged across all participants using Kernel Ridge Regression (KRR), General Regression Neural Network (GRNN), Gaussian Processes Regression (GPR), Support Vector Regression (SVR), and Random Forest (RF). It is clearly shown that increasing the spatial coverage of FMG measurements from a single FMG band to combinations of FMG bands worn on multiple arm positions resulted in significant growth in the regression accuracies. Compared to individual axes of force/torque and 3-axis force and torque results, relatively lower accuracies were achieved for 6-DOF force/torque prediction. This is because increasing the number of outputs to 6-DOF space, a much more complex model is needed to be trained with more samples and features to predict the 6-DOF force/torque accurately [108]. From **Figure 7.3**, it is shown that GPR still achieves the highest accuracy among all regression algorithms with any band combination. While using other regression algorithms declined the accuracy with an

(a)

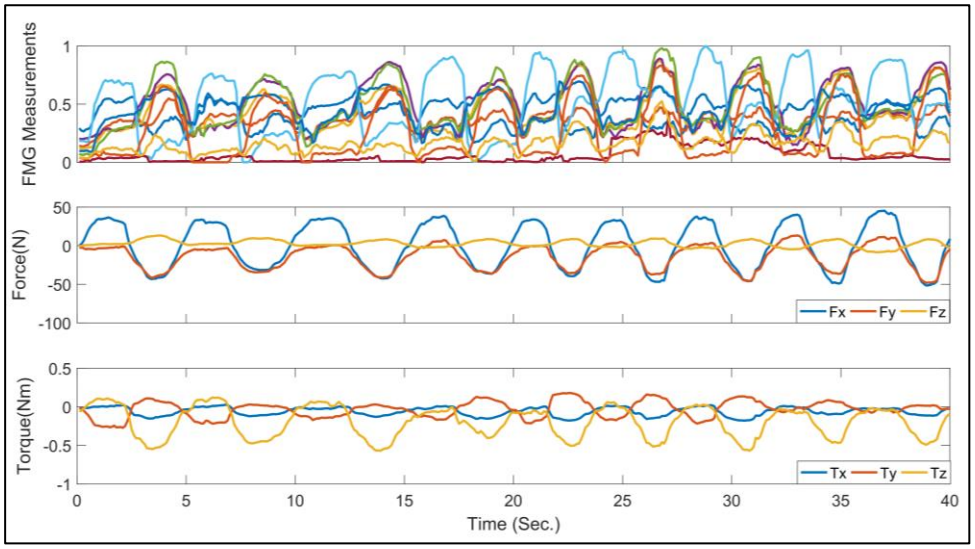

(b)

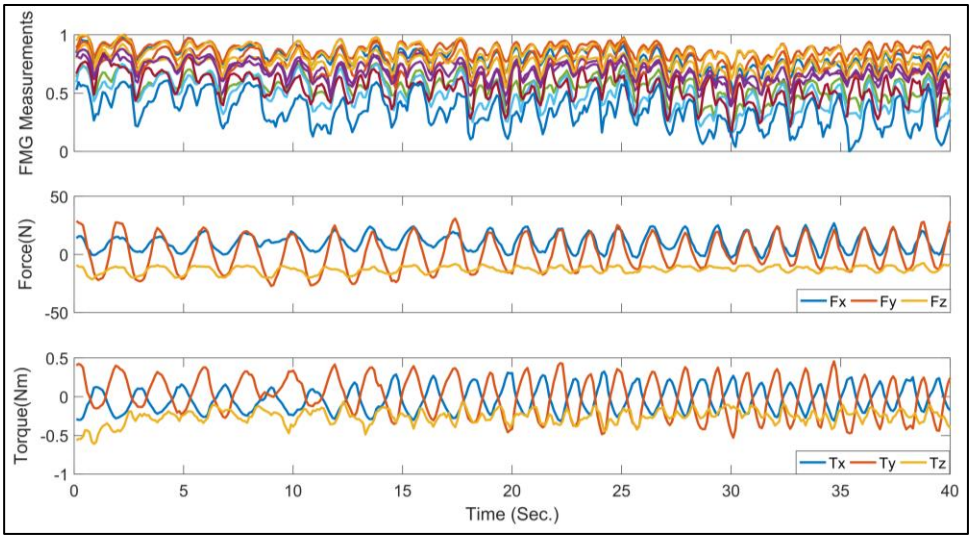

Figure 7.2. (a) A sample of a highly estimation accuracy data of the normalized FMG signals from band 3 vs the exerted force in X, Y and Z, and the exerted torque around the same axes. This sample from subject 2 data. (b) A sample of a lower estimation accuracy data of the normalized FMG signals from band 3 vs the exerted force and torque in X, Y and Z axes, this sample from subject 5 data.

average of 0.18, 0.14, 0.08, and 0.05 using KRR, GRNN, SVR, and RF, respectively, compared to GPR. Among the four landmarks, the band on the forearm muscle belly (band 3) still achieves the highest accuracy of 0.76 ± 0.04 and the NRMSE is 6.47 ± 1.04 %. Considering double-band combinations, the accuracy surged to 0.89 ± 0.03 using the

combination of bands 2 and 3. While the other double-band combinations achieved a similar accuracy of 0.86 ± 0.05, 0.88 ± 0.05, 0.86 ± 0.08, 0.87 ± 0.05, and 0.88 ± 0.05 using the combinations of bands 1 and 2, bands 1 and 3, bands 1 and 4, bands 2 and 4, and bands 3 and 4, respectively. Upgrading the number of the considered bands to three, the accuracy increased to 0.94 ± 0.02 and the NRMSE declined to 3.15 ± 0.98 %using the combination of bands 1, 2, and 3. While the other triple-band combinations achieved a lower accuracy of 0.91 ± 0.02, 0.88 ± 0.02, and 0.92 ± 0.05, using the combinations of bands 1, 2, and 4, bands 1, 3, and 4, and bands 2, 3, and 4, respectively. Using all bands

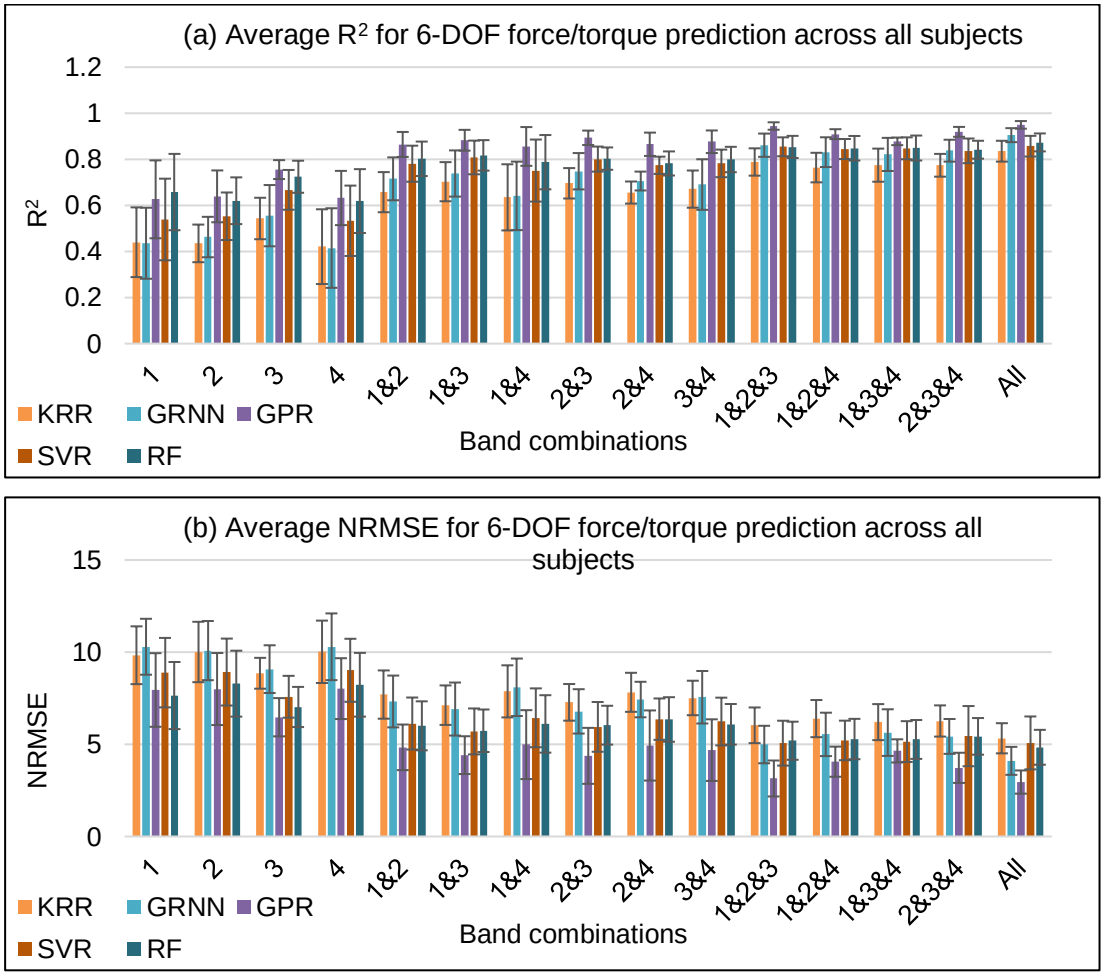

Figure 7.3. (a) The average R^2 across all subjects for 6-DOF force/torque prediction in 10-fold cross validation. (b) The average NRMSE across all subjects for 6-DOF force/torque prediction in 10-fold cross validation. Using Kernel Ridge Regression (KRR), General Regression Neural Network (GRNN), Gaussian Processes Regression (GPR), Support Vector Regression (SVR), and Random Forest (RF).

achieved the highest accuracy among all combinations with an average accuracy of 0.95 ± 0.02 and the lowest NRMSE of 2.95 ± 0.63 %.

Two-way analysis of variance (ANOVA) was performed to examine the effect of the two independent variables: the band combinations and the regression algorithm to the dependent variable of the accuracy R^2. The significant factors at $p < 0.05$ for band combinations and force/torque axis are shown in **Table 6.2**. The table shows the sum of squares (i.e., squared residuals from the average), the degrees of freedom, the mean square (sum of squares divided by the degrees of freedom) and the test statistics for each factor. For the test statistics, the value of the test statistic F and the probability that the variable variance is due to chance are reported. The two-way ANOVA showed both significant effects of the band combinations ($F_{14, 675} = 94.15$, $p < .00001$) and the regression algorithm ($F_{4, 675} = 97.15$, $p < .00001$) to the estimation accuracy R^2 in the cross-validation evaluation. In addition, the interaction between the band combinations and the regression algorithm was marginally significant ($F_{56, 675} = 1.37$, $p < .05$) to the prediction accuracy R^2.

The Post Hoc test (Tukey HSD) on the effect of band combinations showed that the accuracy of using all four bands was significantly higher ($p < .00001$) than the all other single-band and double-band combinations. While there was no significant difference between the four bands together and all triple-band combinations In addition, there was no significant difference between neither all triple-band combinations nor all double-band combinations. Moreover, there was no significant difference between the double-band combinations of: bands 1 and 3, and bands 2 and 3 and triple-band combinations of: bands 1, 2, and 4, bands 1, 3, and 4, and bands 2, 3, and 4. For single-band results, band 3 was significantly higher ($p < .00001$) than band 1, band 2, and band 4. Whereas, there was no significant difference between band 1, band 2, and band 4.

The Post Hoc test (Turkey HSD) on the effect of regression algorithm to the estimation accuracy R^2 showed that using the GPR was significantly higher ($p < .00001$) than all other regression algorithm. Also, DF was significantly higher ($p < .05$) than KRR, GRNN and SVR. Furthermore, KRR was significantly lower than ($p < .01$) all other

algorithms. These algorithms can be ordered from the highest accuracy to the lowest as follows: GPR, RF, SVR, GRNN and KRR.

The second experiment, cross-trial evaluation was motivated by studying the data consistency across different trials and also it is closer to the real situation [65]. In the cross-trial evaluation, the number of validation cycles is the same as the number of repetitions defined in the experiment. In each cycle, one repetition of data that has not been tested will be kept as the testing set, and the rest of data is used as training set. **Figure 7.6** represents the average R^2 and NRMSE for cross-trial averaged across all participants using GPR, as it achieved the highest accuracy in cross-validation evaluation. The resulting accuracy concludes the same trend as cross-validation in increasing the spatial coverage of the FMG results in improving the prediction accuracy and declining the error. The degradation in the cross-trial accuracies compared to the cross validation is because the data was not consistent between different trials and the data was not shuffled as in cross-validation evaluation. Agreed with the cross-validation analysis, using the all bands achieves the peak accuracy with a median of 0.75 ± 0.05 and the NRMSE has a median of 7.71 ± 0.73 %. Decreasing the bands used to 3, the accuracy decreased to 0.70 ± 0.07 and the NRMSE slightly increased to 7.96 ± 0.84 % using the combination of bands 1, 2 and 3 which has the highest accuracy among all triple-band combinations. In addition, using double-band combinations also declined the accuracy significantly to 0.62 ± 0.07 and the NRMSE increased to 8.99 ± 0.88 % using combination of bands 1 and 3 which

Table 7.1. Two-way ANOVA for cross-validation evaluation of 6-DOF force/torque.

Significant Factor	Sum of Squared	Degrees of Freedom	Mean Squares	F	Probability
Band Combinations	10.238	14	0.73129	94.15	0
Algorithm	3.034	4	0.75851	97.15	0
Band Combinations * Algorithm	0.598	56	0.01068	1.37	0.0403
Error	5.2429	675	0.00777		
Total	19.113	749			

has the highest accuracy among all double-band combinations. Using single-band, band 3 is the best among all single-band. However, the accuracy dropped down to 0.49 ± 0.08 and the NRMSE is 10.38 ± 0.74 %.

(a)

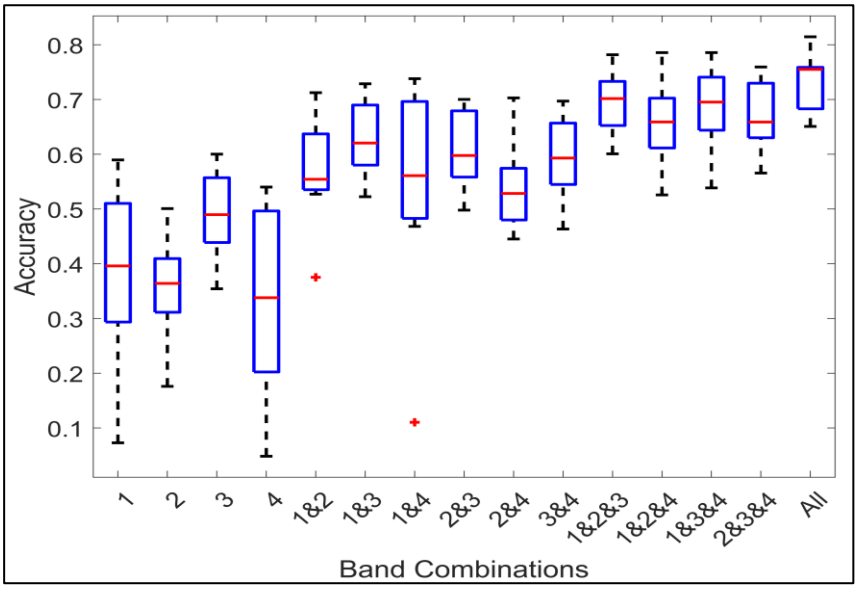

(b)

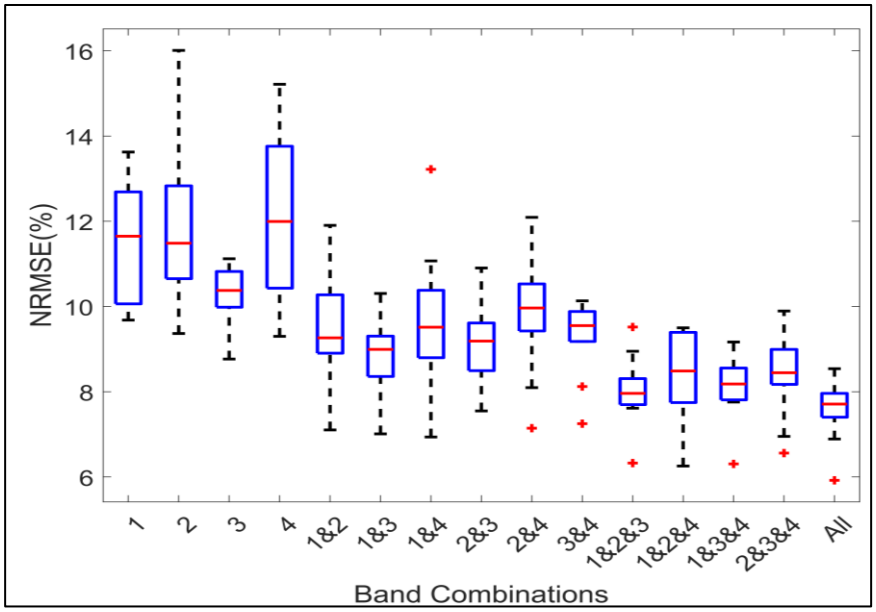

Figure 7.4. (a) The average 6D R^2 across all participants for the cross-trial using GPR (b) The average 6D NRMSE across all participants for the cross-trial using GPR.

Figure 7.5-a shows an example of a good estimation for the force/torque in 6-DOF using all 4 bands from testing one trial from the data of subject 3. The 6D R^2 for this trial is 0.84. On contrary, **Figure 7.5-b** shows an example of a poor estimation with 6D R^2 of 0.63 from testing the model with the third trial of the subject 5 data. In addition, **Figure 7.5**

(a)

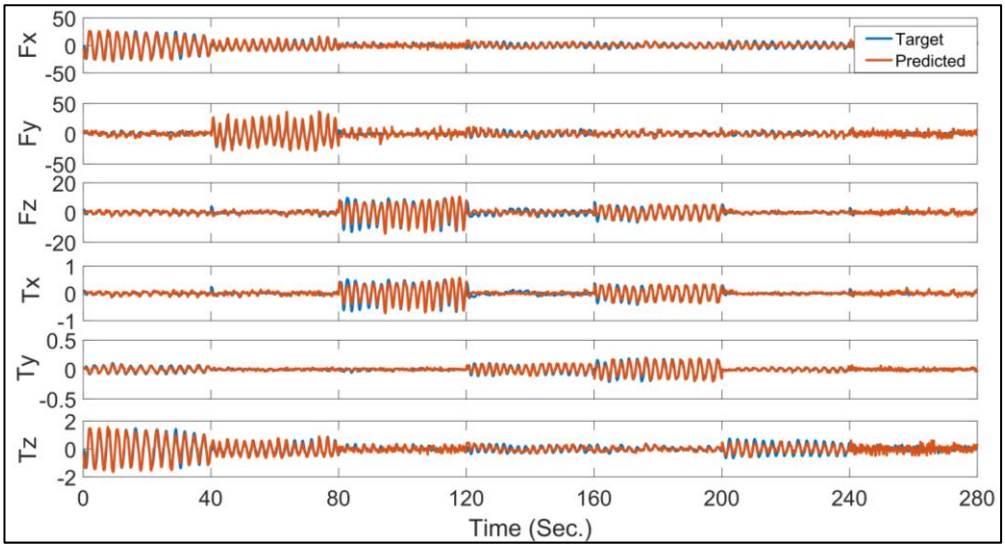

(b)

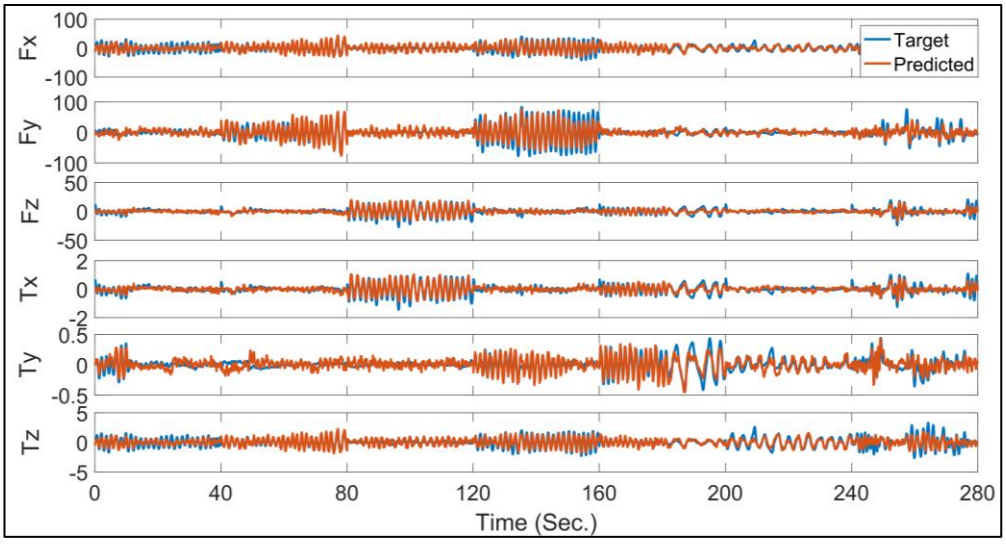

Figure 7.5. (a) An example of the best performance on the force/torque estimation for one trial from the data of subject 3 where all 4 bands were used. (b) A sample of the worst performance. The forces in both charts are in Newton while the torques are in Nm.

shows the order of exerting force/torque on each axis, specifically, in the last part (from 240 to 280) shows the free-degree as the participant exerts force/torque freely in any axis.

One-way analysis of variance (ANOVA) was performed to examine the effect of the independent variable of band combinations to the dependent variable of the accuracy R^2. The significant factors at $p < 0.05$ for band combinations are shown in **Table 7.2**. The table shows the sum of squares (i.e., squared residuals from the average), the degrees of freedom, the mean square (sum of squares divided by the degrees of freedom) and the test statistics for each factor. For the test statistics, the value of the test statistic F and the probability that the variable variance is due to chance are reported. The one-way ANOVA showed significant effect of the band combinations ($F_{14,\ 135} = 14.97$, $p < .00001$) to the estimation accuracy R^2 for the cross-trial evaluation using GPR.

The Post Hoc test (Tukey HSD) on the effect of band combinations showed that the accuracy of using all 4 bands was significantly higher ($p < .05$) than the all other single-, and double-band combinations except the combinations that has band 3 as one of its components: combination of bands 1 and 3, combination of bands 2 and 3, and combination of bands 3 and 4. While there was no significant difference between all triple-band combinations and all double-band combinations. In addition, all double-band combinations were significantly higher ($p < .05$) than all single-band except band 3. However, combination of bands 2 and 4 was not significantly higher than band 3 and band 1 as well. Finally, band 3 was significantly higher ($p < .05$) than band 4, while there was no significance difference between band 3 and either band 1 or band 2.

Table 7.2. One-way ANOVA for cross-trial evaluation of 6-DOF force/torque estimation.

Significant Factor	Sum of Squared	Degrees of Freedom	Mean Squares	F	Probability
Band Combinations	2.22601	14	0.159	14.97	3.20865e-21
Error	1.43363	135	0.01062		
Total	3.65964	149			

7.5. Chapter Summary

In this chapter, the usability of FMG for estimating hand force/torque in 6-DOF was studied. The data was collected from 10 healthy participants. Four FMG bands were donned on the participant's arm in four positions: wrist, forearm midway, forearm muscle belly, and upper arm. 6-DOF force/torque load cell was used for labeling the FMG data. The data was collected for five trials, in each one, the participant exerted force in X, Y, and Z axes and torque around the same axes sequentially. Then, the participant was asked to exert force/torque freely in any direction which was called 'free-degree session'. Five regression algorithms were used to create an FMG-based model to predict hand force/torque in 6-DOF simultaneously: kernel ridge regression (KRR), general regression neural network (GRNN), Gaussian processes regression (GPR), support vector regression (SVR) and random forest (RF). Towards finding the best band(s) combination among the four bands used, the regression model was trained and tested using all possible band combinations and a comparison between them was held based on the resultant accuracy. Two experiments were carried out: 10-fold cross-validation and cross trial. In 10-fold cross, validation, the data from all trials with the free-degree session were combined and divided randomly into 10 permutations, in each validation cycle, one permutation was saved for testing the model while the other nine permutations were used for training the model. The average accuracy in cross-validation evaluation using the four bands was 0.84 ± 0.05, 0.90 ± 0.03, 0.95 ± 0.02, 0.86 ± 0.04 and 0.87 ± 0.04 using KRR, GRNN, GPR, SVR, and RF, respectively. While the accuracy declined dramatically when using the data from single band to 0.54 ± 0.09, 0.56 ± 0.13, 0.76 ± 0.04, 0.67 ± 0.09, and 0.72 ± 0.07, using KRR, GRNN, GPR, SVT, and RF, respectively.

In cross-trial evaluation, one trial was saved each time for testing the model while the other four trials were used for training the model. This was done five times as the data was collected for five trials. The average accuracy using all bands was 0.75 ± 0.05 with GPR as it achieved the highest prediction accuracy in cross-validation evaluation.

Chapter 8.

Discussion

8.1. Chapter Overview

This chapter provides a discussion about the results in all previous chapters. In addition, it provides some insights about the characteristics of the arm muscles that contribute for better understanding of the results and findings.

8.2. Results Discussion

The results showed the viability of employing FMG signals to estimate single- and multi-axis hand force/torque using different regression models. The FMG measurements on four landmarks on the arm demonstrates high accuracies in cross-trial evaluation of 0.86 averaged across the six force/torque axes, 0.81 and 0.78 in 3-DOF force and torque, respectively, and 0.75 in 6-DOF force/torque regression, averaged across the 10 participants using Gaussian processes regression (GPR) algorithm. These results from the present study introduce a potential of FMG in various applications. For instance, the FMG based technology could be employed in human robot collision detection [6], which will enable a ubiquitous and low cost solution for HRI safety through force/torque monitoring. In addition, in tele-assessments of home-based rehabilitation, this FMG-based wearable sensing technology offers a potential for simultaneous multi-DOF force/torque prediction instead of only using a downward axis wrist force detection [32].

Furthermore, towards provide guidelines for the FMG sensors placement on the arm for accurate prediction of hand force/torque in different axes, all band combinations were used for training the regression model and a detailed comparison between them was introduced in **Chapter 5**, **Chapter 6**, and **Chapter 7**. The comparison results showed that reducing the number of the bands worn on the arm decreases the accuracy by 0.05 and 0.12 for triple-band and double-band combinations, respectively compared to the accuracy using the four bands in 6-DOF force/torque prediction. This degradation in the accuracy along with reducing the number of FSR bands used affirms the previous finding

in [19]; that is, higher FSRs density increases the prediction ability. This suggests that only a single band on the arm might not be sufficient for the estimation of hand forces and torques especially with multi-axis.

When using a single band on the arm, band 3 on the forearm muscle belly achieves the best performance among the 4 positions, with average R^2 of 0.70 across the six axes individually, 0.60 and 0.58 in 3-DOF force and torque combinations, and 0.49 in 6-DOF force/torque regression; in contrast, band 4 on the upper arm achieved the worst performance either with single-axis or multi-axis prediction. This interesting finding suggests that the primary location for isometric hand force/torque sensing should be the forearm muscle belly, and the upper arm is not suitable for wrist torque sensing [121][18].

The characteristics and categories of the muscles during isometric hand force/torque exertion can help to explain the above phenomenon. First, band 3 achieves the highest accuracy because the muscles on the forearm muscle belly including anconeus, branchioradialis and pronator teres contribute actively to all the 6 axes isometric force/torque generation, due to the resistance from the object that the subject is pushing against [27]. Secondly, the exertion of the hand forces F_X, F_Y, and F_Z also involves the activation of the muscles on the upper arm, including long bicep brachii, short head bicep brachii, and brachialis muscles [122]. For instance, to exert hand force in X-axis, the participant might try to rotate the upper arm around the shoulder joint, and/or adduct/abduct the shoulder. Lastly, the wrist torques (T_X, T_Y, and T_Z) are mainly resulted from the contraction of the muscle on the forearm [27], which justify low accuracies of band 4 on the upper arm for torque sensing.

The above finding is further confirmed by the results from the double-band combinations. The combination of bands 2 and 3 performs the best among the six combinations of double-band, whereas the combination of bands 1 and 4 is the worst. This finding further reveals the fact that locations close to the forearm muscle belly is better for hand force/torque sensing and suggests that FMG density should be increased along the forearm widest part towards the lower forearm to effectively enhance the performance[123].

The force in Z axis (F_Z) is the most accurately estimated among the six force/torque dimensions, whereas the torque in X axis T_X (pronation-supination) shows the least

accurate estimation. However, even with the increased dimensions of force/torque estimation, which usually leads to increase the prediction difficulty, the 6D R^2 accuracy (R^2 = 0.75) is comparable to those of the studies with less dimension torque prediction, e.g. 3D wrist torque estimations [81]. Furthermore, during the data collection, we did not limit either the values of the exerted force/torque or the speed of force/torque exertion, e.g., by using a predefined visual chart to guide the force/torque exertion. This relatively freely exerted force/torque is usually more challenging to estimate compared to those using more constrained protocols [124][125][126]. In addition, some subjects rotated their elbow and/or adducted/abducted their shoulder slightly during the data collection which made the data inconsistent between different trials and possibly affected the accuracy. Moreover, some participants reported muscle fatigue during data collection and they rested their hand for a while before collecting the data for another session, but this may have an effect on the data consistency among different sessions [123]. Even with these challenges, the results from this study still show comparable accuracies. To our surprise, the T_X (pronation-supination) was well estimated compared to [124][127].

The experimental protocol was defined to instruct the participant to try exerting force/torque each time in one axis, for the purpose of ease and to cover a relatively full range of each force/torque axis in the first 6 sessions of each trial. However, the forces and torques recorded by the 6-DOF load cell show that there are usually more than one degree of force/torque active at the same time. **Figure 7.1-a** shows an example of three trials where in each trial, the participant (subject 7) intentionally exert force in one axis at a time, the figure represents the exerted force in 3 axes as the coordinates of the points. It is shown that the force in three axes always active even the intention is to focus on one axis at a time with the highest value in the axis which was intentionally desired and small values in the other axes. This justify why the points in the trial that focus on X-axis are concentrated around the X-axis and the same observation for the other axes. This phenomenon repeated during the rest segments, and was also reported in [120][119]. Also, the results from 3-DOF force and torque prediction showed that the FMG bands were able to capture the force and torque in multi-axis simultaneously fairly well with R^2 of 0.81 and 0.78, respectively.

Following the exertion on one direction at a time session, the participant was instructed to exert free 6-DOF force/torque which we called ‘free-degree session’. In the

free-session, the data distributed relatively to a 6D space, as shown in **Figure 7.1-b** an example of force visualization in 3D space. The performance of the FSR band decreased to R^2 of 0.75 for predicting 6-DOF force/torque when the free-degree sessions were included. However, this accuracy is still comparable to that of 2-DOF force estimation with R^2 0.78 in [124].

The GPR handled the multiple-axis force/torque prediction well. **Figure 7.5-a** shows an example of a good prediction from the cross-trial evaluation where the 6 axes force/torque were almost perfectly and simultaneously estimated. Mostly the mis-regression happens at the turn-around points of these sinusoidal waves, where the force/torque axis changes. In the worst trial as shown in **Figure 7.5-b**, the predicted force/torque curves are able to capture the pattern of the sinusoidal waves as the true label, but with more mismatch during these turn-around points. This might have referred to several reasons, as shown in **Figure 7.2-b,** the FMG signals from the forearm muscle belly band did not follow the sinusoidal pattern well compared to **Figure 7.2-a**. In addition, the participant exerted the force and torque very fast compared to the data from subject 2 in **Figure 7.2-a** which affect the prediction accuracy as proved in [128]. The number of peaks in the force/torque figure reflects the speed of the force/torque exertion.

Chapter 9.

Concluding Remarks

The aim of this thesis is to explore the viability of using FMG as an additional tool in human-machine interface for estimating hand force/torque, which is crucial for human safety during close interaction with the machines. Increasing the morbidity and disability associated with industrial work settings arise from accidents involving humans and machines, supports the exploration of FMG. FMG provide and easy-to-use and inexpensive technique for monitoring hand force that complement the direct force measurements which limit the human movements, and provide an alternative and potentially more advantageous sensing modality for human-machine interface. The literature review in **Chapter 2** showed a range of applications at which FMG has been successfully utilized. However, we were not able to find any work on hand force/torque estimation. Based on this review, this thesis has three objectives.

Objective 1 of this thesis was to introduce and explore the feasibility of using FMG to predict hand force/torque in single-axis. To meet this objective, a study was designed and executed to recruit healthy participants to exert isometric force/torque in six axes individually while recording the FMG signals. This study was done using two data acquisition systems which were described in **Section 4.3**, the systems were composed of two parts: FMG-based wearable band and force/torque load cell for labeling the data. The key difference between the two systems is the force/torque load cell, where the first acquisition system has 1-DOF torque sensor that needs a different setup each time to measure a new torque axis and one fabricated FMG band was used. The second acquisition system has a 6-DOF force/torque load cell which can measure the force and torque in X, Y and Z axes simultaneously using the same setup with four custom-designed FMG bands were used on the arm to measure muscle contraction. 17 participants were recruited in this study, seven participants in the first experiment using 1-DOF torque sensor, and 10 participants in the second experiment using 6-DOF force/torque load cell. The data was collected for three trials in the first experiment and for five trials in the second experiment. In the first experiment, the participants exerted torque in three deviations: pronation-supination, flexion-extension, and radial-ulnar. While in the second experiment,

the participants exert force in X, Y and Z axis and torque around the same axes sequentially. Five regression algorithms were used in both experiments to map between the FMG signals and the hand force/torque: kernel ridge regression (KRR), general regression neural network (GRNN), Gaussian processes regression (GPR), support vector machine (SVR), and random forest (RF), and a description of each algorithm was provided in **Chapter 3**. 10-fold cross-validation evaluation was used in both experiments. GPR achieved the highest accuracy among the five regression algorithms. The average accuracy across the three-wrist torque and participants in the first experiment was 0.89, while the average accuracy in the second experiment was 0.85 using one band on forearm muscle belly as in the first experiment. This difference between the average accuracies because in the first experiment the participant's arm was fixed to the rig using straps which decrease the possibility of elbow/shoulder movement. Contrarily in the second experiment, participant's arm was free that allow elbow/shoulder movements during data collection as discussed in **Chapter 8**. These results suggest the feasibility of using FMG for predicting isometric hand force/torque in single-axis.

Objective 2 of this thesis was to study the viability of using FMG for hand force/torque estimation in multi-axis at the same time. Towards achieve this objective, two studies were carried out and were described in **Chapter 6** and **Chapter 7**. The first study was to explore the feasibility of using FMG for hand force/torque estimation in 3-DOF. In the first study, two experiments were done: the first experiment provide a preliminary investigation of the usability of FMG for predicting multi-axis torque simultaneously. The data that was collected using 1-DOF torque sensor, were merged into one dataset where the FMG data was the input and the output was the torque values in three axes. One out of three outputs has a value, while the other two were zeros. In the second experiment, the data from the sessions of force exertion were combined in one data set, while the data from torque exertion sessions were combined into another one. It was shown that even the participant intentionally focusses in one axis at a time, there were always more than one axis has a value. Five regression algorithms were used also in these two experiments, and GPR also achieved the highest accuracy. The average accuracy in cross-validation evaluation in the first experiment was 0.91 of the three axes torque prediction. Whereas the average accuracy of 3-DOF force and torque prediction was 0.98, and 0.96, respectively. In this case the accuracy in the second experiment is higher than the

accuracy in the first experiment, as the data was collected using 6-DOF load cell which can measure the force/torque in multi-axis at the same time is the realistic case. Because we can not purely exert force/torque in one axis, there are always more than one axis active at a time. So, using 6-DOF load cell in data collection capture all axes together, while using 1-DOF torque sensor measure only one axis at a time.

The second study was about studying the feasibility of using FMG for hand force/torque estimation in 6-DOF. In the data collection sessions, the participants were instructed to exert force/torque in X, Y, and Z axes sequentially to have enough data for each axis and after that, they exerted force/torque freely in all directions for some sessions which was called 'free-degree session'. The regression model was trained using the data from focusing in one axis at a time as well as the free-degree. The average accuracy in cross-validation evaluation was 0.95 averaged across 10 participants. These results affirmed the usability of FMG for hand force/torque estimation in multi-axis simultaneously.

Objective 3 of this thesis was to provide guidelines about the FMG measurements placement on the arm for single- and multi- axis force/torque estimation. To achieve this objective, the experimental protocol was designed to have four FMG sensing bands, and were donned in four landmarks on the arm: the wrist, forearm midway, forearm muscle belly and upper arm. During all the studies in the thesis to explore the feasibility of using FMG for estimating hand force/torque, all possible band combinations were used to train and test the regression model. After that, using the resultant accuracy, we can compare between different placement positions. In single-axis force/torque estimation, the average accuracy was 0.85, 0.93, 0.96, and 0.97 using one, two, three, and four bands data. It is shown that even with single-band, the estimation accuracy is good and it increased gradually with the increase in the number of bands. In 3-DOF force estimation, the average accuracy increased from 0.88 using single-band to 0.98 using all bands. Similarly, in 3-DOF torque estimation accuracy, it started with an average on 0.80 using single-band and surged to 0.96 using all bands. In addition, in 6-DOF force/torque estimation, increasing the number of bands contributed significantly in improving the accuracy as follows: 0.76, 0.89, 0.94, and 0.95 using single, double, triple and all bands. Furthermore, the band of the forearm muscle belly achieved the highest accuracy among all positions in any experiment, which suggests that the primary location for force/torque sensing is the forearm muscle belly. These results provide guidelines for FMG measurements placement

on the arm for force/torque estimation. Also, the results showed that single-band might be enough for single-axis force/torque sensing, while increasing the number of axes need more bands to have muscles information from different positions.

The results of this thesis provide preliminary confirmation of the feasibility of using FMG for isometric force/torque estimation in single- and multi- axis. In addition, this work has also identified the effect of FMG measurements placement on the force/torque estimation accuracy. This work lays the ground work for investigating FMG and its implementation for hand force/torque estimation to be an additional source of information in human-machine interfaces.

Chapter 10.

References

[1] Data & Analysis Section, *Work-related Injuries Resulting in Hospitalisation*. 2013.

[2] M. D. Backstrom, T., “Moving Parts of Machines,” *Encyclopedia of Occupational Health and Safety. Geneva: International Labor Organization*. 2011.

[3] F. E. M. Nelson, Nancy A., Robert M. Park, Michael A. Silverstein, “Cumulative Trauma Disorders of the Hand and Wrist in the Auto Industry,” *Am. J. Public Health*, vol. 82, no. 11, pp. 1550–1552, 1992.

[4] G. Schöner, “A dynamic theory of coordination of discrete movement,” *Biol. Cybern.*, vol. 63, no. 4, pp. 257–270, 1990.

[5] D. a. Winter, “Kinematic and kinetic patterns in human gait: Variability and compensating effects,” *Hum. Mov. Sci.*, vol. 3, no. 1–2, pp. 51–76, 1984.

[6] S. Haddadin, A. Albu-Schaffer, A. De Luca, and G. Hirzinger, “Collision detection and reaction: A contribution to safe physical human-robot interaction,” in *2008 IEEE/RSJ International Conference on Intelligent Robots and Systems*, 2008, pp. 3356–3363.

[7] S. Kwon and J. Kim, “Real-time upper limb motion estimation from surface electromyography and joint angular velocities using an artificial neural network for human-machine cooperation.,” *IEEE Trans. Inf. Technol. Biomed.*, vol. 15, no. 4, pp. 522–530, Jul. 2011.

[8] M. Ferre, I. Galiana, R. Wirz, and N. Tuttle, “Haptic device for capturing and simulating hand manipulation rehabilitation,” *IEEE/ASME Trans. Mechatronics*, vol. 16, no. 5, pp. 808–815, 2011.

[9] C. Castellini, A. Arquer, and J. Artigas, “SEMG-based estimation of human stiffness: Towards impedance-controlled rehabilitation,” *Proc. IEEE RAS EMBS Int. Conf. Biomed. Robot. Biomechatronics*, pp. 604–609, 2014.

[10] H. J. S. Schreuders, Ton AR, Marij E. Roebroeck, Janine Goumans, Johan F. van Nieuwenhuijzen, Theo H. Stijnen, “Measurement error in grip and pinch force measurements in patients with hand injuries,” *Phys. Ther.*, vol. 83, no. 9, pp. 806–815, 2003.

[11] J. Wang, L. Tang, and J. E Bronlund, “Surface EMG Signal Amplification and Filtering,” *Int. J. Comput. Appl.*, vol. 82, no. 1, pp. 15–22, Nov. 2013.

[12] S. I. Yaniger, “Force Sensing Resistors: A Review Of The Technology,” *Electro International*. pp. 666–668, 1991.

[13] C. Castellini *et al.*, “Proceedings of the first workshop on peripheral machine interfaces: Going beyond traditional surface electromyography,” *Front. Neurorobot.*, vol. 8, no. AUG, p. 22, Aug. 2014.

[14] X. Jiang, L.-K. Merhi, Z. G. Xiao, and C. Menon, “Exploration of force myography and surface electromyography in hand gesture classification,” *Med. Eng. Phys.*, vol. 41, pp. 63–73, 2017.

[15] Interlink Electronics, “FSR 402 Data Sheet FSR 400 Series Round Force Sensing Resistor.”

[16] N. – H. KIM, “Quantification and analysis of hand grasp dynamics and arm reaching kinematics following hemiparesis using a novel assistive robotics approach,” 2007.

[17] N. Li, D. Yang, L. Jiang, H. Liu, and H. Cai, “Combined use of FSR sensor array and SVM classifier for finger motion recognition based on pressure distribution map,” *J. Bionic Eng.*, vol. 9, no. 1, pp. 39–47, Mar. 2012.

[18] M. Rasouli, R. Ghosh, W. W. Lee, N. V Thakor, and S. Kukreja, “Stable force-myographic control of a prosthetic hand using incremental learning,” in *37th Annual International Conference of the IEEE Engineering in Medicine and Biology Society (EMBC)*, 2015, pp. 4828–4831.

[19] A. Radmand, E. Scheme, and K. Englehart, “High-density force myography: A possible alternative for upper-limb prosthetic control,” *J. Rehabil. Res. Dev.*, vol.

53, no. 4, pp. 443–456, 2016.

[20] A. Ferrone *et al.*, “Wearable band for hand gesture recognition based on strain sensors,” in *Biomedical Robotics and Biomechatronics (BioRob), 2016 6th IEEE International Conference on*, 2016, pp. 1319–1322.

[21] Z. G. Xiao and C. Menon, “Towards the development of a wearable feedback system for monitoring the activities of the upper-extremities,” *Xiao Menon J. NeuroEngineering Rehabil.*, vol. 11, no. 2, p. 13, Jan. 2014.

[22] M. Wininger, N.-H. Kim, and W. Craelius, “Pressure signature of forearm as predictor of grip force.,” *J. Rehabil. Res. Dev.*, vol. 45, no. 6, pp. 883–892, 2008.

[23] and R. K. Castellini, Claudio, “Using a high spatial resolution tactile sensor for intention detection,” in *Rehabilitation Robotics (ICORR), 2013 IEEE International Conference*, 2013, pp. 1–7.

[24] V. Ravindra and C. Castellini, “A Comparative Analysis of Three Non-Invasive Human-Machine Interfaces for the Disabled,” *Front. Neurorobot.*, vol. 8, pp. 1–10, 2014.

[25] M. Vergara, J. L. Sancho-Bru, V. Gracia-Ibáñez, and A. Pérez-González, “An introductory study of common grasps used by adults during performance of activities of daily living.,” *J. Hand Ther.*, vol. 27, no. 3, p. 225–33; quiz 234, Jan. 2014.

[26] J. R. C. John R. Cameron, James G. Skofronick, Roderick M. Grant, “Muscle and Forces,” *Phys. Body*, pp. 37–84, 1999.

[27] T. S. Buchanan, D. P. Almdale, J. L. Lewis, and W. Z. Rymer, “Characteristics of synergic relations during isometric contractions of human elbow muscles,” *J. Neurophysiol.*, vol. 56, no. 5, pp. 1225–1241, 1986.

[28] C. Castellini and V. Ravindra, “A wearable low-cost device based upon Force-Sensing Resistors to detect single-finger forces,” in *5th IEEE RAS/EMBS International Conference on Biomedical Robotics and Biomechatronics*, 2014, pp.

199–203.

[29] M. Atzori *et al.*, “Electromyography data for non-invasive naturally-controlled robotic hand prostheses.,” *Sci. data*, vol. 1, p. 140053, Dec. 2014.

[30] M. Moradi, K. Hashtrudi-Zaad, K. Mountjoy, and E. Morin, “An EMG-based force control system for prosthtic arms,” *Can. Conf. Electr. Comput. Eng.*, pp. 1737–1742, 2008.

[31] M. Tavakolan and C. Menon, “Towards the development of a robust model for estimating wrist torque at different wrist angles,” in *Robotics and Biomimetics (ROBIO), 2012 IEEE International Conference on*, 2012, pp. 618–623.

[32] S. Zhang *et al.*, “Muscle Strength Assessment System Using sEMG-Based Force Prediction Method for Wrist Joint,” *J. Med. Biol. Eng.*, vol. 36, no. 1, pp. 121–131, 2016.

[33] M. Ison, I. Vujaklija, B. Whitsell, D. Farina, and P. Artemiadis, “Simultaneous myoelectric control of a robot arm using muscle synergy-inspired inputs from high-density electrode grids,” *2015 IEEE Int. Conf. Robot. Autom.*, pp. 6469–6474, 2015.

[34] C. Yang, S. Chang, P. Liang, Z. Li, and C. Su, “Teleoperated Robot Writing using EMG Signals,” no. August, pp. 2264–2269, 2015.

[35] J. F. Yang and D. A. Winter, “Electromyographic amplitude normalization methods: improving their sensitivity as diagnostic tools in gait analysis.,” *Archives of physical medicine and rehabilitation*, vol. 65, no. 9. pp. 517–21, 1984.

[36] D. a. Yungher, M. T. Wininger, J. B. Barr, W. Craelius, and a. J. Threlkeld, “Surface muscle pressure as a measure of active and passive behavior of muscles during gait,” *Med. Eng. Phys.*, vol. 33, no. 4, pp. 464–471, 2011.

[37] D. A. Yungher, M. T. Wininger, J. B. Barr, W. Craelius, and A. J. Threlkeld, “Surface muscle pressure as a measure of active and passive behavior of muscles during gait.,” *Med. Eng. Phys.*, vol. 33, no. 4, pp. 464–471, May 2011.

[38] C. Allen, K. Z. Karam, P. Le Cam, M. Hill, and T. Tindle, “Application of virtual reality

devices to the quantitative\nassessment of manual assembly forces in a factory environment," *Proc. IECON '95 - 21st Annu. Conf. IEEE Ind. Electron.*, vol. 2, pp. 1048–1053, 1995.

[39] A. Troiano, F. Naddeo, E. Sosso, G. Camarota, R. Merletti, and L. Mesin, "Assessment of force and fatigue in isometric contractions of the upper trapezius muscle by surface EMG signal and perceived exertion scale," *Gait Posture*, vol. 28, no. 2, pp. 179–186, 2008.

[40] A. I. Automation, "F/T Sensor Mini45," 2015. [Online]. Available: http://www.ati-ia.com/app_content/documents/9620-05-DAQ.pdf. [Accessed: 01-Sep-2015].

[41] A. Hill, "The Heat of Shortening and the Dynamic Constants of Muscle," *Proc. R. Soc. London B Biol. Sci.*, vol. 126, no. 843, pp. 136–195, 1938.

[42] L. S. Winters, Jack M., "Muscle models: what is gained and what is lost by varying model complexity," *Biol. Cybern.*, vol. 55, no. 6, pp. 403–420, 1987.

[43] K. R. Mills, "The basics of electromyography.," *J. Neurol. Neurosurg. Psychiatry*, vol. 76 Suppl 2, no. Suppl II, p. ii32-5, 2005.

[44] D. Yang, J. Zhao, Y. Gu, L. Jiang, and H. Liu, "Estimation of hand grasp force based on forearm surface EMG," *Mechatronics and Automation, 2009. ICMA 2009. International Conference on*. pp. 1795–1799, 2009.

[45] F. Mobasser and K. Hashtrudi-Zaad, "Hand force estimation using electromyography signals," in *Proceedings of the 2005 IEEE International Conference on Robotics and Automation*, 2005, pp. 2631–2636.

[46] G. H. Hermens, Hermie J., Bart Freriks, Roberto Merletti, Dick Stegeman, Joleen Blok, Günter Rau, Cathy Disselhorst-Klug, "European Recommendations for Surface ElectroMyoGraphy," *Roessingh Res. Dev.*, vol. 8, no. 2, pp. 13–54, 1999.

[47] C. J. De Luca, "The Use of Surface Electromyography in Biomechanics," *J. Appl. Biomech.*, vol. 13, no. 2, pp. 135–163, 1997.

[48] A. Ziai and C. Menon, "Comparison of regression models for estimation of isometric

wrist joint torques using surface electromyography," *J. Neuroeng. Rehabil.*, vol. 8, no. 1, p. 56, Jan. 2011.

[49] H. Srinivasan, S. Gupta, and W. Sheng, "Estimation of hand force from surface Electromyography signals using Artificial Neural Network," *Proc. 10th World Congr. Intell. Control Autom.*, pp. 584–589, 2012.

[50] J. Mikael Eklund, F. Mobasser, and K. Hashtrudi-Zaad, "Hand force estimation using Fast Orthogonal Search.," *Conf. Proc. IEEE Eng. Med. Biol. Soc.*, vol. 1, no. 2, pp. 695–8, 2004.

[51] C. Castellini, E. Gruppioni, A. Davalli, and G. Sandini, "Fine detection of grasp force and posture by amputees via surface electromyography," *J. Physiol.*, vol. 103, no. 3–5, pp. 255–262, May 2009.

[52] D. Yang, J. Zhao, Y. Gu, L. Jiang, and H. Liu, "EMG pattern recognition and grasping force estimation: Improvement to the myocontrol of multi-DOF prosthetic hands," *2009 IEEE/RSJ International Conference on Intelligent Robots and Systems*. pp. 516–521, 2009.

[53] E. R. N. L. K. Amavuako, D. A. F. Arina, K. E. N. Y. Oshida, and W. I. J. Ensen, "Estimation of Grasping Force from Features of Intramuscular EMG Signals with Mirrored Bilateral Training," *Ann. Biomed. Eng.*, vol. 40, no. 3, pp. 648–656, 2012.

[54] C. Castellini and P. van der Smagt, "Surface EMG in advanced hand prosthetics," *Biol. Cybern.*, vol. 100, no. 1, pp. 35–47, Jan. 2009.

[55] C. Castellini and R. Koiva, "Using surface electromyography to predict single finger forces," in *2012 4th IEEE RAS & EMBS International Conference on Biomedical Robotics and Biomechatronics (BioRob)*, 2012, pp. 1266–1272.

[56] C. Choi, S. Kwon, W. Park, H. Lee, and J. Kim, "Real-time pinch force estimation by surface electromyography using an artificial neural network," *Med. Eng. Phys.*, vol. 32, no. 5, pp. 429–436, 2010.

[57] C. Potluri *et al.*, "Frequency Domain Surface EMG Sensor Fusion for Estimating

Finger Forces," in *Engineering in Medicine and Biology Society (EMBC), 2010 Annual International Conference of the IEEE. IEEE*, 2010, pp. 5975–5978.

[58] D. Formica, S. K. Charles, L. Zollo, E. Guglielmelli, N. Hogan, and H. I. Krebs, "The passive stiffness of the wrist and forearm," *J Neuro-physiol*, vol. 108, no. Ashworth 1964, pp. 1158–1166, 2012.

[59] P. Liang, C. Yang, and Z. Li, "Writing Skills Transfer From Human To Robot Using Stiffness Extracted From sEMG," 2015, no. 1.

[60] S. Paul, "Tele-Impedance: Towards Transferring Human Impedance Regulation Skills to Robots," 2012.

[61] R. H. Chowdhury, M. B. I. Reaz, M. A. B. M. Ali, A. A. A. Bakar, K. Chellappan, and T. G. Chang, "Surface electromyography signal processing and classification techniques.," *Sensors (Basel).*, vol. 13, no. 9, pp. 12431–12466, Jan. 2013.

[62] M. Wininger, N.-H. Kim, and W. Craelius, "Pressure signature of forearm as predictor of grip force.," *J. Rehabil. Res. Dev.*, vol. 45, no. 6, pp. 883–892, Jan. 2008.

[63] E. Cho, R. Chen, L. Merhi, Z. Xiao, B. Pousett, and C. Menon, "Force Myography to Control Robotic Upper Extremity Prostheses: A Feasibility Study," *Front. Bioeng. Biotechnol.*, vol. 4, no. March, pp. 1–12, Mar. 2016.

[64] S. L. Phillips and W. Craelius, "Residual kinetic imaging: a versatile interface for prosthetic control," *Robotica*, vol. 23, no. 3, pp. 277–282, 2005.

[65] V. Ravindra and C. Castellini, "A comparative analysis of three non-invasive human-machine interfaces for the disabled.," *Front. Neurorobot.*, vol. 8, no. October, p. 24, 2014.

[66] D. Merletti, R., Rainoldi, A. and Farina, "Surface Electromyography for Noninvasive Characterization of Muscle Surface Electromyography for Noninvasive Characterization of Muscle," *Exerc. Sport Sci. Rev.*, vol. 29, no. 1, pp. 20–25, 2001.

[67] A. Dementyev and J. A. Paradiso, "WristFlex: Low-Power Gesture Input with Wrist-

Worn Pressure Sensors," in *Proceedings of the 27th annual ACM symposium on User interface software and technology - UIST '14*, 2014, pp. 161–166.

[68] I.Electronics, "FSR ® 400 Series Data Sheet," 2015. .

[69] M. Connan, E. Ruiz Ramírez, B. Vodermayer, and C. Castellini, "Assessment of a Wearable Force- and Electromyography Device and Comparison of the Related Signals for Myocontrol," *Front. Neurorobot.*, vol. 10, no. November, pp. 1–13, 2016.

[70] T. Morris and W. Craelius, "Force Myographic Interface for Ankle Rehabilitation," no. 5, pp. 1–7.

[71] K. Tzu, Y., Murilo, F.M., Egont, A. and Carlos, "Identification of hand postures by force myography using an optical fiber specklegram sensor," in *24th International Conference on Optical Fibre Sensors. SPIE-INT SOC OPTICAL ENGINEERING*, 2015.

[72] G. Sadarangani and C. Menon, "A wearable sensor system for rehabilitation apllications," in *2015 IEEE International Conference on Rehabilitation Robotics (ICORR)*, 2015, pp. 672–677.

[73] H. K. Yap, S. Member, A. Mao, J. C. H. Goh, and C. Yeow, "Design of A Wearable FMG Sensing System for User Intent Detection during Hand Rehabilitation with a Soft Robotic Glove," in *Biomedical Robotics and Biomechatronics (BioRob), 2016 6th IEEE International Conference on. IEEE*, 2016, pp. 781–786.

[74] A. Kadkhodayan, X. Jiang, and C. Menon, "Continuous prediction of finger movements using force myography," *J. Med. Biol. Eng.*, vol. 36, no. 4, pp. 594–604, 2016.

[75] Z. G. Xiao, A. M. Elnady, and C. Menon, "Control an exoskeleton for forearm rotation using FMG," *5th IEEE RAS/EMBS Int. Conf. Biomed. Robot. Biomechatronics*, vol. 1, pp. 591–596, Aug. 2014.

[76] X. Jiang, L.-K. Merhi, and C. Menon, "Force Exertion Affects Grasp Classification using Force Myography," *IEEE Trans. Human-Machine Syst.*, no. January, p.

Accepted, 2016.

[77] C. Delva, M.L., Sakr, M. and Menon, “Pilot study on strategies in sensor placement for robust hand/wrist gesture classification based on movement related changes in forearm volume,” in *Healthcare Innovation Point-Of-Care Technologies Conference (HI-POCT), 2016 IEEE*, 2016, pp. 46–49.

[78] Z. G. Xiao and C. Menon, “Towards the development of a wearable feedback system for monitoring the activities of the upper-extremities,” *J. Neuroeng. Rehabil.*, vol. 11, no. 1, p. 2, 2014.

[79] D. A. Yungher, M. T. Wininger, J. B. Barr, W. Craelius, and A. J. Threlkeld, “Surface muscle pressure as a measure of active and passive behavior of muscles during gait,” *Med. Eng. Phys.*, vol. 33, no. 4, pp. 464–471, May 2011.

[80] V. Ravindra and C. Castellini, “A Comparative Analysis of Three Non-Invasive Human-Machine Interfaces for the Disabled,” *Front. Neurorobot.*, vol. 8, no. October, pp. 1–10, 2014.

[81] M. Sakr and C. Menon, “On the estimation of isometric wrist/forearm torque about three axes using Force Myography,” in *Biomedical Robotics and Biomechatronics (BioRob), 2016 6th IEEE International Conference on*, 2016, pp. 827–832.

[82] M. Sakr and C. Menon, “Regressing force-myographic signals collected by an armband to estimate torque exerted by the wrist: A preliminary investigation,” in *2016 IEEE Canadian Conference on Electrical and Computer Engineering (CCECE)*, 2016, pp. 1–4.

[83] R. L. Abboudi, C. A. Glass, N. A. Newby, J. A. Flint, and W. Craelius, “A biomimetic controller for a multifinger prosthesis,” *IEEE Trans. Rehabil. Eng.*, vol. 7, no. 2, pp. 121–129, Jun. 1999.

[84] N. Carbonaro *et al.*, “An Innovative Multisensor Controlled Prosthetic Hand,” in *IFMBE Proceedings*, vol. 41, L. M. Roa Romero, Ed. Cham: Springer International Publishing, 2014, pp. 93–96.

[85] H. W. Ng, X. Jiang, L.-K. Merhi, and C. Menon, “Investigation of the Feasibility of Strain Gages as Pressure Sensors for Force Myography,” in *Bioinformatics and Biomedical Engineering*, vol. 9044, no. 1, F. Ortuño and I. Rojas, Eds. Cham: Springer International Publishing, 2017, pp. 261–270.

[86] D. Yang, N. Chhatre, F. Campi, and C. Menon, “Feasibility of Support Vector Machine Gesture Classification on a Wearable Embedded Device.”

[87] S. L. K. Rasouli, Mahdi, Karthik Chellamuthu, John-John Cabibihan, “towards enhanced control of upper prosthetic limbs A force-myographic approach,” in *Biomedical Robotics and Biomechatronics (BioRob), 2016 6th IEEE International Conference on. IEEE*, 2016, pp. 232–236.

[88] A. Ferrone *et al.*, “Wearable Band for Hand Gesture Recognition based on Strain Sensors,” *6th IEEE RAS/EMBS Int. Conf. Biomed. Robot. Biomechatronics*, 2016.

[89] G. Ogris, M. Kreil, and P. Lukowicz, “Using FSR based muscule activity monitoring to recognize manipulative arm gestures,” in *2007 11th IEEE International Symposium on Wearable Computers*, 2007, pp. 1–4.

[90] N. Carbonaro *et al.*, “An Innovative Multisensor Controlled Prosthetic Hand,” in *IFMBE Proceedings*, vol. 41, 2014, pp. 93–96.

[91] C. K. S. Fujiwara, Eric, Yu Tzu Wu, Murilo FM Santos, Egont A. Schenkel, “Optical Fiber Specklegram Sensor for Measurement of Force Myography Signals,” *IEEE Sens. J.*, vol. 17, no. 4, pp. 951–958, 2017.

[92] G. Sadarangani and C. Menon, “Gautam Sadarangani, Carlo Menon, Member, IEEE,” in *Rehabilitation Robotics (ICORR), 2015 IEEE International Conference on*, 2015, pp. 672–677.

[93] X. Li, Q. Zhuo, X. Zhang, O. W. Samuel, Z. Xia, and X. Zhang, “FMG-Based Body Motion Registration Using Piezoelectret Sensors,” in *Engineering in Medicine and Biology Society (EMBC), 2016 IEEE 38th Annual International Conference of the. IEEE*, 2016, pp. 4626–4629.

[94] E. R. Ramírez, “Control of a hand prosthesis using mixed electromyography and pressure sensing,” 2016.

[95] A. E. Hoerl and R. W. Kennard, “Ridge Regression: Biased Estimation for Nonorthogonal Problems,” *Technometrics*, vol. 12, no. 1, pp. 55–67, 1970.

[96] C. Saunders, A. Gammerman, and V. Vovk, “Ridge Regression Learning Algorithm in Dual Variables,” *Proc. 15th Int. Conf. Mach. Learn.*, pp. 515–521, 1998.

[97] R. Rifkin, G. Yeo, T. Poggio, and others, “Regularized least-squares classification,” *Nato Sci. Ser. Sub Ser. III Comput. Syst. Sci.*, vol. 190, pp. 131–154, 2003.

[98] S. Van Vaerenbergh, “Kernel Methods for Nonlinear Identification , Equalization and Separation of Signals,” *Science (80-.).*, 2009.

[99] B. Yegnanarayana, *Artificial neural networks*. PHI Learning Pvt. Ltd., 2009.

[100] J. Cholewicki and S. M. McGill, “EMG assisted optimization: a hybrid approach for estimating muscle forces in an indeterminate biomechanical model,” *J. Biomech.*, vol. 27, no. 10, pp. 1287–1289, 1994.

[101] A. L. Hof and J. W. den Berg, “EMG to force processing I: an electrical analogue of the Hill muscle model,” *J. Biomech.*, vol. 14, no. 11, pp. 747755–753758, 1981.

[102] D. F. Specht, “A general regression neural network,” *IEEE Trans. neural networks*, vol. 2, no. 6, pp. 568–576, 1991.

[103] J.-J. Luh, G.-C. Chang, C.-K. Cheng, J.-S. Lai, and T.-S. Kuo, “Isokinetic elbow joint torques estimation from surface EMG and joint kinematic data: using an artificial neural network model,” *J. Electromyogr. Kinesiol.*, vol. 9, no. 3, pp. 173–183, 1999.

[104] C. K. I. Williams and C. E. Rasmussen, “Gaussian processes for regression,” *Adv. Neural Inf. Process. Syst. 8*, vol. 8, no. August, pp. 514–520, 1996.

[105] C. E. Rasmussen, “Gaussian processes in machine learning,” in *Advanced lectures on machine learning*, Springer, 2004, pp. 63–71.

[106] V. V. Harris Drucker , Chris J. C. Burges , Linda Kaufman , Alex Smola, “Support Vector Regression Machines,” *Adv. Neural Inf. Process. Syst.*, vol. 9, pp. 155–161, 1997.

[107] D. Basak, S. Pal, and D. C. Patranabis, “Support Vector Regression,” vol. 11, no. 10, pp. 203–224, 2007.

[108] C. Bishop and N. Nasrabadi, “Pattern recognition and machine learning,” *COMPSTAT*, pp. 325–358, 2006.

[109] C. Chang and C. Lin, “LIBSVM: A Library for Support Vector Machines,” *ACM Trans. Intell. Syst. Technol.*, vol. 2, no. 3, pp. 1–27, Apr. 2011.

[110] W. Wang, Z. Xu, W. Lu, and X. Zhang, “Determination of the spread parameter in the Gaussian kernel for classification and regression,” *Neurocomputing*, vol. 55, no. 3, pp. 643–663, 2003.

[111] P. Refaeilzadeh, L. Tang, and H. Liu, “On Comparison of Feature Selection Algorithms,” *Proc. AAAI Work. Eval. methods Mach. Learn. II*, vol. 3, no. 4, pp. 34–39, 2007.

[112] L. E. O. Breiman, “Random Forests,” *Mach. Learn.*, vol. 45, no. 1, pp. 5–32, 2001.

[113] R. T. Friedman, Jerome, Trevor Hastie, *The elements of statistical learning*. 2001.

[114] E. Criminisi, A., Shotton, J., Robertson, D.P. and Konukoglu, “Regression Forests for Efficient Anatomy Detection and Localization in CT Studies,” in *MCV*, 2010, pp. 106–117.

[115] InterlinkElectronics, “FSR® Integration Guide & Evaluation Parts Catalog with Suggested Electrical Interfaces,” 2010.

[116] Atmel Corporation, “ATmega328 / P Datasheet,” p. 24, 2016.

[117] Y. Xiong and F. Quek, “Hand motion gesture frequency properties and multimodal discourse analysis,” *Int. J. Comput. Vis.*, vol. 69, no. 3, pp. 353–371, 2006.

[118] N. R. Draper and H. Smith, “Applied Regression Analysis,” *Technometrics*, vol. 47, no. 3, pp. 380–380, Aug. 2005.

[119] D. Formica, S. K. Charles, L. Zollo, E. Guglielmelli, N. Hogan, and H. I. Krebs, “The passive stiffness of the wrist and forearm,” *J Neuro-physiol*, vol. 108, no. Ashworth 1964, pp. 1158–1166, 2012.

[120] E. N. Kamavuako, E. J. Scheme, and K. B. Englehart, “Wrist torque estimation during simultaneous and continuously changing movements: surface vs. untargeted intramuscular EMG,” *J. Neurophysiol.*, vol. 109, no. 11, pp. 2658–2665, 2013.

[121] M. Connan, E. Ruiz Ramírez, B. Vodermayer, and C. Castellini, “Assessment of a wearable force-and electromyography device and comparison of the related signals for myocontrol.”

[122] T. S. Buchanan, G. P. Rovai, and W. Z. Rymer, “Strategies for muscle activation during isometric torque generation at the human elbow,” *J. Neurophysiol.*, vol. 62, no. 6, pp. 1201–1212, 1989.

[123] L. A. Jones and I. W. Hunter, “Effect of fatigue on force sensation,” *Exp. Neurol.*, vol. 81, no. 3, pp. 640–650, 1983.

[124] N. Jiang, K. B. Englehart, and P. A. Parker, “Extracting Simultaneous and Proportional Neural Control Information for Multiple-DOF Prostheses From the Surface Electromyographic Signal,” *Biomedical Engineering, IEEE Transactions on*, vol. 56, no. 4. pp. 1070–1080, 2009.

[125] E. N. Kamavuako, E. J. Scheme, and K. B. Englehart, “Wrist torque estimation during simultaneous and continuously changing movements: surface vs. untargeted intramuscular EMG,” *J. Neurophysiol.*, vol. 109, no. 11, pp. 2658–2665, 2013.

[126] J. L. G. Nielsen, S. Holmgaard, N. Jiang, K. B. Englehart, D. Farina, and P. A. Parker, “Simultaneous and Proportional Force Estimation for Multifunction Myoelectric Prostheses Using Mirrored Bilateral Training,” *IEEE Trans. Biomed.*

Eng., vol. 58, no. 3, pp. 681–688, 2011.

[127] J. L. G. Nielsen, S. Holmgaard, N. Jiang, K. B. Englehart, D. Farina, and P. A. Parker, “Simultaneous and Proportional Force Estimation for Multifunction Myoelectric Prostheses Using Mirrored Bilateral Training,” *IEEE Transactions on Biomedical Engineering*, vol. 58, no. 3. pp. 681–688, 2011.

[128] T. S. Buchanan, D. G. Lloyd, K. Manal, and T. F. Besier, “Neuromusculoskeletal modeling: Estimation of muscle forces and joint moments and movements from measurements of neural command,” *J. Appl. Biomech.*, vol. 20, no. 4, pp. 367–395, 2004.